ACTUATORS AND SENSORS

FOR

ACTIVE VIBRATION CONTROL

A THESIS SUBMITTED TO THE UNIVERSITY OF MANCHESTER

FOR THE DEGREE OF DOCTOR OF PHILOSOPHY

IN THE FACULTY OF SCIENCE AND ENGINEERING.

November 1996

BY

MOFTAH MOHAMED BAKUSH

DIVISION OF ELECTRICAL ENGINEERING.

MANCHESTER UNIVERSITY

ProQuest LLC.
789 East Eisenhower Parkway
P.O. Box 1346
Ann Arbor, MI 48106 – 1346

Contents

Abstract.

Scanning probe microscopes (SPM) such as atomic and magnetic force microscopes, have become important devices for the investigation of surfaces in different media. They have proved to be able to produce very high resolution images of the sample under investigation. In its basic form, it involves scanning a very fine tip close to the surface and monitoring the deflection of a cantilever on which the tip is mounted. A detailed model which characterises the dynamic behaviour of the scanning probe microscope cantilever such as its natural frequency and modal shapes is presented

In scanning probe instruments, the cantilevers are extremely susceptible to external disturbances such as acoustic noise and building vibrations, which ultimately limits their performance. This thesis aims to implement active vibration control to minimise the effects of these disturbances and so increase the instrument's sensitivity. In principle the method is very simple: monitor the vibration signal by a suitable sensor, process the signal and feedback to effect actuation. A general description of the behaviour of sensors and actuators used in active vibration control is given.

Piezoelectric elements as actuators have been extensively used to control structures with a wide range of sizes. The effect of piezo-actuator thickness on the magnitude of the deflection of a cantilever beam has been investigated experimentally and the results compared with a theoretical model. Results indicate that there exists a piezo-actuator thickness which maximises the cantilever deflection, and this optimal thickness is a function of ratio of the Young's modulus of the actuator and the cantilever. The significance for actuator design is discussed.

For small structures electrostatic actuation is attractive. An electrostatic actuator is however inherently non-linear. The behaviour of such an actuator is theoretically modelled and experimentally verified. A control system has been developed which enables a linear electrostatic actuation to be realised.

DECLARATION

No portion of the work referred to in this thesis has been submitted in support of an application for another degree or qualification of this or any other university or other institute of learning .

Acknowledgements

I would like to express my gratitude to the Division of Electrical Engineering of Manchester University for providing facilities for this work. I am deeply indebted to my supervisor Dr M.J. Cunningham for inspiring me to take up this exciting and challenging project. I am greatly thankful for his guidance, constructive criticism and encouragement.

I would like also to thank Dr. D.F.L Jenkins for his comments , suggestions and contribution during this work.

I also wish to express my appreciation to the Secretary of Higher education, Libya, for financial support during my study in the United Kingdom.

Finally, special thanks to my wife (Zuhra Emhamed Twati) for her patience and moral support and also to my children (Tahani, Muhannad, Mouad and Esra) for their encouragement in their own ways.

Notation

AFM	Atomic force microscopy.
SFM	Scanning force microscopy.
d_{31}	Piezoelectric charge coefficient (m/V).
g_{31}	Piezoelectric voltage coefficient (V.m/N).
V	Applied voltage (V).
L	Cantilever length (m).
W_b	Cantilever width (m).
E_b	Cantilever Young's modulus (N m^{-2}).
E_p	piezoelectric Young's modulus (N m^{-2}).
E_s	Substructure Young's modulus (N m^{-2}).
ρ	Mass per unit length (kg/m).
M	Equivalent bending moment (N/m).
t_b	Cantilever thickness (m).
t_p	Piezoelectric thickness (m).
Vs	Sensor output (V).
Λ	Free piezoelectric strain.
σ	Interface stress of cantilever-actuator (N/m^2).
σ_b	Cantilever stress (N/m^2).
σ_p	Piezoelectric stress (N/m^2).
ε_b	Strain induced in cantilever by actuator.
ε_p	Strain induced in piezoelectric.
A	Cross-sectional area of composite structure (m^2)
I_b	Second moment of area (m^4) of cantilever about the neutral axis of the composite structure.
ε_o	Permittivity of free space (F/m).
ε_r	Relative permittivity of medium (F/m).
k_o	Cantilever spring constant (N/m)
m	Total mass density (kg)
V_{dc}	DC applied voltage (V).
V_{ac}	AC applied voltage (V).
QF	Quality factor

To WHOM I LOVE MOST

MY FAMILY:

FATHER, MOTHER, WIFE, CHILDREN, BROTHERS AND

SISTERS.

List Of Figures.

List of Tables.

Chapter 1

1. Introduction:

The aim of this thesis is to investigate theoretically and experimentally the behaviour of different types of actuator and sensor systems which are suitable for use in microscale structures such as cantilevers to monitor and suppress unwanted microstructure vibrations whilst allowing micropositioning.

An understanding and modelling of the basic cantilever behaviour such as modal shape, resonance frequencies and deflection is also necessary. Therefore, such behaviour is theoretically modelled in this thesis.

1.1 Objectives of the thesis.

Many flexible structures from large ones found in aerospace engineering down to structures of microscale suffer from undesirable vibration problems. For example advanced spacecraft systems are becoming increasingly complex as large lightweight structure elements become integral parts of the configuration. Disturbances such as the docking of spacecraft or firing of booster rockets will excite structural vibrations. Once excited these vibrations will continue with very little natural damping and, therefore, it is a very difficult task to avoid exciting all of the resonating frequencies. In large structures, the effects of these lead to vibration problems such as material fatigue and instability [1]. On a microscale level, Franks [2] has shown

how atomic force microscope (AFM) images can be adversely affected by induced unwanted cantilever vibrations. This is a general problem common in many scientific instruments, but particularly in scanning force instruments where the cantilevers are typically of microdimensions (size, e.g. 180 x 18 x 0.6 μm). The very high compliance of such structures, necessary for their primary function, makes them extremely sensitive to extraneous vibrations and air-borne acoustic noise. This means great care is normally required to isolate the instruments from these sources, such as by the use of a massive air bearing table. Figure (1.1) shows the scanning force microscopic image affected by vibration problems.

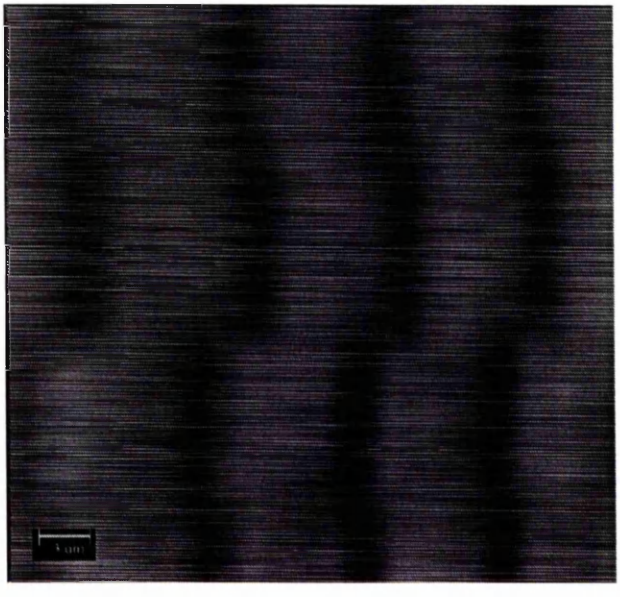

Figure (1-1) Vibration effects on the scanning force microscopic images.

As an alternative to the use of an air bearing table, an effective active vibration control system can be used. This improves the performance of the instrument and reduces the cost. The choice of control techniques has been the focus of a lot of research [3-5]. The control system consists of : a vibration signal monitor (sensor), a signal processor (electronic circuit), a feedback mechanism and finally a damper system (actuator). The advantages of active control over the conventional passive damping is discussed in chapter 2. For an efficient active control strategy, a suitable sensor and actuator should be selected. In the literature [6-11] different types of sensors and actuators used to control cantilever vibrations have been described. The most relevant sensors and actuators and their properties are reviewed in chapter 2. Figure (1.2) shows the improvement in the scanning force microscopic image when the active vibration control is implemented .

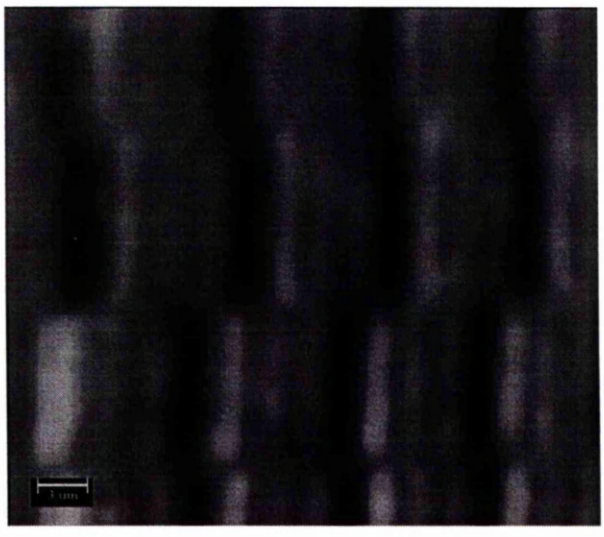

Figure (1-2). Effect of the active vibration control in the SFM images.

In the study of free vibrations of continuous linear systems such as simple cantilevers, effort is mainly concentrated on finding the eigenvalues (frequencies) and corresponding eigenfunctions (modal shapes). The characteristics of inhomogeneous cantilevers (composite structures) is presented in chapter 3.

Leissa and Sonalla [12] have theoretically considered the modal shapes of fixed-free cantilevers with various initial conditions. A cantilever was given various initial shapes and its subsequent non-periodic motion determined. In each case the load was applied at the end of the cantilever. Although this analytical model successfully predicts the behaviour of the simple cantilever, Jenkins *et al* [9] have shown in the modal shape measurement of an inhomogeneous cantilever that the behaviour of a composite structure, such as a cantilever with a piezoelectric element (PZT) which is used for both damping and actuation, is not properly described in Leissa's and Sonalla's model. A new analytical model characterising the composite structure accounting for actuation by a discrete piezo-element located near the root and also the effective clamping point due to the non-ideal behaviour of the clamp is presented in chapter 3.

Since the advent of the atomic fore microscope (AFM) [13], a wide range of physical systems have been investigated from the microscopic to the atomic scale [14]. In one mode of operation, AFMs can resolve individual atoms on both conducting and insulating surfaces. A crucial component for AFM or SFM (Scanning force microscope) is a flexible force-sensing cantilever stylus whose properties should

include, among other things: a sharp tip, a low force constant, a high mechanical factor Q and a high mechanical resonance frequency. For atomic and scanning force microscopy, most cantilevers used are V-shaped [15]. In the past, V-shaped cantilevers have been treated as two rectangular beams in parallel [16] : V-shaped cantilevers have a spring constant which is assumed to be equivalent to two cantilevers in parallel. Chen *et al* [17], report that effective mass of V-shaped cantilevers cannot be determined by assuming rectangular beams in parallel. A model of SFM cantilevers using a finite element model to characterise the most important parameters (i.e. cantilever frequencies, deflection, dimensions and the damping medium surrounding the cantilever) is represented in chapter 3.

For a cantilever beam of a given material and dimensions, it is necessary to determine which factors enable the effective bending moment to be optimised. Such factors include the piezoelectric actuator element material, dimensions, its location and the choice of bonding layer. The choice of the piezoelectric material for an actuator is principally determined by the piezoelectric coefficient d_{31}, which determines the degree of actuation possible for a given drive electric field. The thickness dependency of the actuator has been investigated theoretically by Kim and Jones [18] for plate structures. Their model showed that there is an optimum thickness for a piezoelectric actuator. However, so far no experimental verification of the optimisation of the piezoelectric actuator thickness has been carried out. In Chapter 4 of this thesis, a theoretical and experimental investigation of the optimum piezoelectric element for cantilever actuation are presented.

In recent years, the electrostatic actuator has proven to be an interesting approach in many applications in micromechanical structures such as micro-motors, micropositioners and microactuators in scanning force microscope [19]. Recently, electrostatic actuation was used as an active damper in the control of micro-structures (cantilevers) vibrations [20]. An electrostatic actuator is however inherently non-linear. The behaviour of such an actuator is theoretically modelled in Chapter 5, and a method for linearising the behaviour is also investigated.

1.2 Structure of the thesis:

The thesis is made up of 7 chapters.

Chapter 1, the introduction, lays the foundation for subsequent chapters.

Chapter 2 provides:

a) A detailed survey of the different types of sensors used to detect the cantilever vibration.
b) A description of the piezoelectric material used to model the active damper (actuator).
c) A brief review of previous research on active control models.

Chapter 3 deals with:

a) A derivation of new mode shape analytical solution based on the additional boundary conditions due to the piezo-actuator.

b) The modelling of the behaviour of an inhomogeneous cantilever. The model covers the various effects of the structure parameters such as cantilever materials, dimensions and actuator positions.

c) A literature survey of the most scanning force microscopy (SFM) cantilevers which are either V-shaped or rectangular beams. Although the behaviour of rectangular beams is presented in chapter 3, most previous works used the V-shaped in SFM. The behaviour and advantages of this kind of cantilever are modelled and discussed.

Chapter 4 presents a theoretical and experimental investigation of the optimum piezo-actuator thickness for cantilever actuation.

In Chapter 5 a full description of the electrostatic actuator behaviour is given. The relation between the exciting voltage (dc and ac) and the cantilever deflection is demonstrated theoretically and experimentally .

Chapter 6 presents the experimental investigation of the suppression of cantilever vibrations using active damping and two different detection methods (i.e.capacitance and piezoelectric film).

Chapter 7 presents a summary of the thesis and gives a number of conclusions.

1.3 References.

[1] Roy, P.K and Ganesan, N " Studies on the dynamic behaviour of a cantilever beam with varying thickness " *Journal of Sound and Vibration*, Volume **177**, No 2, 1994, pp 1-13

[2] Franks,A "Progress towards traceable nanometric surface metrology " *Nanotechnology*, Volume **4**, 1993, pp 200-205.

[3] Hansen, C.H and Pan, J " Active control of vibration in a beam", *Mechanical Engineering* , Volume **16** July 1991, pp 57-63.

[4] Meirovitch, L and Bennighof, J.K ." Model control of travelling waves in flexible structures", *Journal of Sound and Vibration*, Volume **111**, pp 131-144, 1986.

[5] Mace, B.R. " Active control of flexible vibrations", *Journal of Sound and Vibration*, Volume **114**, 1987, pp 253-270.

[6] Garratt, J.D "Survey of displacement transducers below 50mm " *Journal of Physics, E Sci, Instrum*, Volume **12**,1979, pp 563-573.

[7] Erlandsson, R , McClelland, G.M , Mate, C.M and Chiang, S " Atomic force microscopy using optical interferometery ", *Journal of Vacuum Science and Technology*, A **6** (2) , Mar/Apr (1988), pp 266-274.

[8] Umeda, N, Ishizaki, S and Uwai, H, " Scanning attractive force microscope using photothermal vibration ", *Journal of Vacuum Science and Technology*, B **9**(2), Mar/Apr 1991, pp 1318-1322.

[9] Jenkins, D.F.L, Cunningham, M.J, Clegg, W.W and Bakush, M.M, " Measurement of the modal shape of inhomogeneous cantilever using optical beam deflection", *IEE Measurement Science and Technology*, Volume **6**, No 2, 1995, pp160-166.

[10] Gregory, C " Intelligent instrumentation" 2nd edition (1981)

[11] Gardner, J.W and Hingle, H.T " Developments in Nanotechnology" Volume **1**, From Instrumentation to Nanotechnology " pp 301-317.

[12] Leiss, A.W and Sonalla, M.I , " Vibration of cantilever beams with various initial condition", *Journal of Sound and vibration*, Volume **150** (1) 1991, pp 83-89.

[13] Binnig, G and Quate, C.F, "Atomic Force Microscope", Physical Review Letters, Volume **56** (9), March 1986, pp 930-933.

[14] Martin, Y and Wickramasinghe, " Magnetic imaging by force microscopy with 1000 A° resolution" , *Applied Physical Letter*, Volume **50** (20), May 1987, pp 1455-1457.

[15] Albrecht, T.R , Akamine, S, Carver, T.E, and Quate, C.F, " Microfabrication of cantilever styli for the atomic force microscope", *Journal of Vacuum Science and Technology*, A **8**(4), July 1990, pp 3386-3396.

[16] Cleveland, J.P, Manne, S, Boeek, D and Hansma, P.K , "A nondestructive method for determing the spring constant of cantilevers for scanning force microscopy", *Review. of Scientific Instrument.*, Volume **64** (40), 1993 , pp 403-405.

[17] Chen, G.Y, Warmack, R.J, Thundat, T. and Allison, D.P, "Resonance Response Of Scanning Force Microscopy Cantilevers", *Review of Scientific Instrument*,Volume **65** (8), August 1994, pp 2532-2537.

[18] Kim, S.J and Jones, J.D " Optima design of piezoelectric for active noise and vibration control", *AIAA journal,* Volume **29**, No 12, December 1991, pp 2047-2053.

[19] Brugger, J, Blanc, N, Renaud , Ph and de Rooij, N.F " Microlever with combined integrated sensor/actuator functions for scanning force microscopy" *Sensors and Actuators A*, Volume **43** , 1990, pp 339-345

[20] Jenkins, D.F.L , Cunningham, M.J and Clegg, W.W, " Sensor and actuators for active vibration control of small cantilevers" Conference presentation: Sensors and their Application VII, Published in Sensors and their applications IOP Publishing, Dublin, Sep 1995.

Chapter 2

2. Background:

2.1 Introduction.

Flexible structures either on a large scale such as satellite receiver systems, or on a very small scale such as devices used in micro-manipulation and measurement, suffer from unwanted vibrations due to low structural internal damping of the materials used in their construction, and the lack of other forms of damping, such as viscous damping. These undesirable vibrations lead to instability and inaccurate measurement. Over the past decade, interest in the control of these vibrations in large flexible structures has increased [1-11]. On a much smaller scale, Franks [12] has shown how atomic force microscope (AFM) images can be adversely affected by induced cantilever vibrations. Recently, different actuation methods to control small structure's vibrations have been implemented [13,14] in the Electrical Engineering Division at Manchester University.

2.2 Damping types.

2.2.1 Passive damping :

This technique aims to increase the damping of a structure by using a passive element as a damper. This will dissipate the energy of vibration by increasing the

relative motion of the structure with respect to the passive element [15]. The drawbacks of this method are:

1. It requires additional masses comparable in many cases to those of the structure itself.
2. The control is not broadband and significantly alters the performance of the structure.
3. It is not easy to implement as the size of the structure becomes very small.

2.2.2 Active damping :

Although passive vibration controllers have the inherent advantage of being simpler to design, Cao *et al* [16] reported that their performance is strongly a function of the external excitation, and the passive controller parameters are generally "tuned" to what is presumed to be the most critical frequency of the external excitation. The effectiveness of these controllers deteriorates significantly because values of the external disturbance are different from the design (tuning) ones. Because of these disadvantages, investigation has turned to active vibration control.

Active control of vibration in flexible structures by means of actuators and sensors distributed about the structure has been the focus of extensive research in recent years. It has been shown by several authors [4,11,12,16] that active control methods that utilise 'intelligent' structures have several advantages over time-proven passive control techniques. The main reasons being:

- This technique is effective for various disturbances without losing too much of its intended effectiveness.
- It is easier to use in controlling vibration in a small structure or even a microstructure.
- Since the size of the active actuator is smaller compared with the structure, the additional mass due to the actuator can be neglected.
- It has the capability of producing high actuation forces.
- It has a wide frequency range of operation.

Active controllers employ force actuators to impose the required control force upon the system to be controlled. The most intuitive technique of active control is to generate a continuous control force of the same amplitude as the external disturbances but in the opposite direction. One goal of this study is to design and experimentally evaluate an active vibration control for small light structures.

2.3 Types of actuator:

In advanced precision engineering there is a need for different types of actuator. In the literature, there is a variety of actuator mechanisms that are capable of operating at the nanometre level such as piezoelectric [13-15], electrostatic [17], electromagnetic [18], magnetostriction [19], shape memory alloy [20-21] and photothermal [22,23]. These actuators have been extensively used in controlling small displacement. In the past, the proper selection of the actuator has been the focus of some effort. When specifying an actuator for applications in

nanotechnology, the decision is usually based upon the following criteria:

1. *Stiffness*- will determine both the dynamic response and the magnitude of the transmissible force.
2. *Positional accuracy* - limits repeatability and is often enhanced by implementing feedback control. This usually results in an increase in the cost of the device.
3. *Range* - at a resolution of one nanometer, the range tends to be rather restricted in terms of normal engineering applications. Costs are generally proportional to the range and accuracy ratio of a given resolution. There are often physical restrictions on the range of some of these actuators such as magnetic saturation, yield stress, etc.

To achieve near-ideal performance, continuous actuators, having minimum interaction with the structure dynamics, have been used. Sensitivity and commercial availability also present restrictions. With all this in mind, many actuators were eliminated.

In what follows, a variety of actuators that are both continuous and capable of operating at the nanometer or even sub-nanometer resolutions are reviewed. For a more detailed discussion see reference [24].

2.3.1 Piezoelectric actuators:

Of the twenty one crystal classes that do not have a centre of symmetry, twenty can experience a dimensional change upon the application of an electrical field and such a material is known as piezoelectric. This effect was discovered in 1880 by

Pierre and Jacques Curie during their systematic study of the effects of pressure on the generation of electrical charges by crystals such as quartz and zinc blend. However, the term "piezoelectricity" (pressure electricity) was first suggested by W. Hankel in 1881. Cady [25] defines piezoelectricity as " electric polarisation produced by mechanical strain in crystals belonging to certain classes, the polarisation being proportional to the strain and changing sign with it ".

Piezoelectric materials exhibit an interesting phenomenon, whereby upon mechanical strain a measurable electric polarisation (or voltage) proportional to the strain is produced. As such, piezoelectric materials have found common use in sensing devices such as accelerometers. However, piezoelectric materials also exhibit an inverse effect, whereby an applied voltage across the material induces a mechanical strain in the material and thus can be used as an actuator. Excellent introductory reviews to piezoelectric materials can be found in references [26,27].

Actuators based upon piezoelectric principles have been variously proposed [4-6,28] and much theoretical work has been done on evaluating their performance-particularly in the context of controlling the vibration of simple beams. The performance of the piezoactuator in controlling the vibration of two dimensional structures has also been considered [9,29-30], where the vibration of a thin plate has been examined.

The piezoelectric materials have been used in recent years as distributed actuators and sensors because they have the following advantages [31].

2.3.2 Advantages of piezoactuators:

1. Accuracy in the sensing and actuating function.
2. Wide frequency range of operation.
3. Inexpensive.
4. Space efficient, light weight, stiff, and come in a variety of sizes.
5. Very high speed and usually operate over a displacement range below 10 μm .
6. Sufficient amplitude range and the provision of short linear drives.
7. The distributed nature of piezoactuators can be used to provide control with minimum of a control spillover (spillover is the interaction between the reduced-order based controller and the actual infinite-order systems).
8. Compared with the frequencies of the structure vibrations, ceramic piezoactuator has a very high resonant frequency,. Therefore, the actuator's dynamic response can be ignored in the system model [11].

2.3.3 Disadvantages of piezoelectric actuators:

1. They show considerable hysteresis. The materials are not mechanically stable over long periods and their parameters are quite temperature sensitive.
2. The piezoactuators become inactive when the material is depolarised by any improper treatments (e.g. high temperature, reverse voltage.)

2.3.4 Electrostatic actuator:

This type of actuator is a non-contact force device that uses the principle that any two electrodes separated by an insulating barrier will be attracted towards one another if there is an electric potential difference between them. The magnitude of this force is given by

$$\mathbf{F} = \frac{\varepsilon \mathbf{A} \mathbf{V}^2}{2\mathbf{x}^2}$$

From this it can be seen that the force is always positive and is related to the permittivity (ε), the cross-sectional area (A), the reciprocal of the separation (x) and the square of the potential (V). Because of the very low force associated with this type of actuator, it is most commonly used for ultrasonic excitation or in microminiature devices such as submillimetre sized motors [32-33], microelectronic resonance accelerometers and also in resonant probe microscopy for the combined excitation and monitoring of small probes. Although the force characteristic is non-linear, it is nonetheless an exact relationship extending over many orders of magnitude and restricted mainly by the dielectric value of the insulating barrier. A disadvantage of this type of device is that, if air is used as the separating dielectric, then ε is known to vary with both temperature and humidity and thus for a very precise application a closely controlled environment is required. A theoretical and experimental investigation of the behaviour of this type of actuator is presented in chapter 5 of this thesis.

2.3.5 Electromagnetic actuator.

Linear characterisable actuators can be produced with an electromagnetic drive. Two types of such actuators can be designed. These, in general , involve the use of the magnetisation and demagnetisation of soft magnets. In precision electromagnetic devices, a saturated permanent magnet is surrounded by a coil with length *L*, and a force (*F)* proportional to both the strength of the magnet (B) and the coil current (I) is generated between the two. This force can be expressed as [24-34]

$$F = B.I.L$$

The electromagnetic actuation method is therefore suited for large electromagnetic applications, but in microengineering the cross-sectional area of the coils (and hence the current passed) reduces as the square of the scaling factor; there is a further linear reduction in the length of the coil, making the force produced reduce as the cube of the scaling factor. Because of this, magnetic actuation becomes quite weak on a microscale.

2.3.6 Magnetostrictive actuators.

The magnetostrictive effect is a similar dimension change as the piezoelectric under the influence of a magnetic field. This means that the displacement per unit field will increase with dimension making this favourable as a large scale or heavy duty actuator. Also the response times of this type of actuation mechanism are short.

2.3.7 Photothermal actuators.

This mechanism works on the principle that heat applied to the top of a cantilever will diffuse down through the structure to create a temperature gradient. Differential thermal expansion of the material will then introduce a mechanical moment to bend the structure. The heat may come form a resistive element or a high intensity light source. The dynamic behaviour of photothermal excitation has always been a problem. However, the need to dissipate the residual heat from the previous cycle before the next can be implemented means that operating frequencies tend to be low compared to other mechanisms [35].

2.3.8 Shape memory alloy actuators:

This family of devices require heat as the actuating mechanism. In shape memory alloy (usually Ni-Ti) the material is bent at a high temperature and then allowed to cool whereby it will return to its original shape. Actuators using this effect are capable of very large displacement for a relatively small device size. A typical example would be a deflection of 20 mm for a cantilever beam of around 100 mm in length and a drive force of 300 N/m with a time constant of approximately 4 seconds [21]. The heating is usually supplied by passing a current through the actuator. The dynamic response of this device is almost invariably very slow.

2.3.9 Summary :

In brief, the above review is summarised in the following table:

Actuator type	Advantages	Disadvantages
Piezoelectric	Wide frequency range, stiff, inexpensive, variety of sizes, low energy consumption, very high resonant frequency, high accuracy.	Non-linear law, temperature and humidity sensitive, applied field is limited.
Electrostatic	Large range to resolution ratio, force generated is small, this makes miniature actuators more favourable.	Sensitive to the permittivity of the gap separation and limited by its dielectric strength.
Electromagnetic	Linear, cheap and easy to implement with a fast dynamic response.	Interference, available range and accuracy are not easy to assess.
Magnetostriction	Gives large displacements. Output depending on the size of the device.	Exhibits considerable hysteresis
Photothermal	Large bending moment.	Dissipates heat.
Shape memory alloys	Large range actuators.	Dynamic response is slow, requires heat as the actuating mechanism, low stiffness.

Table (2-1) Advantages and disadvantages of different types of micro-actuation.

2.4 Selection of actuator:

After this analysis of the most relevant actuators that are capable of operating at the nanometre level, the piezoelectric actuator is selected for in-depth study and research because of its low cost and many other advantages listed above.

2.4.1 Selection of piezoelectric material.

A wide variety of piezoelectric materials are currently available, such as piezo-film, piezoceramics and piezoelectric bimorph elements. In the selection of the materials to be used, certain criteria had to be considered. These materials must have:

1. A high piezoelectric charge constant d_{31}, since for a large d_{31} a large strain is produced for a small voltage.
2. A high modulus of elasticity E_p. If E_p is small compared to the modulus of the substructure E_s, then only a small fraction of the strain produced in the piezoelectric will be transferred to the substructure.
3. The capability for a high field to be applied to the piezoelectric before depoling occurs, which destroys the piezoelectric properties of the material.
4. A Curie temperature (the temperature above which the piezoelectric permanently loses its piezoelectric properties) of the actuator material higher than the curing temperature of the composite structure. If this is not the case, the piezoelectric nature of the material will be destroyed during the curing process.

Work over the last twenty years [8,10,13] has shown significant piezoelectricity in polarised ceramics such as barium titanate, lead zirconate titanate (PZT) and polarised polymers PVDF. PZT is the piezoelectric material of choice for many applications because of its large piezoelectric charge constant (d_{31}) that in turn allows the actuators to output sufficiently large power. Several authors [7,36] have used the piezo-polymer PVDF, because it is convenient to use (can be cut to any shapes easily) and easy to apply. Nevertheless it has a weak actuator when compared to PZT. Therefore, PZT material is selected for work reported in this thesis.

2.4.2 Nature of piezoelectric ceramics (PZT).

Piezoelectric ceramics show different properties depending on variations in material composition and treatment during the manufacturing process. This makes optimisation for different applications possible. For actuator applications, PZT ceramics, which show high expansion efficiency, are generally used.

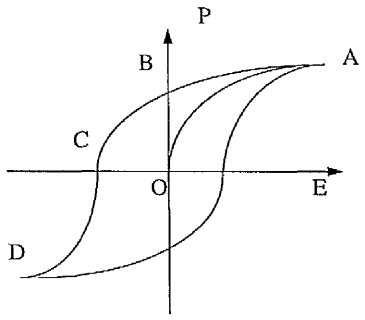

Figure (2-1). Polarisation of piezoelectric ceramics by applying an alternating electric field E.

The essential characteristics of piezoelectric ceramics are :

I. Unpolarised material (point O) is polarised by an electric field and saturation is observed for strong fields (point A).

II. After removing the electric field E, a residual polarisation is maintained (point B).

III. This remenant polarisation is removed by a compensating field called the coercive field (point C).

IV. By increasing the inverse field, polarisation changes to the opposite direction but limited by saturation (point D).

The coercive field's strength depends strongly on material composition. For common actuator materials it is in the range of one hundred to several hundred volts/mm. A consequence of hysteresis in the P-E (polarisation-field) diagram is dissipative loss which occurs during the dynamic operation of the actuators, leading to the actuators warming up.

2.4.3 Nature of polyvinylidene fluoride (PVDF):

Polyvinylidene fluoride is a polymer that can be polarised or made piezoelectrically active by melting and cooling it then stretching the film. In its polarised form, PVDF is essentially a tough, flexible piezoelectric crystal. In the nonpolarised state, PVDF is a common electric insulator. The polarisation process requires the application of a strong electric field of the order of 10 V/ μm at temperatures in the region of 100^{o} C. Electrodes are first applied to the PVDF film by vacuum evaporation on either side.

The field is applied for about 20 minutes and is then maintained while the temperature is reduced to ambient. The result is a permanent piezoelectric material. The degree of piezoelectric activity being a function of polarising voltage, temperature and time. In this polarised form, PVDF is commercially available as a thin polymeric film. Generally the film has a layer of nickel or aluminium deposited on each face to act as an electrode. For the proposes of this thesis, this material is used as an active damper.

For a uniaxially polarised film, a voltage or field applied across its faces results in a longitudinal strain. The strain occurs over the entire plated area of the film, making it a distributed parameter actuator. If the field is distributed spatially, the strain will also vary spatially. This gives the added possibility of varying the control spatially as well as with time. In summary the features of PVDF are :

- A frequency response from $\cong$ DC to GHz.
- It senses from 10^{-5} to 10^{8} N/m^2 (286 dB).
- Infrared responsivity $\geq$ 1.5 $\mu A/W$.
- Low acoustic impedance and low mechanical Q.

2.4.4 Features of the piezoelectric materials:

Compared with the frequencies of the substructural vibrations, piezoelectric materials have a very high resonant frequency. Therefore, their dynamic response can be ignored in the system model. These materials are suitable for resonators because of their high mechanical stiffness and low mechanical loss.

2.4.5 Comparison of PVDF film and PZT ceramic actuators:

While it is generally believed that the PZT ceramics are more efficient than the PVDF films for actuation, there has been little attempt to compare quantitatively the performance differences between the two types. Since the two materials have quite different material properties, a number of factors should be considered. The properties of these materials are summarised in the following table:

Actuator properties	Ceramic PZT	Polymeric PVDF
charge coefficient d_{31} 10^{-12} (m/v)	**123-200**	**23**
Young's modulus Ep (10^{10} N/m^2)	6.1	0. 2
Breakdown voltage (V/μm)	100	10000
Max tensile strength σ (MN/m^2)	45	33-55
Voltage constant g_{31} 10^{-3}	**9.1**	**216**
ρ (kg/m^3) density	7500	1780

Table (2-2) . Comparisons between ceramic PZT and polymeric film PVDF.

As can be seen from the table, the degree of piezoelectricity, PVDF has almost order of magnitude lower piezoelectric charge constant (d_{31}) than PZT, therefore, the effective moment (M) which is proportional to this constant as given by the following simple expression [31], is expected to be higher in PZT actuators. This makes PZT actuators superior over the PVDF ones.

$$M = d_{31}.w_p.E_p\ V.$$

where w_p is the PZT actuator width in m.

Figure (2.2) shows the effective bending moment as a function of the piezo-actuator thickness using the maximum allowable electric field strengths for PZT (100 V/m) in continuous use. It is clear that the bending moment of PZT actuators is an order of magnitude higher than that which is produced by PVDF films.

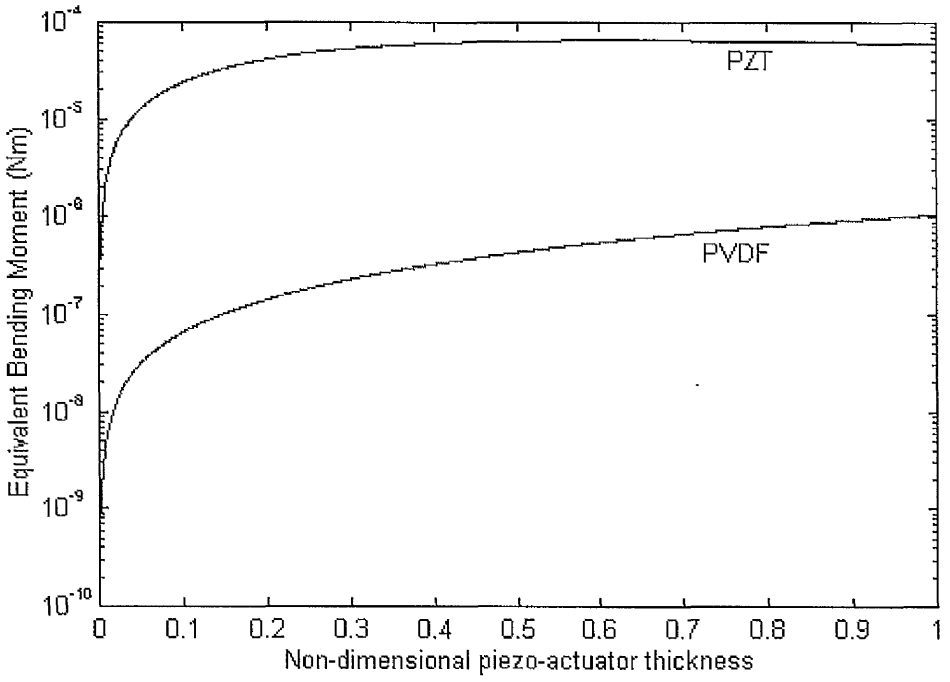

Figure (2-2) Comparison of the effective bending moment induced by PZT actuators (upper trace) and PVDF actuators (lower trace).

On the other hand, the sensor output is a function of the voltage constant g_{31} and can be written as [37]:

$$Vs = g_{31} * F/w_b$$

- Where F is applied force in Newtons.
- w_b is the cantilever width in m .

Therefore, the PVDF is more effective as a sensor than the PZT (output $\cong$ 20 times).

2.4.6 The optimum location of the actuator.

The choice of the actuator location is an important issue in the design of actively controlled structures. The actuators should be placed at locations to excite the desired modes most effectively. Previous works [5,6] indicated that piezoelectric actuators, which locally strain the substructure, should be placed in regions of high average strain and away from areas of zero strain. For maximum effectiveness authors have indicated that it is preferable to place the actuator near the fixed end where the curvature is maximum.

2.5 Choice of the Transducer.

2.5.1 General considerations:

The quantity to be measured for most instrumentation systems is nonelectrical. In order to use electrical methods and techniques for measurement, manipulation, or control, the nonelectrical quantity is converted into an electrical signal by a device called a transducer. One definition states, " a transducer is a device which, when actuated by energy in one transmission system, supplies energy in the same form or in another form to a second transmission system" [38]. This energy transmission may be electrical, mechanical, chemical, or thermal.

Many physical parameters and biological variables can be measured conveniently with the aid of this sensor. When choosing a transducer type, its inherent performance is vital. Performance is defined by a number of specifications including range, resolution, dynamic response, susceptibility to change of

environment, overall accuracy, stability and linearity. Possible choices of the sensor used for displacement measurements are listed below with typical performance data:

2.5.2 Displacement transducers:

The displacement created by the action of a force is converted into a change of some electrical parameters. The electrical methods most commonly used in the measurement of displacement are discussed below.

2.5.2.1 Strain gauges

A strain gauge is a passive transducer that converts a mechanical displacement into a change of resistance. It is a thin device that can be attached to a variety of materials to measure applied strain. Figure (2.3) shows a various forms of strain gauge [38] .The strain gauges can be classified into:

a) Metallic strain gauges formed from thin resistance wire or etched from thin sheets of metal foil. These gauges are generally small in size and can be used in high temperature applications.

b) Semiconductor strain gauges often used in high-output transducers such as load cells. These gauges have a very high sensitivity, with gauge factor (i.e. ratio of resistance change to strain = $\frac{\Delta R / R}{\Delta L / L}$) from 50 to 200, allowing measurement of small strain, for example 0.01 microstrain. They are, however, sensitive to temperature fluctuations and often behave in a non linear manner.

Since metallic gauges and semiconductor gauges are very sensitive to temperature they must be operated in a bridge circuit with reliable temperature compensation. Their extension is limited to approximately 0.3 % of their length. A typical resolution is 10 micrometers and linearity is about 1%.

The main problem in providing a good bonding between the gauge and the structure is very difficult to overcome. The adhesive material must hold the gauge firmly to the structure, yet it must have sufficient elasticity under strain without losing its adhesive properties. The adhesive should also be resistant to temperature, humidity, and other environmental conditions.

To summarise, the strain gauge is fairly economical, small in size and uses a minimum of processing electronics. But it requires matching of gauges to minimise temperature effects and general drift.

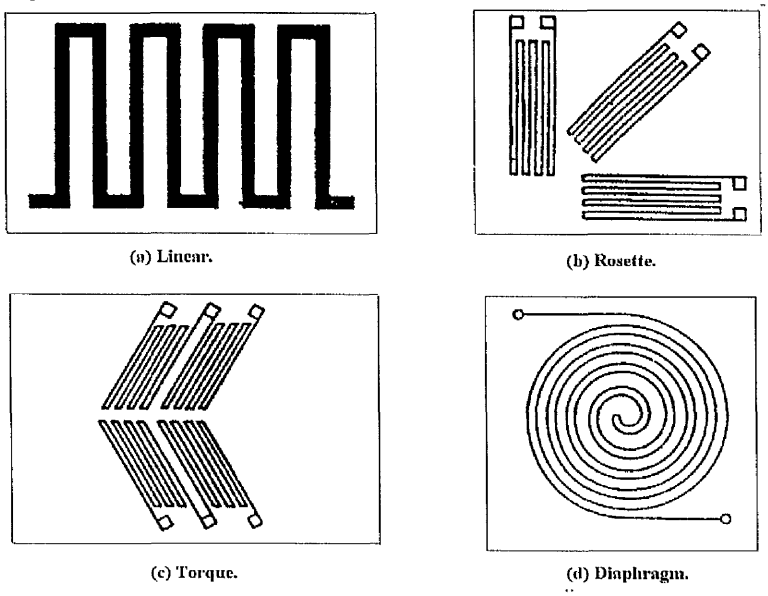

Figure (2-3). Strain gauge configurations

2.5.2.2 Optical Interferometry.

The optical interferometer has a capability to measure static deflection of the lever as well as its vibration amplitude at high frequencies with minimum of disturbance to the cantilever. In 1986 McClelland *et al* [39] and Martin *et al* [40] presented optical interferometers based on homodyne and heterodyne interferometery. These methods are based on measuring the phase shift between a reference laser beam and a measurement beam reflected from the object being moved. Long range accuracy is excellent and resolution is limited to a fraction of the wavelength of light or approximately 10 nanometres.

In the following, a brief review of four optical methods used to detect the deflection of a cantilever is given. An extensive study of these methods is given in reference [41].

2.5.2.2.1 Homodyne detection system:

The basic homodyne detection system [42] is shown schematically in figure (2.4). A laser beam passes through a beam splitter (BS), an optical flat and finally is incident on a cantilever on which the force-sensing tip is mounted. The laser beam reflects back to the same beam splitter through the optical flat and deflects into a photodetector that generates a photocurrent used to image the force acting on the tip. In a differential homodyne detection system, the laser beam is split into two components. One is diverted by a beam splitter to a first photodetector and serves as a reference signal. The other passes through the beam splitter, optical flat, reflects back from the cantilever, and deflects into a second photodiode. The difference

between the two photodetector currents yields a signal that represents the cantilever deflection. A drawback of the homodyne technique is that the signal depends on the optical pathlength which can drift because of thermal or mechanical instabilities.

To summarise, the homodyne technique can be made to operate in the differential mode thus eliminating part of the laser noise.

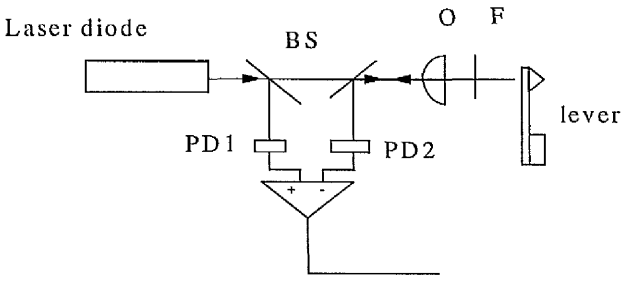

Figure (2-4). A schematic diagram of the homodyne detection system showing, the beam splitter (BS), a lens (O), the optical flat (F), and the photodetector PD.

2.5.2.2.2 Heterodyne detection system:

The heterodyne detection system is described by Martin *et al* [40] and Sarid [41]. This system is shown schematically in figure (2.5). The laser beam divides into two components. One passes through an acoustic-optic modulator (AO) that shifts

the laser beam frequency by $\Delta\omega$, a beam splitter, a quarter-wave plate, and finally, a microscope objective which focuses it onto the cantilever end. The incident laser beam reflects back through the microscope objective and the quarter-wave plate. The polarising beam splitter then deflects the laser beam through an analyser that adjusts the power of the beam incident on the photodetector. The other laser beam component reflects onto a mirror as a reference beam. The reference laser beam deflects by a second mirror, passes through the beam splitter, analyser and is incident on the same photodetector. The interference between the reference and signal beams, generates a photocurrent that represents the force acting on the tip. The unique feature of the heterodyne detection system is that it is independent of optical pathlength drifts. The drawback of the heterodyne system is that it cannot operate in the direct-current (dc) mode.

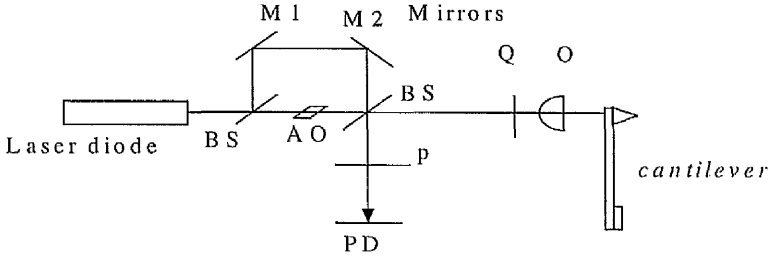

Figure (2-5) The heterodyne detection system, showing beam splitter (BS), acoustic-optic modulator (AO), quarter-wave plate (Q), focusing lens (O), the polariser (P), the photodetector (PD).

2.5.2.2.3 Polarisation detection system

The polarisation detection system given in figure (2.6) [43,44], differs from the other optical detection systems in that the amplitude of vibration of the cantilever is first converted into a polarisation modulation that is subsequently converted into amplitude modulation. The conversion from polarisation to amplitude modulation is carried out by two polarising prisms rotated 45° relative to each other. The output from the differential system, has a high common -mode rejection which cancels most of the laser noise. A full description to the function of this system is given by Sarid [41].

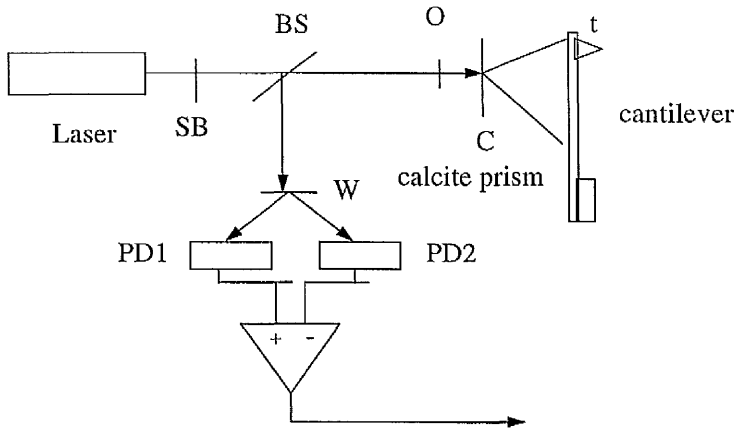

Figure (2-6). The polarisation detection system.

2.5.2.3 Optical beam deflection:

The method of optical beam deflection is currently used in atomic and magnetic force microscopy [43,44] to measure the displacement of the cantilever tip as it scans across the sample under investigation. Optical beam deflection has been extensively applied in photothermal deflection spectroscopy [45] where photothermal induced variations in the refractive index of a gas (or liquid) cause a non-invasive 'probe' laser beam to be deviated from its original path.

Recently, in 1994 Fujisawa *et al* [46] have investigated experimentally the difference between the forces measured by an atomic force microscope (AFM) with an optical lever deflection method and with an optical interferometer method. They demonstrated that the optical deflection method can detect not only the surface corrugation but also the frictional force, while the optical interferometer method detects only the surface corrugation.

In an optical beam deflection system shown in figure (2.7), a collimated laser beam is focused on the cantilever and is reflected back into two closely spaced photodetectors whose photocurrents are fed into a differential amplifier. A minute deflection of the cantilever causes one photodetector to collect more light than the other and the output of the differential amplifier is proportional to the deflection of the cantilever.

2.5.2.3.1 Advantages of the optical beam deflection:

Optical beam deflection is suitable for the measurement of the cantilever vibration because:

- It is experimentally simple.
- It permits a high degree of spatial resolution along the cantilever (limited by the wavelength of the laser beam).
- It is non-intrusive.
- Its resolution is very high, better than 0.1 nm.

At the present time an extensive work in the Electrical Engineering Division at Manchester University is progressing using optical beam deflection method towards achieving a practical system that will detect and control unwanted vibrations of the microscale cantilevers (e.g. 200 μm x18 μm x 0.6 μm) used in scanning force microscopy.

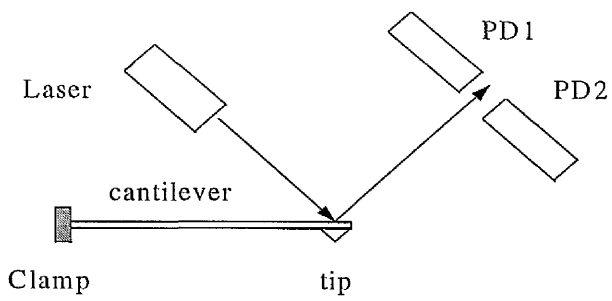

Figure (2-7). A schematic diagram of the optical beam deflection.

2.5.2.4 Capacitive detection method:

2.5.2.4.1 General considerations.

Capacitance sensors are widely employed in many measurement systems in both laboratory and industrial activities. They measure different physical quantities such as displacement, force, pressure, and density. They are particularly useful in applications where dynamic measurements are needed involving a measurement of a capacitance variation with a resolution of 10^{-4} to 10^{-5}. Although the first apparatus using a change in electrical capacitance to measure a small displacement appears to be that of Valley (1910), it was Whiddington's 'ultramicrometer' (1920) which led to widespread interest in the method. Since then there has been continuous development.

A capacitor consists of two conducting metal plates separated by an insulator. When a voltage is applied to the metal plates, equal and opposite electric charges appear on the plates. The ratio of that charge to the voltage is the capacitance. The capacitance of a parallel-plate capacitor is proportional to the area A of the plates and inversely proportional to their separation d,

$$C = \varepsilon_0 \varepsilon_r A/d$$

where ε_0 is the permittivity of free space with a value of 8.854×10^{-12} F/m.

Thus capacitance is a function of geometrical configuration and permittivity. Variation in the area A or separation d requires physical connection to the moving part, while permittivity ε_r variation does not. Transducers which depend on the area of overlap give a change in the capacitance that varies linearly with the displacement.

These devices are suitable for the measurement of large displacements. On the other hand, those devices which depend on a change in the distance, *d*, give a change in capacitance which is inversely proportional to the displacement and are used for the measurement of small displacements [47]. In the simple arrangement with two parallel plates capacitance variation between the plates is hyperbolic and is only useable over a small range of displacement. The sensitivity $\Delta C/\Delta d$ in this case is inversely proportional to d^2, and so the smaller the separation *d* the greater the sensitivity, but a practical limit is set by the voltage breakdown of the air in the gap. A capacitance transducer used to measure the displacement by varying either the area between the plates, or the plate separation or position of the dielectric is shown in figure (2.8).

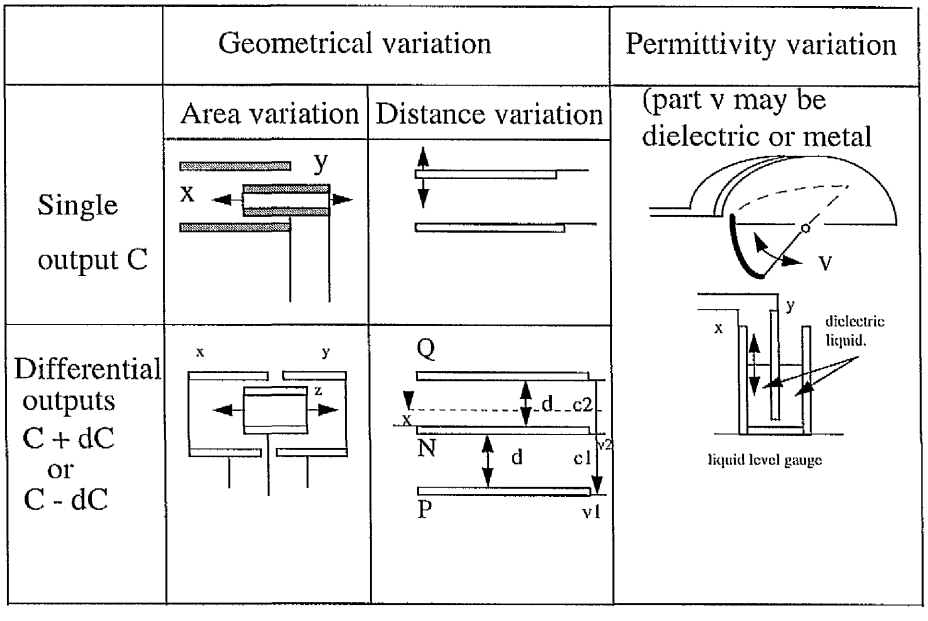

Figure (2-8) Capacitance displacement transducers [47].

2.5.2.4.2 Advantage of capacitor sensor.

In an analysis of various capacitive transducers Hugill [48] and Garratt [49] gave comparisons of capacitive sensors with other displacement transducer. In comparison with strain gauges, capacitor sensor systems are much more sensitive and less temperature dependent. The characteristics of a capacitive sensor depend only on its planar geometry, while resistive strain gauges depend on the thickness of the wire forming the resistor and the specific resistance of the material used. For the sensing of bending elements, the capacitor sensors have the advantage of being used contactless and can be installed in places where they do not disturb bending. Resistive strain gauges, on the other hand, have to be integrated into places where the bending has its maximum. In the capacitor sensors there is no need for local trimming, while with resistive strain gauges, not only the resistive bridge balance has to be made, but also the resistors have to be trimmed for thermal compensation.

In comparison with laser interferometric systems, much smaller displacement can be measured with a capacitive sensor system, sometimes much less than a nanometre (0.01 nm) as demonstrated by Jones [50]. The interferometeric systems tend to have thermal instabilities due to a variety of optical components used and can be bulky and expensive due to the coherent light source and precision optics used.

In comparison with inductance measurement techniques, capacitor geometries are typically planar structures while inductive systems are essentially three dimensional.

Therefore capacitor sensors can easily vary in size from a few to even several centimetres. Such a change in dimension is more difficult for inductive sensor . Also the frequency range that can be used for inductive sensors is much smaller than for capacitive sensor systems. Capacitive sensors are most suitable in applications requiring high levels of accuracy, stability, discrimination and low power dissipation and excitation forces. Also these transducers have excellent frequency response and can measure both static and dynamic phenomena. Their disadvantages are sensitivity to temperature variations and possibility of erratic or distorted signals due to long lead length. Based on these behaviours the capacitor transducer has been designed in this thesis to control the displacement vibration.

2.5.2.4.3 The capacitor transducer configuration:

In this thesis, a three nearly equally spaced parallel plates differential arrangement as given in figure 2.10 is employed. The outer two (P,Q) being at a fixed distance apart, d cm, from the moveable plate N. A displacement of the middle plate N causes one of the two capacitances so formed, C1 to increase and the other, C2, to decrease. If the N plate is moved by a distance x centimetre towards plate P, the capacitances C1 and C2 can be calculated as [48].

$$C_1 = \varepsilon_o \varepsilon_r \frac{A}{d + x}$$

$$C_2 = \varepsilon_o \varepsilon_r \frac{A}{d - x}$$

If voltage V is applied across PQ, the difference in the voltages ΔV across the two capacitors can be expressed as

$$\Delta V = V_1 - V_2 = V\left[\frac{C_2}{C_1 + C_2} - \frac{C_1}{C_1 + C_2}\right] = V\frac{x}{d}$$

This differential method has been used for accurate measurement of displacement between 10^{-8} mm and 10 mm with accuracy of 0.1% [47] . Theoretical studies [47-51] indicate that the range is equal to twice the gap distance, i.e. $x = \pm d$ and resolution is very high. But in reality values are limited by noise, humidity, temperature and stray capacitance (given below) in parallel with the transducer's output. Also, these factors cause both nonlinearity and a reduction in sensitivity.

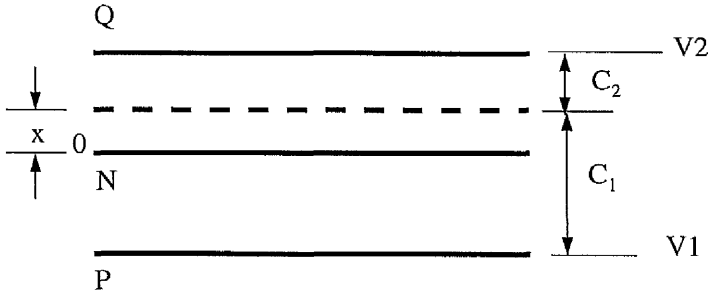

Figure (2-9) Capacitance displacement transducer.

The above arrangement has the following advantages:

a) doubled output,

b) reduced nonlinearity,

c) greatly increased transducer stability,

d) reduced excitation forces.

e) C_1 and C_2 have nearly the same response to environmental changes when they form the variable arms of a bridge circuit.

2.5.2.5 Stray capacitance:

In most capacitance applications, problems arise from the presence of parasitic capacitors that can be greater than the mean value of the sensor capacitance. This is due to the shield used to minimise noise interference and to the unavoidable variations both of the mean value of the sensor capacitance and of the parasitic capacitances due to environmental effects such as temperature, humidity, and geometric variations not related to the physical quantity being measured. Also because conductors in the neighbourhood of the plates are not set to definite potentials (i.e. are left electrically floating), they can have a large effect on any capacitance measurement, and it is essential to connect them to common terminals which will most conveniently be earthed. Each plate of the transducer now has a capacitance to earth which may be much larger than the transducer. The effects due to the parasitic capacitances can be avoided by measuring the change of capacitance following a, b, c and d steps

a) electronic circuit should be insensitive to capacitance to earth,

b) the complete transducer should be mounted on a rigid metal enclosure,

c) the flexible leads to the plate must be arranged with care,

d) environmental effects (i.e. humidity, and temperature) must be carefully considered.

2.5.2.6 Techniques for measurement of capacitance:

A wide variety of capacitance measuring circuits suitable for industrial measurement of capacitance in the range 0.1 to 10 pF have been reported in the literature [48]. In 1980, Kanno [51] arranged industrial capacitance measuring circuits into four main categories:

1) resonance method,

2) oscillation methods,

3) charge/discharge method

4) AC bridge methods

The measurement circuits should have the required measurement frequency range, low baseline drift , high, stable sensitivity , and be insensitive to stray capacitances to achieve high accuracy and a good signal-to-noise ratio .

2.5.2.6.1 The resonance method.

This method is capable of measuring both the unknown capacitance and its parallel loss element over a wide frequency range from a few hundred kHz to several hundred MHz. This circuit is shown in figure 2.10.

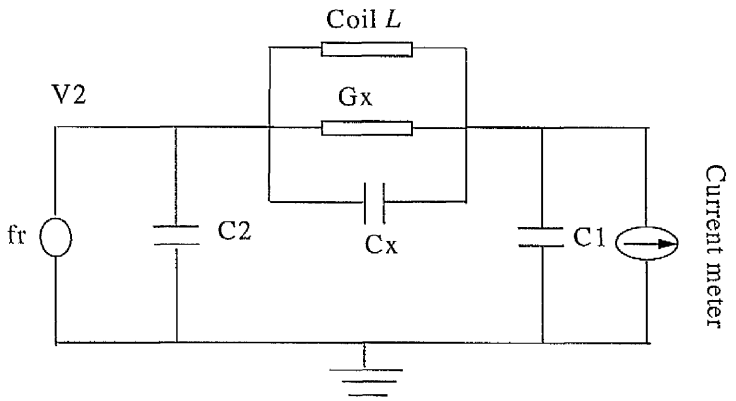

Figure (2-10) The resonance method [51].

The sine wave source provides an excitation voltage V_1 to an LCG parallel circuit consisting of a known inductance *L*, the electrode capacitance C_x and loss G_x . The circuit is tuned to resonance by adjusting the source frequency to f_r, and then the unknown capacitance C_x can be determined from:

$$(2\pi.f_r)^2 L.(C_X + C_1 + C_2) = 1.$$

The conductance of the parallel loss element G_x is given by :

$$G_x = \frac{I_x}{V_1}.$$

where I_x is the current measured by the detector when the circuit is at resonance.

Measurements using the resonance method requires several operating steps such as

- adjusting the resonance frequency,
- detecting the resonance conditions,
- calculating the unknown capacitance and loss.

The first two steps are often done manually and therefore this method is not suitable for the continuous monitoring of a physical variable. Hence currently it is not used in on-line capacitance transducers.

2.5.2.6.2 The oscillating methods:

In this method, the oscillation frequency of an LC or RC oscillator depends on the unknown capacitance C_x. The frequency is measured, either by using a digital counter to obtain a digital output or by using a frequency-to-voltage converter to obtain analogue output, and then used to determine the unknown capacitance.

a) The RC oscillation method.

The RC oscillation method is perhaps the most popular method used in general purpose capacitance meters. The circuit types include multivibrator, various timers and phase-locked loops.

Generally these circuits suffer from some common drawbacks -poor immunity to strays, oscillation frequency influenced by the shunting conductance of C_x, poor sensitivity to small capacitance changes and poor frequency stability. Therefore, the RC oscillation method is generally not suitable for applications requiring a measurement resolution of better than 0,01 pF.

b) The LC oscillation method.

This method can provide measurement frequencies ranging from several hundred kHz to a few hundred MHz [52]. Figure 2.11 (a) shows the principle of a typical LC oscillator transducer. The change in the oscillation frequency can be expressed as

$$\Delta f = \frac{f_o}{2(C_s + C_x)} \Delta C_x$$

where C_s is the overall energy stray capacitance in parallel with C_x and f_o is the standing oscillation frequency.

A design suitable for steady-state measurement has been described by Floyed *et al* [53], and uses a reference oscillator (figure 2.11 (b)). The difference between the two oscillation frequencies is obtained from the output of a frequency mixer. This low-frequency signal can be measured using a digital counter or a frequency-to-voltage converter (FVC) .

The oscillation frequency of the LC oscillator is not very sensitive to a loss component parallel with C_x. This and its capability to produce a high oscillation frequency make this method useful for applications concerning the measurement of high loss materials. The main disadvantage of this method is the stray capacitance C_s is included in the measurement.

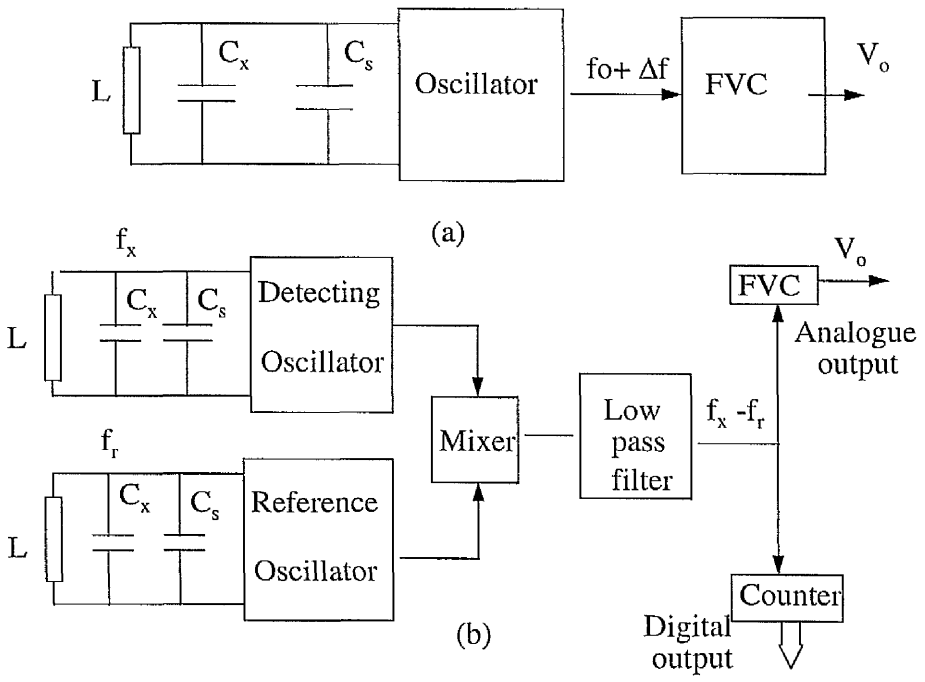

Figure (2-11). The LC oscillation method. [51].
(a) Normal method. (b) The balanced method.

2.5.2.6.3 The charge-discharge method:

A typical example of this method is the charge transfer device shown in figure (2.12) developed by Fielden and described in a patent assigned to the company Endress and Hauser Ltd [54].

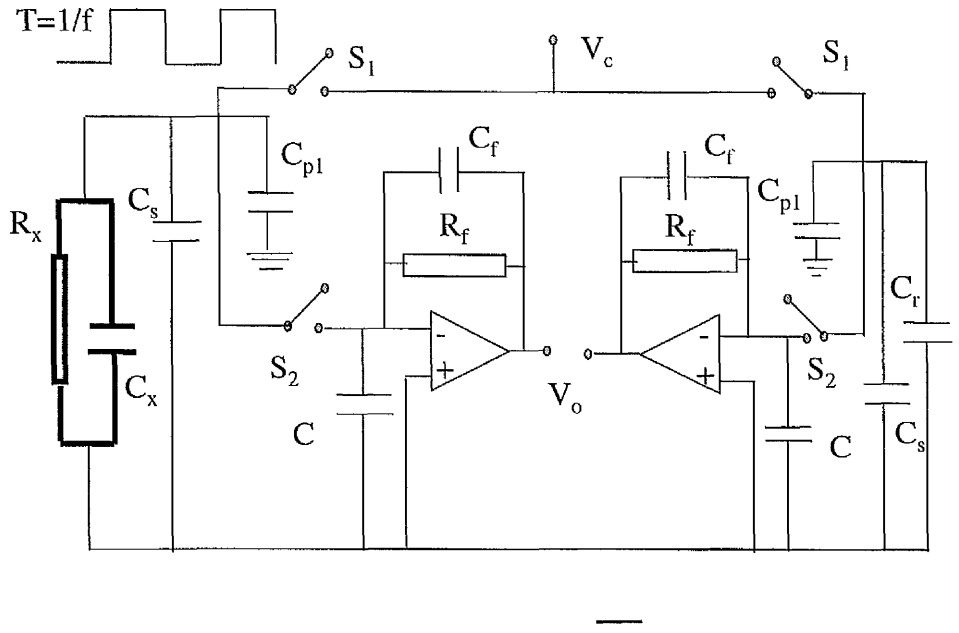

Figure (2-12). The charge transfer device.

The operation of this transducer consists of charging the unknown capacitance C_x to voltage V_c via a CMOS switch S_1, then discharging it into the detector via a second switch S_2. The charge transferred from C_x to the detector in single charging/discharging cycle is

$$Q = V_c C_x$$

The charging and discharging operations are repeated at a frequency f, under the control of a clock. This method has several advantages;

- The charge detector is a current integrator amplifier, and by choosing large values for C and $R_f C_f$, the output of the detector is dependent only upon the DC

component of the discharge current pulses. This enables a good measurement accuracy to be maintained even at high switching frequencies up to several MHz.

- Its differential circuit structure reduces the drifts caused by the common inputs to both halves of the system, such as the variation in f, V, etc. This results in a low baseline drift due to changes in ambient temperatures. However, this transducer is not a stray-immune type.
- The measurement of the unknown capacitance is almost unaffected by any parallel loss component provided that the 'On' resistance of the switches are small compared with the loss resistance, R_x, and the 'turn-on' and 'turn off' time of the switches are shorter compared with the time constant $C_x R_x$.

2.5.2.6.4 The AC bridge method:

a) General form of the AC bridge:

The Ac bridge method has a long history of development including the Schering bridge in the 1920s and various automatic ratio-arm bridges in the 1980s. It is still recognised as the most accurate and stable method for capacitance measurement (Heerens) [55-56]. The basic principle and design methods of Ac bridge techniques have been described in detail by Hague and Foord [57].

The general form of the Ac bridge consists of four bridge arms, a source of excitation, and a null detector. The power source supplies an ac voltage to the bridge at the desired frequency. For measurement at low frequencies, the powerline may

serve as the source of excitation. At higher frequencies, an oscillator generally supplies the excitation voltage. The null detector must respond to ac unbalance currents or voltages. A basic bridge circuit is illustrated in figure (2.13) and is similar in principle to the d.c. Wheatstone bridge.

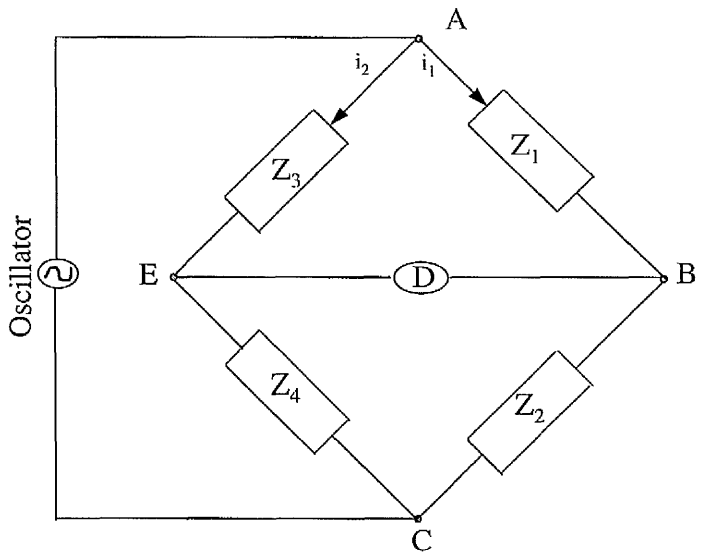

Figure (2-13). The basic a.c bridge circuit.

b) Conditions for bridge balance:

The general equation for bridge balance is obtained by using complex notation for the impedances of the bridge circuit. The condition for bridge balance requires that the potential difference between E to B (in figure 2.13) be zero. This will be the case when the voltage drop from B to A equals the voltage drop from E to A in both magnitude and phase. In complex notation, i.e. the two conditions for bridge balance

$$|Z_1||Z_4| = |Z_2||Z_3|$$

$$\angle\Phi_1 + \angle\Phi_4 = \angle\Phi_2 + \angle\Phi_3$$

the products of the magnitudes of the opposite arms must be equal and the sum of the phase angles of the opposite arms must be equal. To satisfy both balance conditions, the bridge must contain two variable elements in its configuration. Any two of the available four elements could be chosen..

2.5.2.7 **Piezoelectric detection:**

In recent years, piezoelectric materials have been used very effectively as distributed actuators and sensors in the vibration control of large structures. This is due to their accuracy as transducers, being inexpensive, having a high output and fairly simple processing electronics. Disadvantages are the non-linear law, the high operating force, temperature and humidity-sensitive and requiring a high-impedance-matching interface.

2.5.2.8 Summary:

The main advantages and disadvantages of different detection systems are given below.

Transducer	Advantages	Disadvantages
Strain gauge.	Adaptable to conveniently sensing displacements in more than one axis .Minimum of processing electronics. Fairly economical, small size.	Requires matching of gauges to minimise temperature effects and general drift. Requires adhesion and positioning on mechanical coupling.
Interferometric system.	Digital output. Extremely high accuracy, high resolution. Resolution independent of range.	Thermal instabilities due to variety of optical components used. Expensive due to coherent light source and precision optics used.
Optical beam deflection.	Extremely sensitive. Resolution better than 0.1 nm. Experimentally simple.Wavelength independent large magnification, and it is differential.	Thermal and mechanical drift. Laser noise.
Capacitive detection.	Easy mechanical design, allowing choice of electrode materials to give high stability and low temperature coefficients. High resolution possible. Small size. Large range.	Stray capacitance, shielding being required. Accuracy affected by dielectric changes between electrodes. Non-linear law.
Piezoelectric	High output. High upper frequency. Fairly simple processing electronics. Variety of size. Inexpensive. High resolution.	Non-linear law. High operating force. Temperature-and humidity sensitive. Requires high impedance matching interface.

Table (2-3) Advantages and disadvantages of different types of transducers.

2.5.2.9 Selection of transducer.

Based on the previous analysis of the possible transducers which have good accuracy, the following three sensors are selected:

- The optical beam deflection.
- Piezo-electric sensor.
- Capacitive sensors.

The first two systems are selected because

1. They are experimentally simple.
2. They have very high accuracy and high resolution.
3. Space efficient and inexpensive.

The capacitance transducer is selected due to

1. Its high accuracy and high sensitivity.
2. Less temperature dependent.
3. Inexpensive.
4. Easy mechanical design.

At the same time, interferometric detection methods are under consideration by different research groups in the Electrical Engineering Division at Manchester University for sensing the vibration of microstructure cantilevers used in scanning force microscopy (SFM).

2.6 Review of the previous investigations.

In 1987, Crawley and de Luis [4] developed a rigorous analysis of the piezoactuator/substructure coupling for a one-dimensional structure (beam). In this analysis, several important assumptions were made including linear strain across the beam thickness, uniform strain across the piezoactuator and a shear stress carrying viscoelastic bonding layer for the surface bending configuration of the piezoactuator . The surface shear stresses of the beam/bonding layer interfacing surfaces were obtained from a static analysis of the beam and showed that the shear stresses become uniform along the piezoactuator length when the bonding layer becomes infinitely thin. It was also shown that stiffer piezoactuators provide higher bending moments. Uniform strain across the piezoactuator implies that the piezoactuator will not bend.

Baz And Poh [5] investigated the effects of piezoelectric actuators and bending layers on elastic and inertial properties of composite flexible beams. They drew similar conclusions and in addition stated the effects of actuator's location.

The prototype experiment by Bailey and Hubbard [7] utilised a uniform layer of the piezoelectric material bonded to one face of a cantilevered beam. They implemented a control strategy using simple constant gain method and showed that vibrational modes of the beam could be controlled based upon the measurement of the velocity at the beam's tip.

In 1989, Dimitriadis and Fuller [30] extended the application of piezoactuators to the plate vibration control problem. Under the assumptions of zero bonding layer thickness (perfect bonding) and linear strain variation across the combined structure thickness, a relationship for the effective bending moments exerted on the plate by the piezoactuators was derived. It was shown that the effect of the piezoactuator is equivalent to a constant edge moment around the boundaries of the patch. This work is an important contribution from the perspective that the potential use of piezoactuators was proven for the two dimensional plate vibration problem.

Kim and Jones [58] presented a significant study on the effective bending moment induced by twin, rectangular shaped piezoactuators bonded to the upper and lower surfaces of a thin flat plate. They showed that, for commercially available piezoactuators and bonding materials, there exists an optimal thickness of the piezoactuator that maximises the bending moments under a constant applied electric field. It was also demonstrated that the optimal thickness for commercial piezoactuators is approximately a half-plate thickness for a steel substructure and approaches a quarter of the thickness of the plate for an aluminium substructure. An increase in the Young's modulus of the piezoactuators reduces the optimal thickness of the actuators and gives larger bending moments.

In 1992, Dosch *et al* [59] successfully developed a new technique by means of which a single piece of piezoelectric material can sense and actuate simultaneously in a closed loop system. This self-sensing actuator has a number of desirable properties not easily achieved with a separate piezoelectric sensor and actuator. One property is

that the self-sensing actuator is truly collocated. Another desirable property is the elimination of possible closed loop control problems arising from the capacitive coupling between the sensor and the actuator elements.

The above review is a small proportion of the work available in the literature. The researchers are interested in the control of the vibration of very large scale structures such as an aerospace station. The control of vibration of small structures and even microstructures is one of the main interests of the author's research group. In this thesis the application of previous techniques used for large scale structures is investigated for more small size structures (fraction of mm dimensions) to demonstrate the feasibility of using these techniques to suppress vibration at such levels of dimension or even for microstructure size structures.

2.7 References.

[1] Hansen, C.H and Pan, J " Active control of vibration in a beam", ME Volume **16** July 1991, pp 57-63.

[2] Meirovitch, L and Bennighof, J.K ." Model control of travelling waves in flexible structures", *Journal of Sound and Vibration*, Volume **111**, 1986, pp 131-144.

[3] Mace, B.R. "Active control of flexible vibrations", *Journal of Sound and Vibration*, Volume **114**, 1987, pp 253-270.

[4] Crawley, E.F and De Luis, J " Use of piezoelectric actuators as elements of intelligent structures" *AIAA Journal* , Volume **25**, No 10, Oct 1987, pp 1373-1384.

[5] Baz, A and Poh, S " Performance of active control systems with piezoelectric actuators" *Journal of Sound and Vibration*, Volume **126**, No 2, 1988, pp 327-343.

[6] Baz, A " Static deflection control of flexible beams by piezo-electric actuators" NASA report .1993, NASA contract 30429-D , pp 1-42

[7] Bailey, T and Hubbard, J.E " Distributed piezoelectric- polymer active vibration control of a cantilever beam", *Journal.Guidance*, Volume **8**, No 5, 1985, p 605-611.

[8] Varadan, V.K , Hong, S,Y and Varadan, V.V, " Piezoelectric sensors and actuators for active vibration damping using digital control." *Ultrasonic symposium* ,1990, pp 1211-1215.

[9] Irons, J and Kennedy, W "Active vibration control of a centrally clamped disc by means of a piezoelectric polymer", Report in the division of dynamics & control, University of Strathclyde Glasgow, 1989.

[10] Burdess, J.S and Fawcett, J.N " An experimental evaluation of a piezoelectric actuator for the control of vibration in a cantilever beam." *Journal of systems and control Engineering* , 1992, Volume **206**, pp 99-107.

[11] Cox , D.E and Lindner, D.K " Active control for vibration suppression in a flexible beam using a model domain optical fibre sensor " *Journal of vibration and acoustics*, Volume **113**, July 1991, pp 368-381.

[12] Franks, A " Progress towards traceable nanometric surface metrology " *Nanotechnology* , Volume **4**, 1993, pp 200-205.

[13] Cunningham, M.J , Jenkins, D.F.L , Clegg, W.W and Bakush, M.M " Active vibration control and actuation of a small cantilever for applications in scanning probe instruments" *Sensor and Actuators A(50),* 1995, pp 147-150.

[14] Jenkins, D.F.L, Cunningham, M.J and Clegg, W.W " The use of composite piezoelectric thick films for actuation and control of miniature cantilevers" *Microelectronic Engineering,* Volume 29, 1995, pp 71-74.

[15] Azvine, B , Wynne, R.J and Tomlinson, G.R " Active damping for the control of flexible structures" *Conference publication No 389* , March 1994, p 1296.

[16] Cao, S and Semercigil, S.E, " A semi-active controller for excessive transient vibrations of light structures " *Journal of Sound and Vibration*, Volume **178**, No 2, 1994, p 145.

[17] Jenkins, D.F.L , Cunningham, M.J and Clegg, W.W, " Sensor and actuators for active vibration control of small cantilevers" Conference presentation: Sensors and their application VII, Published in " *Sensors and their applications*" IOP Publishing, Dublin, Sept 1995.

[18] Smith, S.T, and Chetwynd, D.G, " An optimised magnet-coil force actuator and its application to linear spring mechanisms", *Proc, Inst, Mech.Eng*, 1990, **204** (C4), pp 243-253.

[19] Clark, A.E, Teter, J.P, and McMasters, O,D " Magnetostriction "jumps" in twinned $Tb_{0.3}$ $Dy_{0.7}$ $Fe_{1.9}$ " *Journal. Appl. Phys.*, **63**(8),1988, pp 3910-3912.

[20] Schetky, L.M. " Shape memory alloys " Scientific American, 1979, p 74.
Golestaneh, A. A. " Shape-memory Phenomena " *Physics Today*, 1984, **37** (4), pp 62-70.

[21] Kuribayashi, K, " Millimeter-sized joint actuator using a shape memory alloy", *Sensors and Actuators*, 1989, Volume **20**, pp 57-64.

[22] Flynn, A.M, Tavrow, L.S, Bart, S.F and Brooks, R.A " Piezoelectric micromotors for microrobots " *Proc. 1990 IEEE Ultrasonics Symp.* (Honolulu, Hawaii), p 1163.

[23] Moroney, R.M, White, R.M and Howe, R.T, " Ultrasonic micromotors Proc", *IEEE Ultrasonics Symp*, 1989, (Montreal, Canada), p 749.

[24] Gardner, J.W and Hingle, H.T " Developments in Nanotechnology " Volume **1**, *From Instrumentation to Nanotechnology* " pp 301-317.

[25] Cady, W " Piezoelectricity' McGraw-Hill, New York, 1964.

[26] Jaffe, H and Berlincourt, D.A., " Piezoelectric transducer materials " Proc. IEEE, 1965, **53**(10), pp 1372-1386.

[27] Buchanan, R.C "Ceramic materials for electronics".

[28] Crawley, E.F and Anderson, E.H " Detailed models of piezoceramic actuation of beams", *Journal of intelligent material system and structure*, Volume **1**, January 1990, pp 4-25.

[29] Dimitriadis, E.K ,and Fuller, C.R, "Piezoelectric actuators for noise and vibration control of thin plates," *12th ASME conference on Mechanical vibration and noise*, Montreal, 1989.

[30] Dimitriadis, E.K, Fuller, C.R and Rogers, C.A " Piezoelectric actuators for distributed vibration excitation of thin plates" *journal of vibration and acoustics*,Volume **113**, January 1991, pp 100-107.

[31] Hong, S.Y , Varadan, V.V. and Varadan, V.K " Comparison of analog and digital strategies for automatic vibration control of lightweight space structures " Structures sensing and control, SPIE Volume **1489**, 1991, pp 75-83.

[32] Fan, L.,Tai, Y. and Muller, R. S. " IC-processed electrostatic micromotors", *Sensors and Actuators*,1989, Volume **20**, pp 41-47.

[33] Tai, Y. and Muller, R. S. " IC-processed electrostatic micromotors", *Sensors and Actuators*,1989, Volume **20**, pp 49-55.

[34] Hadfield, D, " Permanent Magnets and Magnetism" London: J. Wiley and Sons, Chapters 2, 6 and 7, 1962.

[35] Wood, D, Burdess, J.S and Harris, A, J " Actuators and their mechanisms in microengineering" *IEE digest no: 96/110* , 1996.

[36] Burke, E. S, and Hubbard, J.E, " Distributed actuator control design for flexible beams " *Automatica*, 1988, **24**(5), pp 619-627.

[37] Morgan-Matroc limited " Piezoelectric Ceramics" Vernitron Division , Thornhill Southampton SO9 5QF ,U.K.

[38] Cooper, W.D " Electronic instrumentation and measurement techniques " 2nd edition , Prentice-Hall, Inc. Englewood Cliffs, New Jersey , 1978.

[39] McClelland, G.M, Erlandsson, R, and Chiang, S, " Review of progress in Quantitative Nondestructive Evaluation ", edited by D.O. Thompson and D.E Chimenti (Plenum, New York), 1987, Volume **6B**, p 307.

[40] Martin, Y, Williams, C.C and Wickramasinghe, H. K, " Atomic force microscope-force mapping and profiling on a sub 100-A° scale," *Journal Applied physics*, 1987, Volume **61**, pp 4723-4729.

[41] Sarid, D, " Scanning force microscopy with applications to electric, magnetic and atomic forces." Oxford University Press, New York, 1994.

[42] Sarid, D, Iams, D, Weissenberger, V and Bell, L.S, " Compact scanning force microscope using a laser diode," *Optical letter*, 1988, Volume **13**, p 1057.

[43] Alexander, S et al " An atomic -resolution atomic-force microscope implemented using an optical lever ", *Journal Applied physics*, 1989, Volume **65** , pp 164-167.

[44] Hipp, M. Bielefeldt, H. Colchero, J. Marti, O, and Mlynek, J , " A standalone scanning force and friction microscope," *Ultramicroscopy* **42-44**, 1992, p 1498.

[45] Jackson, W.B, Amer, N.M, Boccara, A.C, and Fournier, D, " Photothermal deflection specroscopy and detection" *Applied optical*, 1981, Volume **20**, pp 1333-1344.

[46] Fujisawa, S, Ohta, M, Konishi, T, Sugawara, Y and Morita, S, " Differnce between the forces measured by an optical lever deflection and by an optical interferometer in an atomic force microscope" *Review Scintific Instrumentation*, 1994, **65**(3), pp 644-647.

[47] Jones, B.E, " Instrumentation measurement and feedback" McGraw-Hill U.K.

[48] Hugill, A.L "Displacement transducers based on reactive sensors in transformer ratio bridge circuits" *J.Phys,E ; SCI ,Instrum*, Volume 15, 1982, pp 597--605.

[49] Garratt, J.D " Survey of displacement transducers below 50 mm", *Journal Physics E .Scintific Instrumentation*, 1979, Volume **12**, p 563-573.

[50] Jones, R.V and Richards, J.C.S " The design and some applications of sensitive capacitance micrometers", *Journal Physics E .Scintific Instrumentation*, 1973, Volume **6**, pp 589-600.

[51] Kanno M "Measurement and applications of small capacitance " *Oyo Buturi* (Japan) Volume **49** ,pt 9, 1980, pp 905-912 .

[52] Harrop,P.J " Dielectrics" London : Butterworths, 1972.

[53] Floyed, R.E , Mcdermott, L.F and Smith, H.C, 1985, IBM Tech. Disclosure Bull, Volume **27**, pp 5449-5450.

[54] Endress and Hauser Ltd 1984 " On a capacitance comparator measuring circuit" Patent 84087.

[55] Heerens, W.C " Multi-terminal capacitor sensors" *Journal. of Scientific Instruments . J of physics, E,* Volume **15**, 1982, p 137.

[56] Heerens, W.C " Microelectric sensor technology" *Journal Physics E .Scintific Instrumentation*, Volume **19** p 897.

[57] Hague, B and Foord, T.R " Alternating Current Bridge Methods" London: Pitman 1971.

[58] Kim , S.J and Jones, J.D " Optimisation of piezo-actuator/ substructure coupling for active noise and vibration control " *Sensor and Actuators*, pp78-91.

[59] Dosch, J.J and Inman, D.J, " A self-sensing piezoelectric actuator for collocated control ", *Journal of intellgent material system and structure*, 1992, Volume **3**, pp 166-185.

Chapter 3

3. Theoretical work.

3.1 Introduction:

Scanning force microscopes (SFM) are a new class of high resolution imaging instruments. They have proved to be powerful tools for the investigation of surfaces in air, liquid, and ultrahigh vacuum environments. The SFM operates by sensing the interaction force acting between a specimen surface and a very sharp tip mounted on a small highly compliant cantilever. The forces may be of an interatomic , magnetic or electrostatic nature and are in the Nano-Newton range causing a small deflection of the cantilever. By monitoring the cantilever deflection by one of the detection methods mentioned in the previous chapter, and scanning the specimen in a raster-fashion under the tip, it is possible to build up a high resolution map of the surface features of interest.

The design of a scanning force microscopic system requires an understanding of the behaviour of its components such as force-sensing cantilevers, to obtain the desired performance and to appreciate the main design problems. A crucial component for the SFM is a flexible cantilever and its force-sensing tip, whose

dynamic properties (i.e. resonance frequency, spring constant, and modal shape) determine the sensitivity and resolution of the scanning force microscope. Therefore, these properties must be investigated to understand their behaviour. One practical problem associated with SFMs is unwanted vibrations of the cantilever which has a great effect on the resolution of the SFM instrument. The purpose of this chapter is to review and model the behaviour of scanning force microscope cantilevers. This chapter is organised as follows:

Section 3.2 treats the mechanical properties of cantilever's design specifications.

Section 3.3 presents the active vibration control system.

Section 3.4 discusses the model's results as compared with experimental results.

Section 3.5 presents an analytical model which describes the modal shapes of inhomogeneous cantilevers.

Section 3.6 deals with the characteristic of V-shaped cantilevers.

3.2 Properties of cantilevers.

In 1989 Albrecht *et al* [1] carried out an investigation of the microfabrication of cantilever styli used in the scanning force microscope. They reported that the cantilever styli used in the SFM may be rectangular V-shaped and they should meet the following criteria:

3.2.1 Low force constant.

When the scanning force microscope is operated in non-contacting modes with attractive forces, the lower limit for the force constant is chosen to prevent

instabilties which would allow the cantilever to snap into contact with the sample surface. In the contacting mode, the cantilever is chosen to be stiff enough to reduce the mechanical vibration of the cantilever. Since the frequency and mass of vibration of a typical atom are $\omega \cong 10^{13}$ rad /s and $m = 10^{-25}$ kg respectively, the atom equivalent spring constant is $k = \omega^2 m = 10$ N/m. The spring constant of an SFM cantilever should therefore be smaller than 10 N/m to avoid damaging the surface of the sample [2]. The spring constant (k) of a rectangular cantilever can be determined by:

$$\kappa = \frac{E_b . w_b . t_b^3}{4 . L^4} \qquad (3.1)$$

where E_b is the cantilever Young's modulus, wb, tb and L are the cantilever width, thickness and length respectively.

3.2.2 High resonant frequency.

The imaging rate, in scanning force microscopy is limited by the mechanical resonant frequency of the cantilever. To achieve a best imaging, SFM cantilevers should have resonant frequencies > 10 kHz to avoid excitation by ambient noise and allow sufficiently high scan rates. The resonance frequency of the rectangular cantilever can be expressed as [3]

$$f = \frac{1}{2 . \pi} \cdot \sqrt{\frac{k}{m^*}} \qquad (3.2)$$

where m* is the effective cantilever mass.

3.2.3 High mechanical factor QF.

The mechnical factor QF of the cantilever should have a high value. High Q-values are needed for a stable oscillation. The resonance curve detection methods (i.e. FM and AM detection) are sensitive modulation techniques for measuring small force gradients. The sensitivity of these methods is mainly determined by the mechanical quality factor QF. The higher the quality factor, the sharper the resonant peak, and thus the higher the sensitivity. In the AM and FM mode the minimum detectable force gradient F'_{min} is given by

$$F'_{min} = \sqrt{\frac{4.k.k_B.T.B}{\omega_o.QF.\langle A^2 \rangle}}$$

where k_B is the Boltzmann constant, T is temperature, B is measurement bandwidth, ω_o resonant frequency of the cantilever and $\langle A^2 \rangle$ is the mean-square cantilever deflection amplitude.

To maximise the sensitivity of the system the minimum detectable force gradient has to be minimised. Increasing the QF factor decreases the force gradient and increases the system sensitivity.

3.2.4 High lateral stiffness.

High lateral stiffness in the cantilever is desirable to reduce the effects of lateral forces in the SFM. For example, when the SFM is operated in a contact profiling

mode, frictional forces can cause appreciable lateral bending of the cantilever. Choosing an appropriate geometry for the shape of the cantilever can yield substantial lateral stiffness.

3.3 Active vibration control.

3.3.1 Introduction.

The deflection of very small cantilevers typical of 100 μm long is at the heart of SFM instruments. These instruments are extremely sensitive to building and air borne vibrations and great care is required to isolate the instruments from these sources, such as by the use of a passive damping like a massive air bearing table. Nevertheless, mechanical vibration of the cantilever limits the resolution of the instruments. Therefore, to improve the resolution and control these unwanted cantilever vibrations, it is interesting to investigate the use of active vibration control. In principle this method is very simple and can be divided into three parts; actuation, sensor and feedback mechanism

3.3.2 Modelling inhomogenous cantilevers.

3.3.2.1 Structural configurations.

The simplest possible configuration is shown in figure (3.1). It is composed from a simple cantilever beam partially covered by single piezoelectric elements. The piezoelement is placed near the root where the stress is maximum.

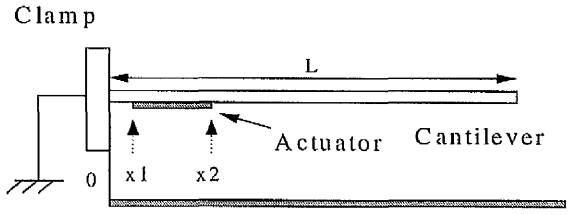

Figure (3-1) The cantilever and actuator configuration.

3.3.2.2 Theoretical considerations.

The problem is analysed using the Energy method assuming series approach. It is assumed that the transverse displacement y(x,t) of the cantilever can be written as the product of two functions, one depending only on x and the other depending only on t to be [4,5]

$$y(x,t) = \sum_{j=1}^{n} q_j(t).\Phi_j(x) = \underline{\Phi}^T.\underline{q} \qquad (3.3)$$

where $\underline{\mathbf{q}}$ is vector of unknown coefficent, Φ is known assumed shape function and can be expressed for clamped-free cantilever as

$$\Phi_j(x) = \zeta_j \sin\left(\frac{\lambda_j x}{L}\right) - \cos\left(\frac{\lambda_j x}{L}\right) - \zeta_j \sinh\left(\frac{\lambda_j x}{L}\right) + \cosh\left(\frac{\lambda_j x}{L}\right) \qquad (3.4)$$

where ζ_j and λ_j are constants and tabulated in textbooks as given in reference [6]

The stress-strain relationship for cantilever and piezoelectric layer excited by applied voltage (V) is given as [7].

$$\sigma_b = E_b . \varepsilon_b \tag{3.5 a}$$

$$\sigma_p = E_p\left(\varepsilon_p - \mu . V\right) = E_p . \varepsilon \tag{3.5 b}$$

$$\varepsilon = \varepsilon_p - \mu V \tag{3.5 c}$$

where $\mu = d_{31} / t_p$.

In the case of undamped cantilever, the equation of motion is developed using Lagrange's equations [4]

$$-\frac{\partial T}{\partial q_j} + \frac{d}{dt}\left(\frac{\partial T}{\partial \dot{q}_j}\right) + \frac{\partial U}{\partial q_j} = 0 \tag{3.6}$$

where **T** is kinetic energy and **U** is potential energy.

In the case of free vibration

$$\frac{\partial T}{\partial q_j} = 0.$$

The general equation of motion can be expressed in a matrix form as

$$[m]\ddot{q}(t) + [k]q(t) = F \tag{3.7}$$

Therefore the resonance frequency can be calculated by

$$f_j = \frac{1}{2\pi}\sqrt{\frac{k}{m}}$$

where [m] , [k] are mass and stiffness matrices and F is modal force vector due to excitation of the piezoelectric element.

The equation (3.7) can be derived by following the next steps:

Firstly the kinetic energy T is given as [5]

$$T = \frac{1}{2}\int m.\dot{y}^2(x,t)dx \tag{3.8}$$

$$T = T_b \text{ (cantilever)} + T_p \text{ (piezoelectric)}$$

$$T = \frac{1}{2}\int_0^L m_b\dot{y}^2(x,t)dx + 2*\frac{1}{2}\int_{x1}^{x2} m_p\dot{y}^2(x,t)dx \tag{3.9}$$

Differentiating (3.3) gives

$$\dot{y}(x,t) = \sum_{j=1}^{n}\dot{q}_j(t).\Phi_j(x) = \underline{\Phi}^T.\underline{\dot{q}}$$

$$\dot{y}^2(x,t) = (\underline{\Phi}^T.\underline{\dot{q}})^2 = \underline{\Phi}\ \underline{\Phi}^T\underline{\dot{q}}^2 \tag{3.10}$$

Substituting equation (3.10) into equation (3.9) yields

$$T = [\frac{1}{2}\int_0^L m_b\underline{\Phi}\underline{\Phi}^T dx + \int_{x1}^{x2} m_p\underline{\Phi}\underline{\Phi}^T dx]\underline{\dot{q}}^2 \tag{3.11}$$

where m_b and m_p are cantilever and piezoelectric element masses respectively, x_1 and x_2 are defined in figure (3.1). $\underline{\Phi}^T$ is the transpose of the shape function.

Secondly the strain energy expression is defined by [4],

$$U = \int \sigma.\varepsilon.A.dx$$

$$U = U_b + U_p \tag{3.12}$$

1. For the cantilever:

$$U_b = \frac{1}{2}\int_0^L E_b I_b y''^2 dx$$

$$U_b = \frac{1}{2}\cdot\int_0^L E_b I_b \underline{\Phi''\Phi''^T}\underline{q}^2 dx \qquad (3.13)$$

and

$$I_b = \frac{w_b . t_b^3}{12}$$

where w_b and t_b are the cantilever width and thickness respectively.

2. For the piezoelectric element:

Using the appropriate stress-strain relationships (i.e. equations (3.5), (3.12)), it follows that :

$$U_p = \int_{x1}^{x2} E_p A_p \varepsilon^2 dx = \int_{x1}^{x2} E_p A_p \left(\varepsilon_p - \mu V\right)^2 dx$$

$$U_p = \int_{x1}^{x2} E_p A_p \left(\varepsilon^2{}_p - 2\varepsilon_p \mu V + \mu^2 V^2\right) dx \qquad (3.14)$$

Consider the section of the cantilever between x1 and x2. If a point P on the neutral axis of the composite structure is deflected by an amount y, then from simple bending theory , the axial strain developed by the piezoelectric element in the cantilever is given by [8]

$$\varepsilon_p \approx \frac{\partial^2 y}{\partial x^2} \qquad (3.15)$$

Substituting equation (3.15) into equation (3.14) yields

$$U_p = \int_{x1}^{x2} A_p E_p \underline{\Phi''\Phi''^T} dx \underline{q}^2 - 2\int_{x1}^{x2} A_p E_p \underline{\Phi''^T} \mu V dx \underline{q} + \int_{x1}^{x2} A_p E_p \mu^2 V^2 dx \tag{3.16}$$

Substituting equations (3.16), (3.13), (3.12) and (3.11) into Lagrange's equation (3.6) yields

$$\left[m_b \int_0^L \underline{\Phi\Phi}^T dx + 2m_p \int_{x1}^{x2} \underline{\Phi\Phi}^T dx \right].[\ddot{\underline{q}}] + \left[E_b I_b \int_0^L \underline{\Phi''\Phi''^T} dx + 2A_p E_p \int_{x1}^{x2} \underline{\Phi''\Phi''^T} dx \right].[\underline{q}]$$

$$= \left[2A_p E_p \int_{x1}^{x2} \mu V \underline{\Phi''} dx \right] = \left[2A_p E_p \mu V \left(\Phi'(x2) - \Phi'(x1) \right) \right] \tag{3.17}$$

Comparing equation (3.17) with equation (3.7) yields

$$[m] = \left[m_b \int_0^L \underline{\Phi\Phi}^T dx + 2m_p \int_{x1}^{x2} \underline{\Phi\Phi}^T dx \right]$$

$$[k] = \left[E_b I_b \int_0^L \underline{\Phi''\Phi''^T} dx + 2A_p E_p \int_{x1}^{x2} \underline{\Phi''\Phi''^T} dx \right]$$

$$F = \left[2A_p E_p \int_{x1}^{x2} \mu V \underline{\Phi''} dx \right] = \left[2A_p E_p \mu V \left(\Phi'(x2) - \Phi'(x1) \right) \right]$$

In [Appendix A] a Matlab routine to analyse the above model is given.

3.3.3 Modelling the detection method :

The sensor based on the piezoelectric element bonded to the cantilever can be modelled. The governing equations for the voltage generated from the piezo-element positioned over the region x1 to x2 (see figure 3.2) can be represented as follows:

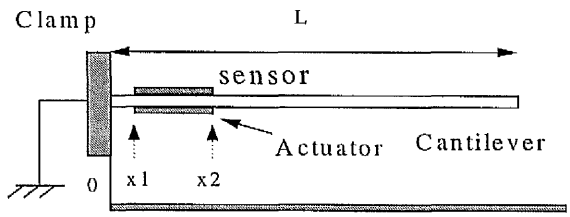

Figure (3-2) Sensor and actuator configuration.

The governing equation of the piezoelectric element is given by [9]

$$D = d_{31}.E_p.\varepsilon_p \qquad (3.18)$$

where D is the charge per unit area.

The total charge generated is [10]

$$Q = \int D.\, dA = C.\, V_s \qquad (3.19)$$

Substituting equation (3.18) into equation (3.19), the sensor ouput can be defined as

$$V_s = \frac{d_{31}.\ E_p}{C} \int_{surface} \varepsilon_p.\ dA \tag{3.20}$$

where C is the piezoelectric capacitance

$$C = \frac{\varepsilon^T_{33}}{t_p}.A \tag{3.21}$$

where ε^T_{33} is the permittivity of the piezoelectric material and t_p is the piezoelectric element thickness.

The piezoelectric charge constant (d_{31}) and piezoelectric voltage constant (g_{31}) are related by [8]

$$d_{31} = g_{31}.\ \varepsilon^T_{33} \tag{3.22}$$

Substituting equations (3.21) and equation (3.22) into equation (3.20) yields

$$V_s = \frac{g_{31}.\ E_p.\ t_p}{w_p.\ (x2 - x1)} \int_{x1}^{x2} \varepsilon_p.\ dA \tag{3.23}$$

Substituting equations (3.3) and (3.15) into equation (3.23) and integrating over the sensor length yields

$$V_s = \frac{g_{31}.\ E_p.\ t_p}{w_p.\ (x2 - x1)} * [\Phi'(x2) - \Phi'(x1)].\ \underline{q} \tag{3.24}$$

3.3.4 Feedback mechanism.

The control system is to damp the free vibrations of the first two modes (higher than the second mode may give rise to instability - spillover) of the cantilever using the close loop feedback strategy. A number of feedback strategies have been proposed for active vibration control. These range from simple techniques such as constant gain or variable gain feedback [11] to control algorithms using neural networks [12]. In this thesis constant gain feedback is modelled. Active vibration control is applied to the cantilever by feeding back a suitably amplified sensor signal (Vs) to the piezoelement (actuator) throughout the electronics circuit with gain (G).

Therefore, the feedback voltage can be given as

$$Vfb = G * Vs \tag{3.25}$$

A schematic diagram of the control system is shown in figure (3.3). The overall control flow chart is given in figure (3.4)

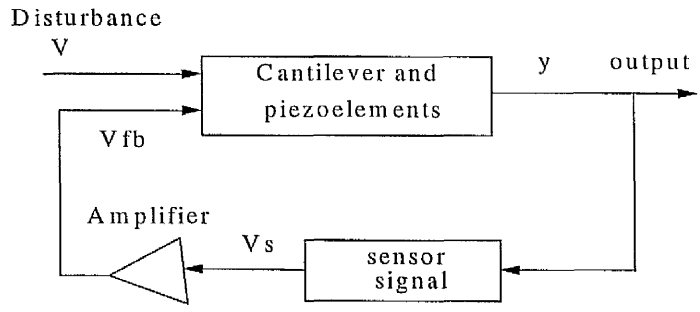

Figure (3-3) Feedback control scheme.

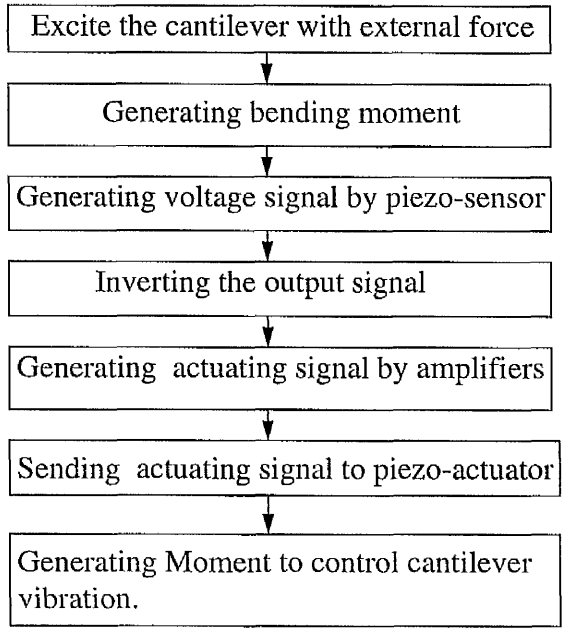

Figure (3-4) Control system flow chart.

3.4 Discussion.

In performing the calculation, the following physical properties of cantilever and properties of piezoelectric material shown in tables (3.1) and table (3.2) were used.

	Cantilevers		
Material	Corning-7 glass	Steel	Aluminium
Length (L) mm	23.5	60	500
Width (w) mm	2	40	40
Thickness (tb) mm	0.5	1.5	1.5
Density (ρ) kg/m^3	7800	7860	2700
Young's modulus N/m^2	8.1E+10	20.7E+10	7.1E+10

Table (3-1) Properties of the cantilevers used.

	Piezoelectric materials	
Material	PZT Ceramics	PVDF Films
Length (L) mm	≅ 2	1-20
Width (w) mm	≅ 0.5	0.1 -0.5
Thickness (tp) mm	≅ 0. 2	28 - 110 μm
Density (ρ) kg/m^3	7700	1780
Young's modulus N/m^2	6.29E+10	2 E+9
piezoactuator edges mm	x1 =0.5 x2=2.5	10 70
Charge constant d_{31} m/V	- 160 E-12	22 E-12

Table (3-2) Properties of piezoelectric materials.

3.4.1 Comparisons with experimental results.

The results of the above model are confirmed by comparing them with measured data published in literature [8,13] and shown in figures (3.5) -- (3.7) for different cantilevers and actuator materials.

Figure (3.5) shows the predicted first four modal frequencies of glass cantilever with one piezoelement bonded on its face near the clamp side. See table (3.3) for frequency values.

Figure (3.6) shows the experimental results for the same conditions as in figure (3.5). These data were supplied by the research group in the Electrical Engineering Division, Manchester University [13]. It is clearly seen that the agreement between the experimental data and predicted values is very good.

Figure (3.7) predicts the same modal frequencies for an aluminium cantilever with dimensions given in table (3.1). A comparison between predicted values and experimental ones is given in table (3.4). Again close agreement with experimental data were obtained.

	Frequency	
Mode Number	Theoretical (kHz)	Experimental (kHz)
1	0.690	0.694
2	4.3	4.2
3	12.2	11.5
4	23.8	21.7

Table (3-3) A comparison of predicted model with experimental frequencies (reference 13) for a glass cantilever.

	Frequency	
Mode Number	Theoretical (Hz)	Experimental (Hz)
1	23	20
2	138	140

Table (3-4) A comparison of predicted model with experimental frequencies (reference 8) for aluminium cantilever.

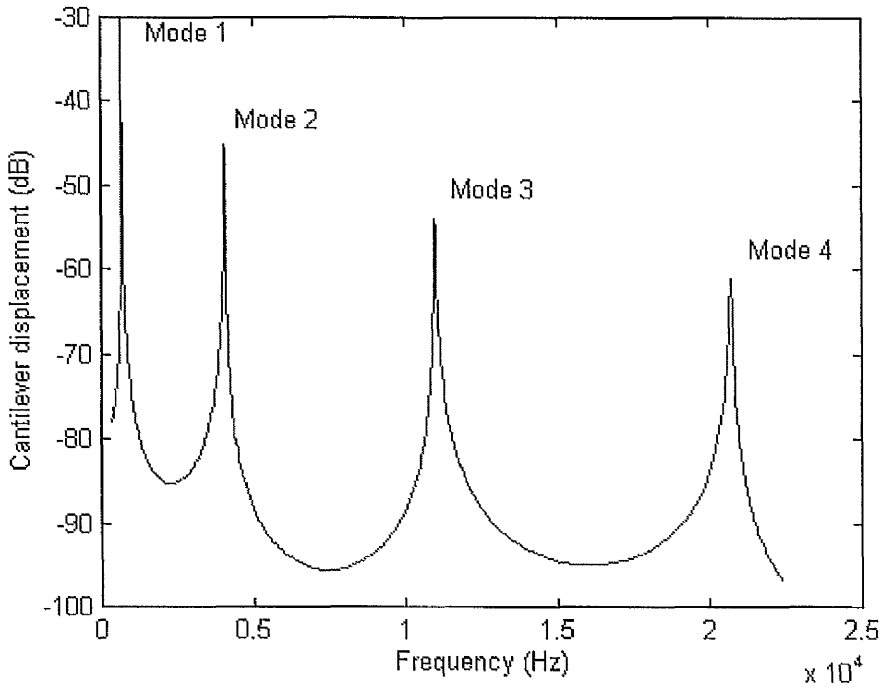

Figure (3-5) Spectrum showing the predicted bending modes for glass cantilever.

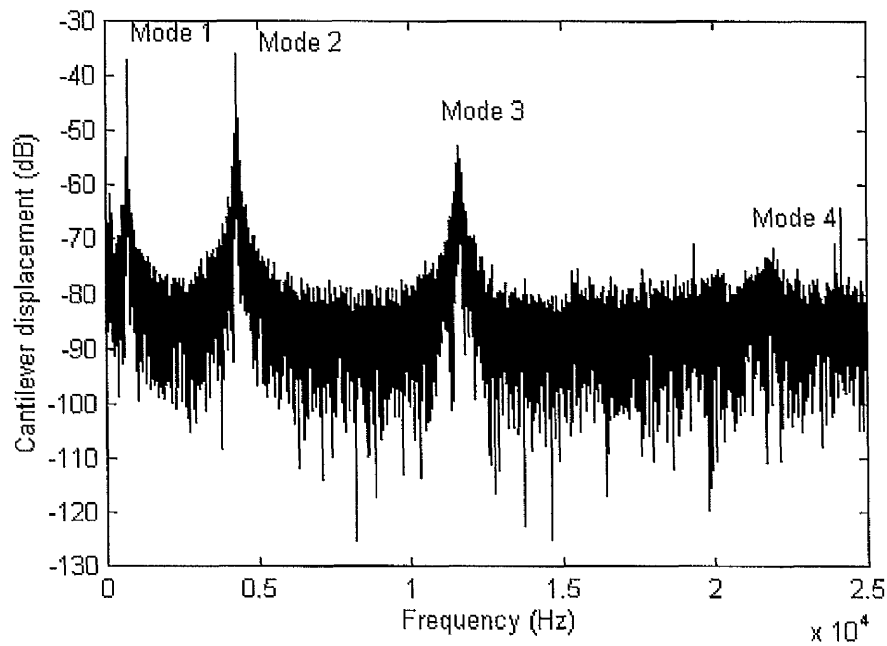

Figure (3-6) Spectrum showing the measured cantilever modes [13].

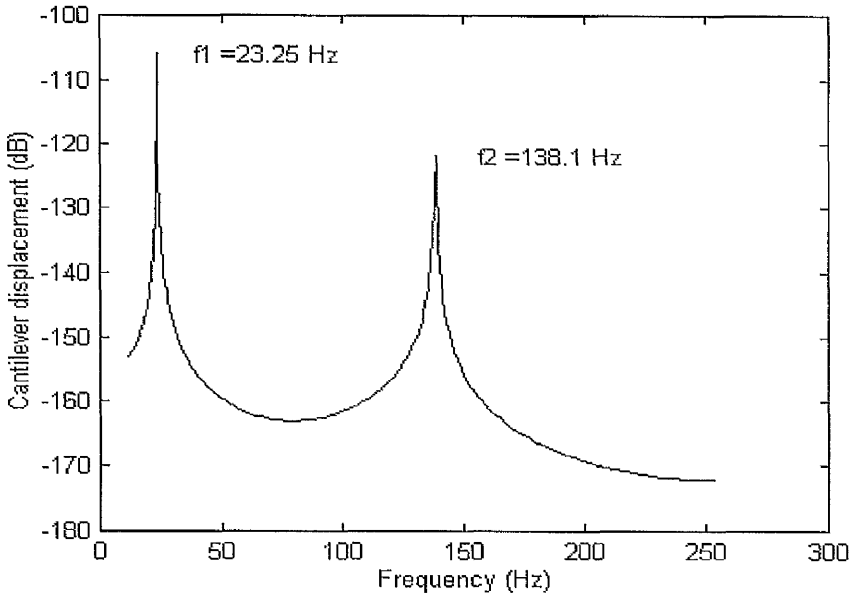

Figure (3-7) A spectrum showing the aluminium cantilever bending modes.

Figure (3.8) illustrates the first four mode shapes as predicted by the model (the three dimensional modal shapes are given in appendix C for the first three modes). As can be seen from this figure the first two modes have higher amplitudes than other modes. Therefore these two modes are more important when the vibration control strategy is undertaken.

In brief, from these figures, the theoretical values are very close to the experimental data. The difference between the measured data and calculated values is probably due to sample variations and the uncertainty about dimensions of the structures and the values of various parameters.

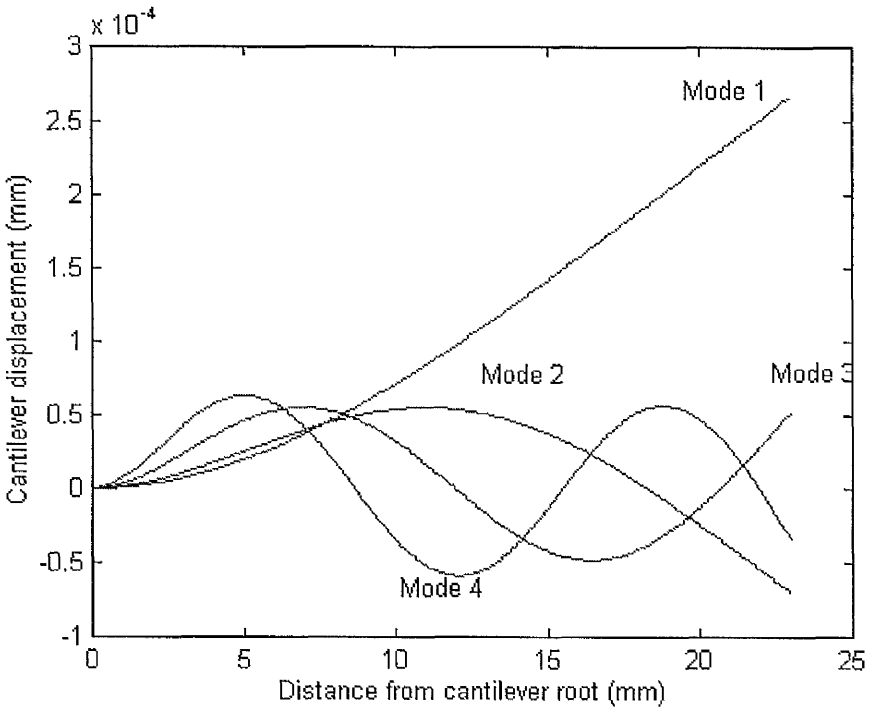

Figure (3-8) Predicted model shapes for the first four bending modes of a cantilever.

The sensitivity of modal frequencies with the various parameters is demonstrated by figures (3.9) and (3.10). The configuration and parameters in figure (3.7) are used.

Figure (3.9) describes the effects of changing the cantilever thickness. As can be seen from this figure the cantilever frequencies are proportional to cantilever thickness. An increase in the cantilever thickness increases the mode frequency but decreases the mode amplitude .

Figure (3.10) illustrates the effects of piezoactuator thickness. Again the composite structure frequencies were increased as the piezoactuator thickness increased. The effects of piezoactuator thickness is discussed in detail in the chapter 4.

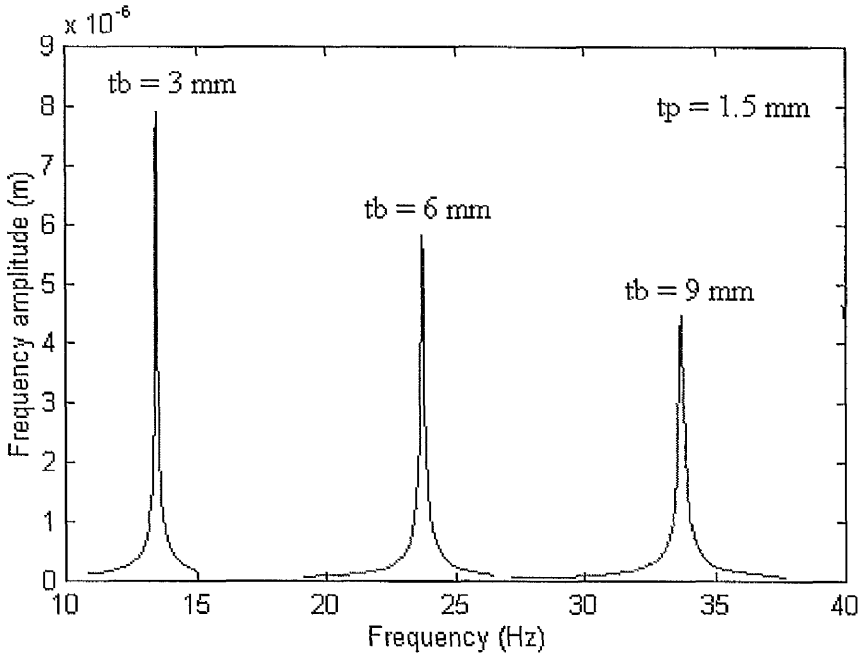

Figure (3-9) The effect of changing the cantilever thickness.

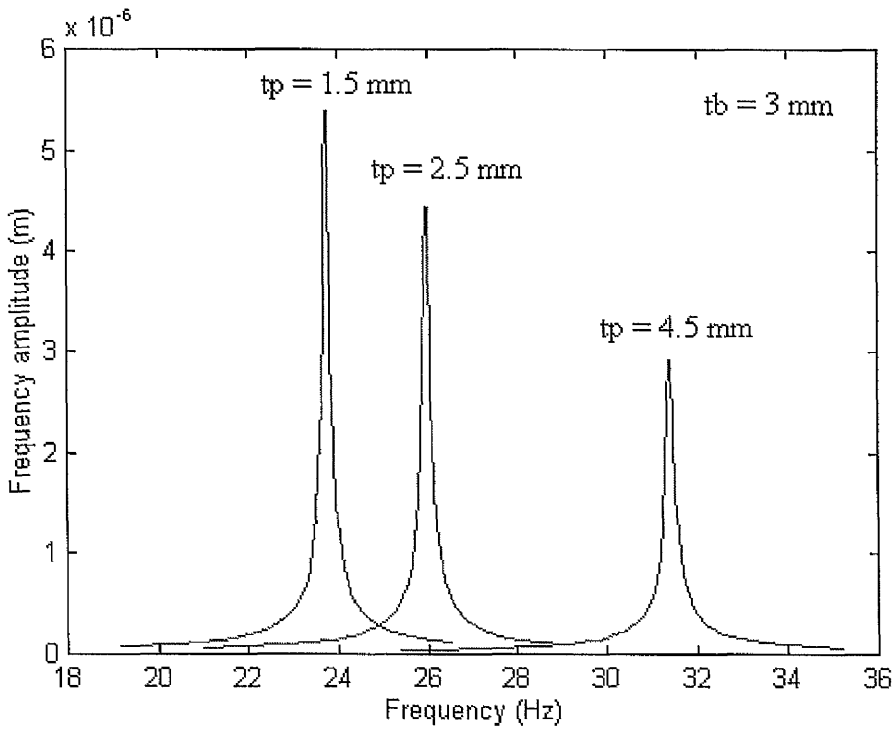

Figure (3-10) The effect of changing the piezoactuator thickness.

Figures (3.11) and (3.12) show free and controlled vibrations of the first two modes of the aluminium cantilever using feedback control system. Although, when the gain is increased, the vibration became progressively more damped. It was found experimentally [8] that the gain of the feedback signal must not be increased much beyond 70 dB of the last stage amplifier gain, because the system became unstable. Also, the gain had be set so that the maximum voltage amplitude would not exceed the voltage breakdown limit of the piezoactuator.

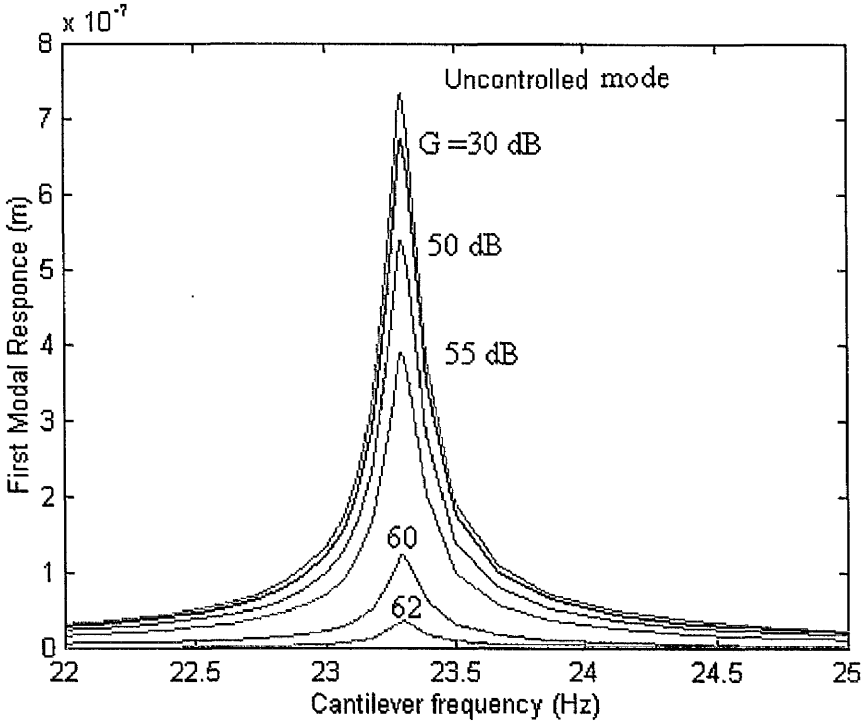

Figure (3-11) Open loop and closed loop response (First mode).

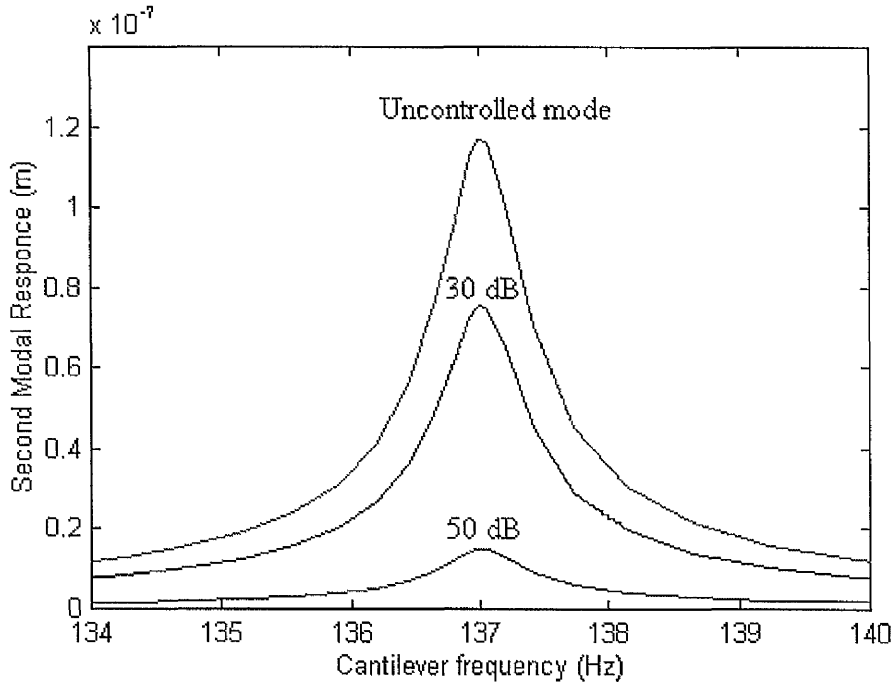

Figure (3-12) Open loop and closed loop response (Second mode).

3.4.2 Summary

In this chapter, a detailed model which characterises the dynamic behaviour of inhomogeneous structure based on Energy method is presented. This model provides a good prediction of the measured resonance frequencies. As can be seen from the figures (3.5) and (3.6) the model accuracy is good. The effects of various parameters were also taken into consideration to investigate their sensitivity relative to measured data. The difference between the predicted data and measured data is mainly due to uncertainty about dimensions and the values of various parameters. In brief, the model can predict the effects of the most important parameters with acceptable accuracy.

3.5 Modal shapes of inhomogeneous cantilevers.

In the past efforts in the determination of modal frequencies of vibration and shapes has largely been concentrated on the theoretical modal analysis of beams, plates and shell structures. Leissa and Sonalla [14] have theoretically considered the modal shapes of simple fixed-free cantilevers with various initial conditions (equation 3.4). A cantilever was given various initial shapes and its subsequent non-periodic motion determined. In each case the load was applied at the end or the centre of the cantilever. In 1995 Jenkins *et al* [13] reported that the previous models can not accurately represent the behaviour of inhomogeneous cantilevers This is due to non-ideal clamp and effects of piezoelectric element. In what follows, a new analytical model for modal shapes of composite structures taking into account the above effects is presented (the mathematical derivation is given in appendix B).

3.5.1 Theoretical model .

(a) General form:

The fourth-order differential equation, given below, which describes the behaviour of simple fixed-free cantilever may be found in many standard texts [4]:

$$\frac{d^4\Phi_n(x)}{dx^4} - \lambda^4{}_n\Phi_n(x) = 0 \qquad (3.26)$$

This equation can be solved by applying the appropriate boundary conditions. Owing to the non-ideal behaviour of the clamp, ΔL is used to account for the location of the effective clamping point which lies within the clamped region. The additional

boundary condition at x = X2 accounts for the moment produced by the piezoactuator.

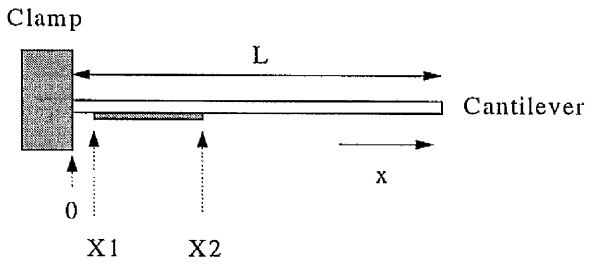

Figure (3-13) The cantilever-piezoactuator arrangement

(b) Boundary conditions:

At $x = -\Delta L$

$$\Phi(x) = 0 . \qquad \frac{d\Phi}{dx} = 0.$$

At $x = X2$

$$EI. \frac{d^2\Phi_n(x)}{dx^2} = \pm gV.$$

At $x = L$

$$EI. \frac{d^2\Phi_n(x)}{dx^2} = 0 \qquad EI. \frac{d^3\Phi_n(x)}{dx^3} = 0$$

The solution of equation (3.26) using the above boundary conditions can be given as

$$\Phi_n(x) = C\left[\alpha \cosh(\lambda_n x) - \cos(\lambda_n x) + \beta \sinh(\lambda_n x) - \gamma \sin(\lambda_n x)\right] \tag{3.27}$$

In this case EI is the total flexural rigidity of the composite structure, defined as [15]

$$EI = E_b I_b + E_p I_p$$

The required eigenvalues, λ_n, are obtained from the numerical solution of the characteristic frequency equation [4],

$$1 + \cos(\lambda_n L).\ \cosh(\lambda_n L) = 0$$

The solution of the above characteristic equation is given in [16]. The terms C, and λ_n are defined in appendix B.

3.5.2 Comparisons and discussion:

A Matlab routine was written to evaluate the modal frequencies and shapes of the first four modes. Figure 3.14 and 3.15 show the experimental results and the results from the previous model (equation 3.4) for third and fourth modes respectively. As can be seen from these figures, there is a significant discrepancy between the old model and the measured modal shapes. The discrepancy may be due to imperfect clamp and behaviour of the piezoactuator.

Figures 3.16 and 3.17 describe the experimental and new theoretical modal shapes for the third and fourth modes respectively. It can be seen that the agreement between the new modal shapes and experimental data is remarkably good.

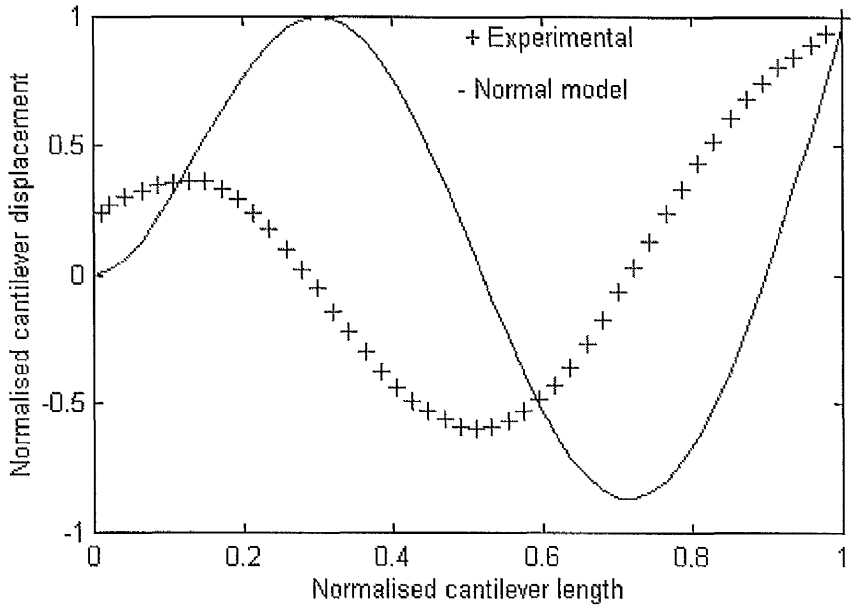

Figure (3-14) A comparison of experimental and simple modal shapes for the third bending mode of a cantilever .

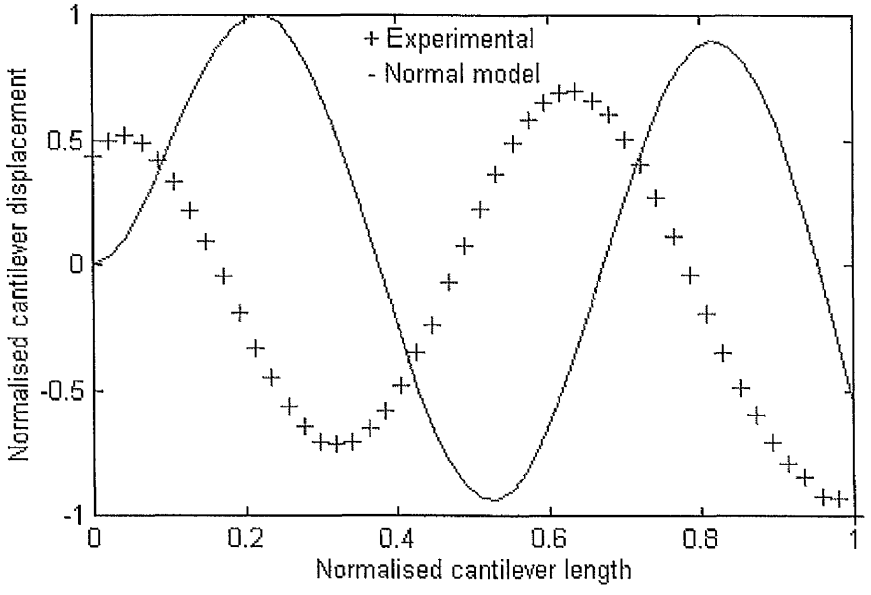

Figure (3-15) A comparison of experimental and simple modal shapes for the fourth bending mode of a cantilever.

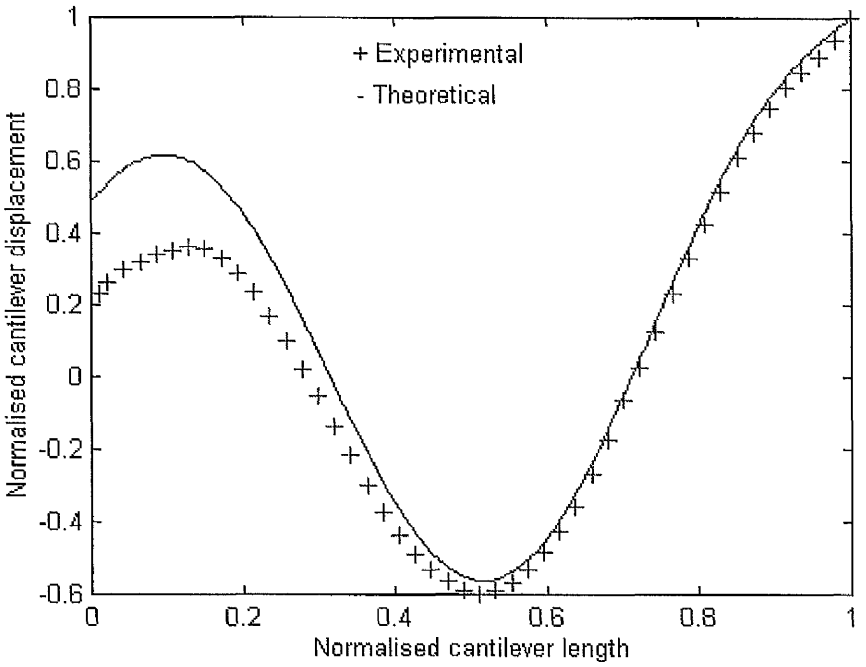

Figure (3-16) A comparison of experimental and new theoretical modal shapes for the third bending mode of a cantilever [13].

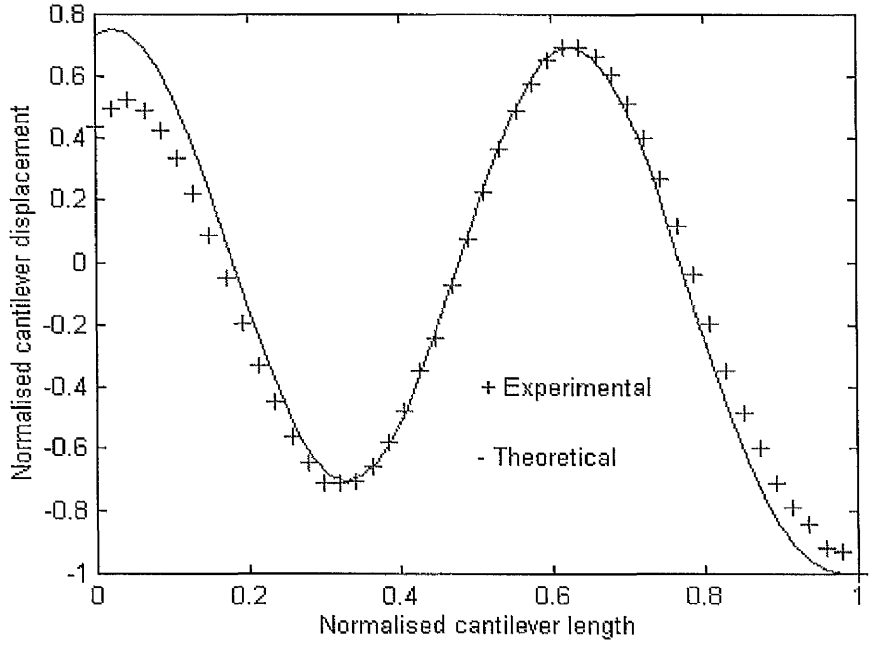

Figure (3-17) A comparison of experimental and new theoretical modal shapes for the fourth bending mode [13].

3.5.3 Summary:

A model describing the modal shapes of inhomogeneous cantilever is analytically presented. The effect of imperfect clamp was taken into account. An additional boundary condition at the edges of the actuator accounting for the moment produced by the piezoactuator element, is considered. The model provides a good fit to the measured modal shapes. The difference with the experimental data near the clamp is probably due to material hysteresis, damping or dry friction damping at the boundary. In brief, further analysis is required to determine how the node and anti-node locations of such cantilevers can be affected because the exact positioning of actuators, relative to anti-node locations, is critical for optimal active vibration control.

3.6 Modelling V-shaped cantilevers:

3.6.1 Why V-shaped cantilevers ?

Most cantilevers used in scanning probe microscopic are V-shaped, as shown in figure (3.18). The additional rigidity of the V-shaped lever reduces lateral bending of the cantilever in response to frictional and other lateral forces which are present when scanning over the sample. In addition, V-shaped cantilevers have a more stable resonance than rectangular cantilevers because they provide low mechanical resistance to vertical deflection and high resistance to lateral torsion [17]. Figure (3.19) shows the deflection of the V-shaped and rectangular cantilevers for similar length, width and applied force. As can be seen, the rectangular cantilever has a higher deflection due to less rigidity than the V-shaped cantilevers. This makes the V-shaped cantilevers less responsive to external disturbances such as air borne

vibrations. They are therefore more appropriate for use in scanning force microscopy.

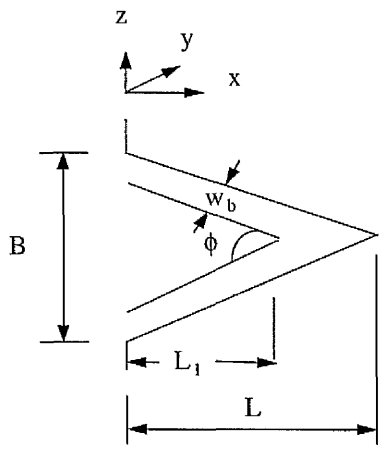

Figure (3-18) Schematic diagram of the V-shaped cantilever.

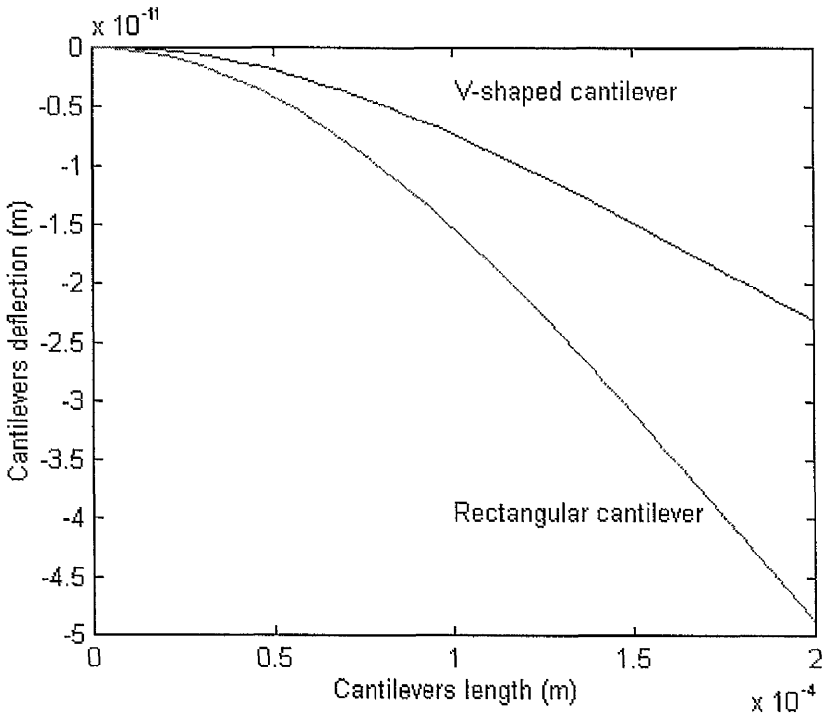

Figure (3-19) Comparison of V-shaped cantilever with Rectangular cantilever.

3.6.2 Previous studies.

In the past years, V-shaped cantilevers have been treated as two rectangular beams in parallel [18]. Therefore, in the case of V-shaped cantilevers, the equations characterising the behaviour of rectangular cantilevers are assumed still valid. These equations can be rewritten as below.

(a) The natural resonant frequency.

The natural resonant frequency for the free undamped vibration is given as [19]

$$f_o = \frac{\lambda^2_i . t_b}{4\pi L^2}\left(\frac{E_b}{3\rho}\right)^{\frac{1}{2}}$$

where f_o is the natural resonant frequency, λ_i is the eigenvalue and ρ is the cantilever density. For the first mode λ_i is given by [4] as $\lambda_i = 1.875$ and therefore the fundamental resonant frequency f_o of the cantilever is given by

$$f_o = \frac{3.52. t_b}{4\pi L^2}\left(\frac{E_b}{3\rho}\right)^{\frac{1}{2}} \qquad (3.28)$$

The value λ_2 for the second mode of resonance is given as $\lambda_2 = 4.69$ and so the second mode of resonance will be 6.25 times of that of the fundamental.

(b) The quality factor QF.

The quality factor is related to the energy dissipated by the system per period. The following definition for the quality factor can be found [20-21]

$$QF = \left[\frac{(E_b \rho)^{\frac{1}{2}} \cdot w_b}{24\mu} \right] \left(\frac{t_b}{L} \right)^2 \qquad (3.29)$$

where μ is the viscosity of the medium in which the cantilever is resonated.

(c) The Air damping.

In the above equations the air damping is neglected . The influence of air damping on the resonant frequency using the quality factor QF is given by [21],

$$f_r = f_o \left(1 - \frac{1}{4QF^2} \right) \qquad (3.30)$$

where f_r is the resonant frequency of the damped cantilever.

According to [18] the equations (3.28), (3.29) and (3.30) for the rectangular cantilever can also be used for the V-shaped cantilever if the width w is taken to be the width of both arms of the cantilever.

Using a variational method Chen *et al* [22] have recently demonstrated the resonance response of V-shaped cantilevers used in scanning force microscope. They reported that the V-shaped cantilever can not be accurately modelled by assuming two rectangular beams in parallel . In the following an investigation of the dynamic behaviour of V-shaped cantilever based on the Finite Element method is given.

3.6.3 Model of the V-shaped cantilever behaviour.

(a) General considerations:

The equation of motion of the cantilever for an undamped system is given by [22]

$$\frac{\partial^2}{\partial x^2}\left(E_b I_b \frac{\partial^2 Y(x,t)}{\partial x^2}\right)+\rho_b . A_b \frac{\partial^2 Y(x,t)}{\partial t^2}=0 \qquad (3.31)$$

where Y(x,t) describes the deflection of the cantilever for oscillation at a resonant frequency. For a V-shaped cantilever as shown in figure (3.18), the second moment of inertia, I_b, is defined by a rectangle with a varying width and constant thickness t_b as

$$I_b = \begin{cases} \dfrac{A_b t_b^{\,2}}{12} & \text{for} \quad 0 \le x \le L_1 \\ \dfrac{B.t_b^{\,3}}{12}\left(1-\dfrac{x}{L}\right) & \text{for} \quad L_1 < x \le L \end{cases}$$

The cross-sectional area is given by

$$A_b = \begin{cases} 2.w_b.t_b & \text{for} \quad 0 \le x \le L_1 \\ Bt_b\left(1-\dfrac{x}{L}\right) & \text{for} \quad L_1 < x \le L \end{cases}$$

(b) Boundary conditions:

The boundary conditions for the cantilever can be expressed as follows:

(a) For the fixed end:

$$y(0) = 0 \qquad \text{(zero deflection)}$$

$$\frac{\partial y(0)}{\partial x} = 0 \qquad \text{(zero slop)}$$

(b) For the free end:

$$\frac{\partial^2 y(L)}{\partial x^2} = 0 \qquad \text{(zero bending)}$$

$$\frac{\partial^3 y(L)}{\partial x^3} = 0 \qquad \text{(zero shear)}$$

Since A_b and I_b are not constant, it is very difficult to find the exact solution for equation (3.31). Chen *et al* [22] used the variational method to solve this problem. In this thesis the solution (appendix C) based on the Finite Element method is presented.

3.6.4 Comparisons and discussion.

The following analysis will be justified by comparing the predicted scanning force microscopy cantilever's resonant frequency with the results of Chen's *et al* [22] numerical model which is based on the variational method, and with measured data.

In performing the calculations, the following cantilever dimensions and data (as in table 3.5) were used.

Dimension	Silicon cantilevers				Silicon Nitride			
Type	A	B	C	D	E	F	G	J
L (μm)	190	190	200	200	85	140	220	320
L1 (μm)	87.	87.5	115	115				
B (μm)	165	165	165	165				
w (μm)	33.	33.5	20	20	18	18	22	22
T (μm)	0.6	0.3	0.6	0.3	0.6	0.6	0.6	0.6
E (N/m)	1.79×10^{11}				1.5×10^{11}			
ρ (kg/m3)	2330				3253.4			

Table (3-5) The cantilevers dimensions were measured from electron micrographs.

Cantilever Type	Measured data	Finite Element method FEM	Chen model	Calculation according to(3.28)
A	33	34.7	34	23.6
B	17.4	17.4	17.3	11.8
C	25.8	25.8	25.8	21.26
D	13.1	13.2	12.9	10.6
E	120	125		91.2
F	38	37.9		33.6
G	15	16.7		13.6
J	7	7.3		6.4

Table (3-6) Calculated and measured resonant frequencies in kHz

Table (3.6) shows the results of the analytical models and experimental data . As can be seen, the agreement between the Chen *et al* , FEM models and measured data is remarkably good. Also from this table, it is clear that the results of the rectangular

model (equation 3.28) shows disagreement with the experimental data and is not appropriate to represent the behaviour of the V-shaped cantilevers.

Figure (3.20) shows a FEM image of the V-shaped mesh cantilever used in SFM.

Figure (3.21) shows the first three V-shaped modes of free vibration . As can be seen the modal shapes of V-shaped cantilevers are similar to the modal shapes of rectangular cantilevers given in figure (3.8). The three dimensional modal shapes are given in appendix C for the first three modes .

Figures (3.22-3.24) show the effect of changing of the V-shaped cantilever arms width and the angle between its arms (see figure 3.18). It is clear that the cantilever frequencies are functions of the cantilever width which is not the case for rectangular cantilevers. Also, these results confirm that the V-shaped cantilevers cannot be assumed as parallel rectangular cantilevers.

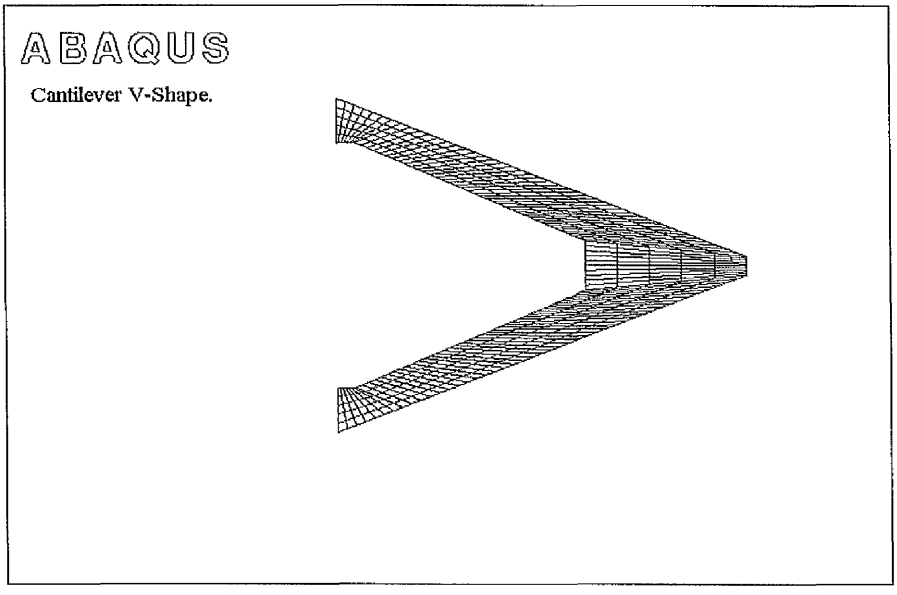

Figure (3-20) FEM mesh for the cantilever used in scanning force microscopy.

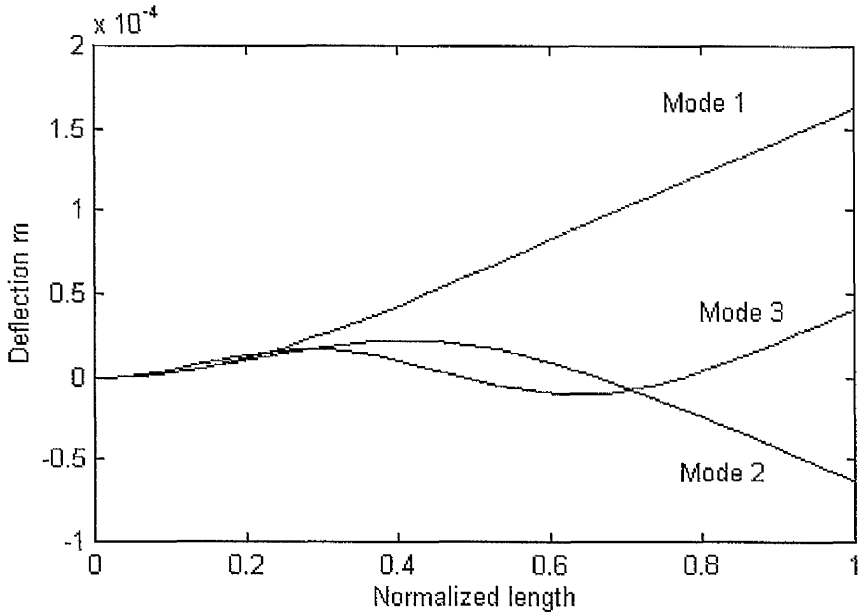

Figure (3-21) The first three normal modes of vibration for a V-shaped cantilever.

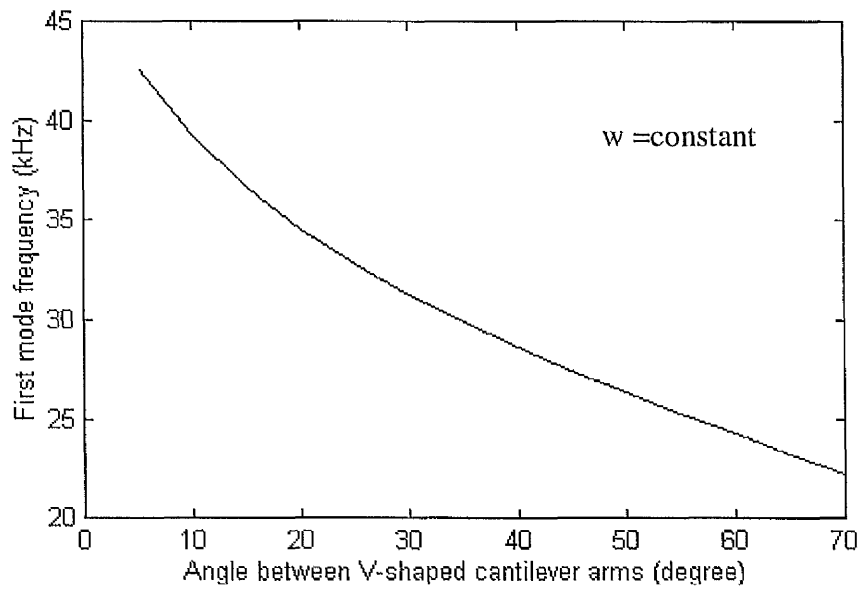

Figure (3-22) Effect of the angle change between cantilever arms (Assuming constant cantilever arms width w_b)

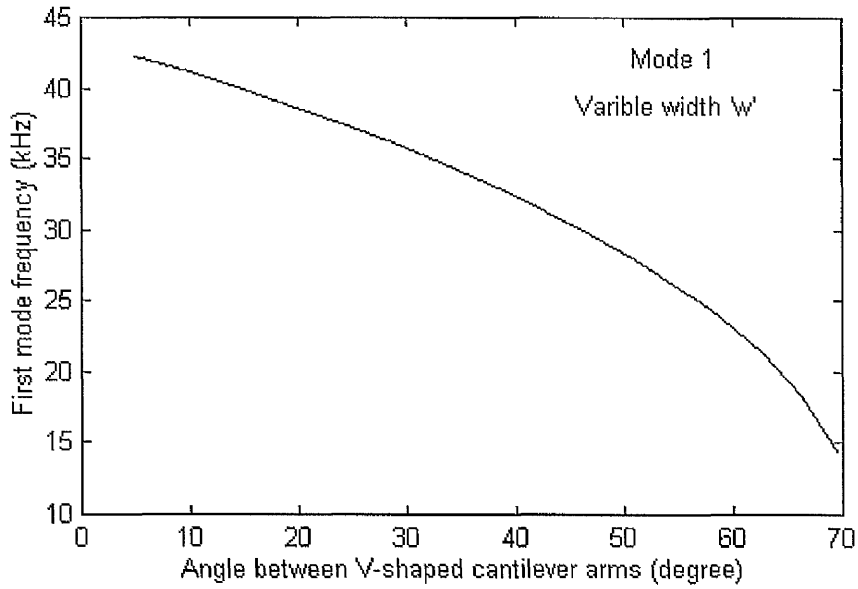

Figure (3-23) Effect of the angle change between cantilever arms (Assuming variable cantilever arms width w_b)

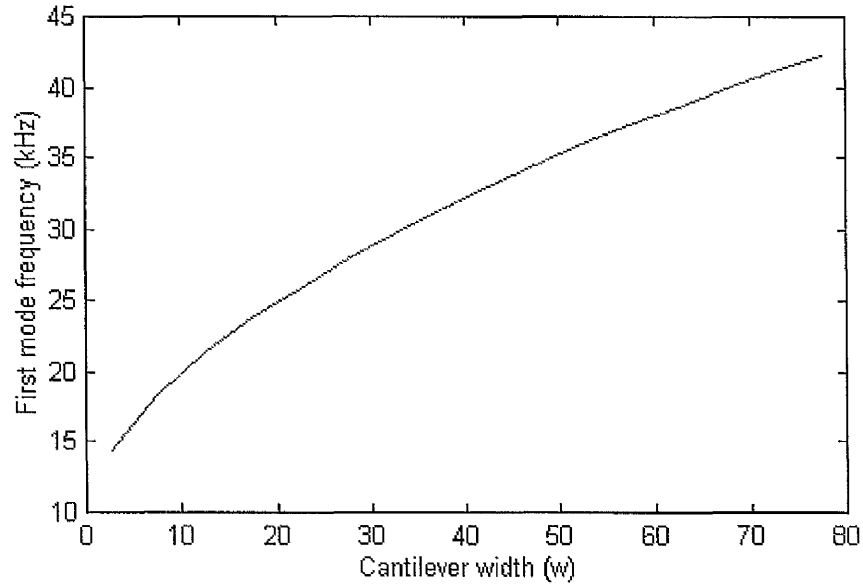

Figure (3-24) Effect of the cantilever width (w_b) variation on the cantilever frequency.

3.7 Summary.

A general description of scanning probe microscopy cantilevers has been given. The dynamic behaviour of these cantilevers is analytically modelled . The results of these models are remarkably good and provide a good fit to the measured data. The effects of piezoelectric elements bonded to the cantilevers are also investigated. A new theoretical model describing a modal shapes of composite structure is derived. The effects of non-ideal behaviour of clamp and piezoelement additional moment are considered. This model overcomes the discrepancy between measured data and the previous analytical models, and yields a very good fit to measured data.

3.8 References.

[1] Albrecht, T.R , Akamine, S, Carver, T.E, and Quate, C.F, " Microfabrication of cantilever styli for the atomic force microscope ", *Journal of Vacuum Science and Technology*, A **8**(4), July 1990, pp 3386-3396.

[2] Cooper, W.D " Electronic instrumentation and measurement techniques " 2nd edition , Prentice-Hall, Inc. Englewood Cliffs, New Jersey , 1978.

[3] Sarid, D, " Scanning force microscopy with applications to electric, magnetic and atomic forces." Oxford University Press, New York, 1994.

[4] Thomson, W.T , " Theory of vibrations with applications' 1981, (George Allen Unwin).

[5] Daniel, J.I, " Engineering Vibration" 1994, Prentice-Hall, Inc., New Jwrsey .

[6] Young, D and Felgar, R.P " Tables of characteristic functions representing normal modes of vibration of a beam", *The University of Texas, Publication No 4913*, 1949.

[7] Crawley, E.F and Anderson, E.H " Detailed models of piezoceramic actuation of beams", *Journal of intelligent material system and structure*, Volume **1**, January 1990, pp 4-25.

[8] Burdess, J.S and Fawcett, J.N " An experimental evaluation of a piezoelectric actuator for the control of vibration in a cantilever beam." *journal of systems and control Engineering* , 1992, Volume **206**, pp 99-107.

[9] Morgan-Matroc limited " Piezoelectric Ceramics" *Vernitron Division* , Thornhill Southampton SO9 5QF ,U.K.

[10] Cox , D.E and Lindner, D.K " Active control for vibration suppression in a flexible beam using a model domain optical fibre sensor " *Journal of vibration and acoustics*, Volume **113**, July 1991, pp 368-381.

[11] Crawley, E.F and De Luis, J " Use of piezoelectric actuators as elements of intelligent structures " *AIAA Journal* , Volume **25**, No 10, October 1987, pp 1373-1384.

[12] Chen, C.I, Napolitano, M.R and Chen, C.L " A new learning algorithm for neural network state for estimation in active vibration control " *Smart material and structure*, Volume **1** , 1992, pp 250-257.

[13] Jenkins, D.F.L, Cunningham, M.J, Clegg, W.W and Bakush, M.M, " Measurement of the modal shape of inhomogeneous cantilever using optical beam deflection ", *Measurement Science and Technology*, Volume **6**, No 2, 1995, pp160-166.

[14] Leiss, A.W and Sonalla, M.I , " Vibration of cantilever beams with various initial condition ", *Journal of Sound and vibration*, Volume **150** (1) 1991, pp 83-89.

[15] Baz, A and Poh, S " Performance of active control systems with piezoelectric actuators" *Journal of Sound and Vibration*, Volume **126**, No 2, 1988, pp 327-343.

[16] Howard, B.W and Gupta, S, " Math Software Package Simplifies Structural Analysis", *Journal of Sound and Vibration*, Aug 1992, pp 24-29.

[17] Schmidt, M.D " Imaging of Magnetic Domain structures by Magnetic Force Microscopy " MS.c Thesis submitted to Division of Electrical Engineering, Manchester University, October 1995.

[18] Cleveland, J.P, Manne, S, Boeek, D and Hansma, P.K , " A non-destructive method for determining the spring constant of cantilevers for scanning force microscopy ", *Review. Scientific .Instrument.*, Volume **64** (40), 1993 , pp 403-405 .

[19] Young, D.J " Roark's Formulas for Stress and Strain" McGraw-Hill, 1989.

[20] Blohm, F.R , Bouwstra, S, Elwenspoeck and Fluitman, J.H.J, " Dependence of the quality factor of micromachined silicon beam resonators on pressure and geometry, *Journal of Vacuum Science and Technology*, **B 10**, January 1992, pp 19-26.

[21] Kiesewetter, L, Zhang, J.M, Houdeau,D, and Steckenborn,A " Determination of Young's moduli of micromechanical thin films using the resonance method" *Sensors and Actuator* **A** 35, 1992, p 153.

[22] Chen, G.Y. Warmack, R.J. Thundat, T. and Allison, D.P, " Resonance Response Of Scanning Force Microscopy Cantilevers ", *Review Scientific .Instrument.*,Volume **65** (8), August 1994, pp 2532-2536.

Chapter 4

4. Optimal thickness of piezoactuators:

4.1 Introduction:

Recently, piezoelectric materials have received great attention since they have proved to be experimentally effective both as actuators and as sensors. When a piezoelectric material is strained then an output voltage proportional to the strain is produced. The inverse effect is such that when a voltage is applied across a piezoelectric material a mechanical strain is induced in the material. The latter effect enables the piezoelectric transducer to be used as an actuator. Piezoelectric materials, such as lead zirconium titanate (PZT), are found mainly in the form of bulk ceramics and in this form they are available in a variety of shapes and sizes. For example, a PZT cylinder with suitable electrodes is capable of actuation in three-dimensions and makes very precise positional control possible. An example of the application of this type of actuator is to be found in scanning force microscopes. In such an instrument the piezoelectric scan tube is used to move the sample in the x, y and z directions [1]. It is however more common for square or rectangular plate PZT elements to be used. They are commonly used to actuate cantilever beams [2]. For a cantilever beam of a

given material and dimensions, it is of practical importance to determine the value of the actuator parameters which enable the effective bending moment to be optimised. If there exists an optimum thickness of a piezoelectric actuator, for a given cantilever thickness, then not only can the effective bending moment be optimised, but also the effectiveness of actuation. The actuator parameters which enable the effective bending moment to be optimised include the piezoelectric element material, its dimensions, its location and the nature of the bonding layer. The choice of the piezoelectric material for an actuator is principally determined by the piezoelectric coefficient d_{31} which determines the magnitude of actuation which is possible for a given drive voltage. There is little difference in Young's modulus for the commonly used PZT bulk ceramics. The effect of the actuator's thickness has been investigated theoretically by Kim and Jones [3] for plates. They produced theoretical models for the effective bending moments produced by piezoelectric actuators bonded to stainless steel and aluminium plates. Their model demonstrated that in designing a piezoelectric actuator, one parameter of critical importance is the actuator thickness. They have shown that there exists an optimal piezoelectric actuator thickness which maximises the bending of the plate. For a cantilever, the most favourable location of the actuator is governed by the position of maximum strain [4] and this dictates that the actuator should be located very near to, but not at, the root of the cantilever. Plantier *et al* [5] have investigated the effect of the bonding layer and have shown analytically that the effectiveness of actuation increases as the bonding layer thickness decreases and also that the resonant frequencies are slightly decreased as the bonding layer thickness increases. They also compared some experimental results

with their model and deduced that if the bonding layer was assumed to be ideal then the model over-estimated the experimental actuation effectiveness. This work investigates theoretically and experimentally the effect of actuator thickness on the magnitude of the cantilever actuation. A model which describes the effective bending moment induced by single and double piezo-actuator bonded to a cantilever beam is presented in the next section.

4.2 Derivation of the Effective Bending Moment:

Based upon work which was first published by Kim *et al* [3] for plate substructure, a model which describes the effective moment induced by twin and single piezo-actuator bonded to the cantilever beam is presented. In order to derive an expression for the effective bending moment, M, a number of assumptions are made, namely [6,7]:

(1) The composite structure is assumed to be very thin.

(2) A linear strain distribution is assumed across the thickness of the composite structure.

(3) The cantilever is fully covered by the piezo-actuator.

(4) The electric field strength (V/t_p) is held constant.

(5) The bonding layer thickness is assumed to be zero (i.e. perfect bonding).

The appropriateness of these assumptions is discussed later when considering the experimental investigation. Figure (4.1) shows a schematic drawing of a piezo-actuator bonded to a flexible cantilever.

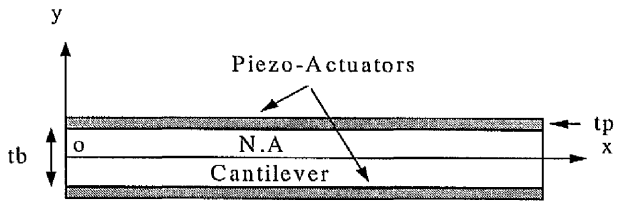

Figure (4-1). Schematic drawing of double layer actuators.

The stress-strain relationship for piezoactuator is given by Crawley *et al* [4],

$$\sigma_p = E_p\left(\varepsilon_p - \Lambda\right) \tag{4.1}$$

where

$$\Lambda = \frac{V}{t_p} d_{31}$$

Similarly, a stress-strain expression for the cantilever can be expressed as

$$\sigma_b = E_b \cdot \varepsilon_b \tag{4.2}$$

From assumption (2), the strain distribution is assumed to be a linear function of **y** across the composite structure. Therefore,

$$\varepsilon(y) = \Delta . y \tag{4.3}$$

where Δ is the strain slope. Since a linear strain distribution was assumed across the composite structure thickness, the corresponding stress distribution can also be assumed to be linear and is expressed as a function of the interface stress σ between piezoactuator and cantilever.

(a) For cantilever.

$$\sigma_b = 2\frac{\sigma}{t_b}y \tag{4.4}$$

Comparing equations (4.2-4.4), the strain slope Δ can be expressed as a function of the interface stress

$$\Delta = \frac{2\sigma}{E_b t_b}$$

(b) For piezoactuator.

$$\sigma_p = 2\frac{E_p}{E_b}.\frac{\sigma}{t_b}y - E_p\Lambda$$

$$\sigma_p = 2E.\frac{\sigma}{t_b}y - E_p\Lambda \tag{4.5}$$

where $E = E_p/E_b$.

The interface stress σ can be determined by use of the moment equilibrium condition about neutral axis [3, 8] .

$$\int_{\text{beam}} \sigma_b dA + \int_{\text{PZT}} \sigma_p dA = 0 \tag{4.6}$$

4.2.1 Two piezo-actuators:

In this section, a piezo-actuator bonded to each face of a flexible cantilever is assumed. The case of a single piezoactuator will be treated in the next section. Exploiting symmetry about the neutral axis, the moment equilibrium condition can be expressed as

$$\int_0^{\frac{t_b}{2}} \sigma_b y dy + \int_{\frac{t_b}{2}}^{\frac{t_b}{2}+t_p} \sigma_p y dy = 0 \qquad (4.7)$$

Substituting equations (4.4) and (4.5) into equation (4.7), the interface stress of the cantilever-actuator is found to be

$$\sigma = \frac{6E_p t_p t_b \left(t_p + t_b\right)}{t_b^3 + 2Et_p\left(3t_b^2 + 4t_p^2 + 6t_b t_p\right)} \Lambda$$

$$\sigma = \frac{6E_p T(1+T)}{1 + 2ET\left(3 + 6T + 4T^2\right)} \cdot \Lambda \qquad (4.8)$$

where $T = \frac{t_p}{t_b}$,

The effective bending moment, *M*, applied to the cantilever by the piezo-actuator can now be expressed as a function of the known interface stress σ as:

$$M = w_b \int_{-\frac{t_b}{2}}^{\frac{t_b}{2}} \sigma_b y dy = \frac{w_b . t_b^2 . \sigma}{6}$$

$$M = \frac{w_b . E_p t_b^2 T(1+T)}{1+2ET(3+6T+4T^2)} \Lambda \qquad (4.9)$$

4.2.2 Single piezo-actuator.

The schematic drawing of an actuator bonded to the upper surface of a flexible cantilever is shown in figure (4.2). The distance of the neutral axis from the lower edge of the cantilever D can be expressed as [8]

$$D = \frac{E_b t_b^{\,2} + 2E_b t_b t_p + E_p t_p^{\,2}}{2\left(E_b t_b + E_p t_p\right)}$$

so

$$D = \frac{t_b(1 + 2ET + ET^2)}{2(1 + ET)}$$

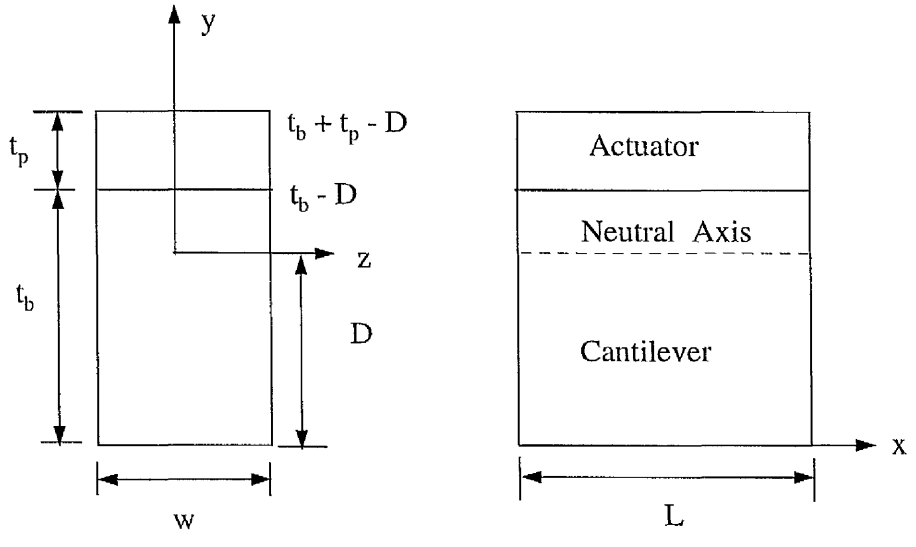

Figure (4-2). Schematic drawing of a cantilever with single actuator.

In this case, the strain can also be expressed as a linear function of y

$$\varepsilon(y) = \Delta.(y+D) \tag{4.10}$$

Therefore for the cantilever the strain can be expressed as

$$\sigma_b = \frac{\sigma}{t_b}(y + D) \tag{4.11}$$

Again, comparing equations (4.2), (4.10) and (4.11), the strain slope Δ in this case is

$$\Delta = \frac{\sigma}{E_b t_b}$$

For the piezo-actuator

$$\sigma_p = \frac{E_p}{E_b}.\frac{\sigma}{t_b}(y+D) - E_p\Lambda$$

$$\sigma_p = E.\frac{\sigma}{t_b}(y+D) - E_p\Lambda \tag{4.12}$$

Substituting equations (4.10) and (4.12) into equation (4.6) enables this to be expressed as:

$$\int_{-(t_b+t_p-D)}^{-(t_b-D)} \left[E\frac{\sigma}{t_b}(y+D) - E_p\Lambda \right] y dy + \int_{-(t_b-D)}^{D} E\frac{\sigma}{t_b}(y+D) y dy = 0 \tag{4.13}$$

By applying equation (4.13), the interface stress of cantilever-actuator is found to be:

$$\sigma = \frac{\frac{E_p \Lambda}{2}\left[-T^2 - 2T + 2T\frac{D}{t_b}\right]}{\frac{t_b}{3}\left[1 - 3\frac{D}{t_b} + 3\left(\frac{D}{t_b}\right)^2 + E\left(T^3 + 3T^2\left(1 - \frac{D}{t_b}\right) + 3T\left(1 - 2\frac{D}{t_b} + \frac{D}{t_b}^2\right)\right)\right] + \frac{D}{2}\left[E.T\left(\frac{2D}{t_b} - T - 2\right) + \left(\frac{2D}{t_b} - 1\right)\right]} \quad (4.14)$$

The effective bending moment, M, applied to the cantilever by a single piezo-actuator can now be expressed as

$$M = w_b \int_{-\frac{t_b}{2}}^{\frac{t_b}{2}} \sigma_b y dy = \frac{w_b . t_b^2 . \sigma}{6}$$

Thus,

$$M = \frac{w_b . t_b^2 E_p \left[-T^2 - 2T + 2T\frac{D}{t_b}\right]\frac{\Lambda}{12}}{\frac{t_b}{3}\left[1 - 3\frac{D}{t_b} + 3\left(\frac{D}{t_b}\right)^2 + E\left(T^3 + 3T^2\left(1 - \frac{D}{t_b}\right) + 3T\left(1 - 2\frac{D}{t_b} + \frac{D}{t_b}^2\right)\right)\right] + \frac{D}{2}\left[EI\left(\frac{2D}{t_b} - T - 2\right) + \left(\frac{2D}{t_b} - 1\right)\right]} \quad (4.15)$$

4.2.3 Comparison and discussion.

As specified in equations (4.9) and (4.15), the final expression for the effective bending moment is a function of the thickness and the material properties of the cantilever and the piezo-actuator. The bending moment also depends on the free piezoelectric strain Λ. It is also apparent that theoretically much greater moments can

be expected with thinner piezo-actuators under a constant applied voltage. However, this observation leads to the spurious conclusion that thinner piezo-actuator perform better. In practice, most piezoelectric materials have maximum allowable electric field strengths . If the maximum allowable field strength is exceeded, the material will degrade and eventually lose its piezoelectric properties (being depolled). Thus, in optimising the piezo-actuator thickness, the electric field strength should be held constant rather than the applied voltage to correctly represent the true nature of the piezoelectric materials

Figure (4.3) shows that the maximum moment generally occurs for slightly thinner piezo-actuators for double-sided rather than for single-sided piezo-actuator. The optimal thickness of the double-sided PZT actuator is about 60 % of the stainless steel cantilever thickness and approaches 80 % for single-sided actuator. Note that the effective bending moment produced by double-sided PZT actuators is slightly higher than the bending moment produced by single-side PZT actuator as soon as the actuator thickness is less than the cantilever thickness.

Figure (4.4) describes the same comparison using PVDF as the actuator. In this case the piezo-actuator thickness is about 2.5 times using double-sided actuators and 3.3 times using single-sided actuator.

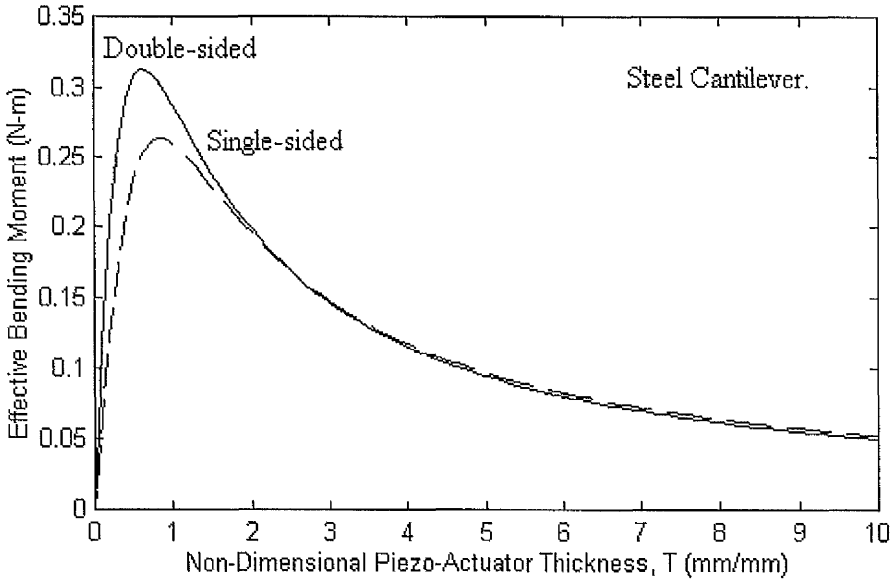

Figure (4-3) A comparison of the effective bending moment induced by double and single PZT-Actuators.

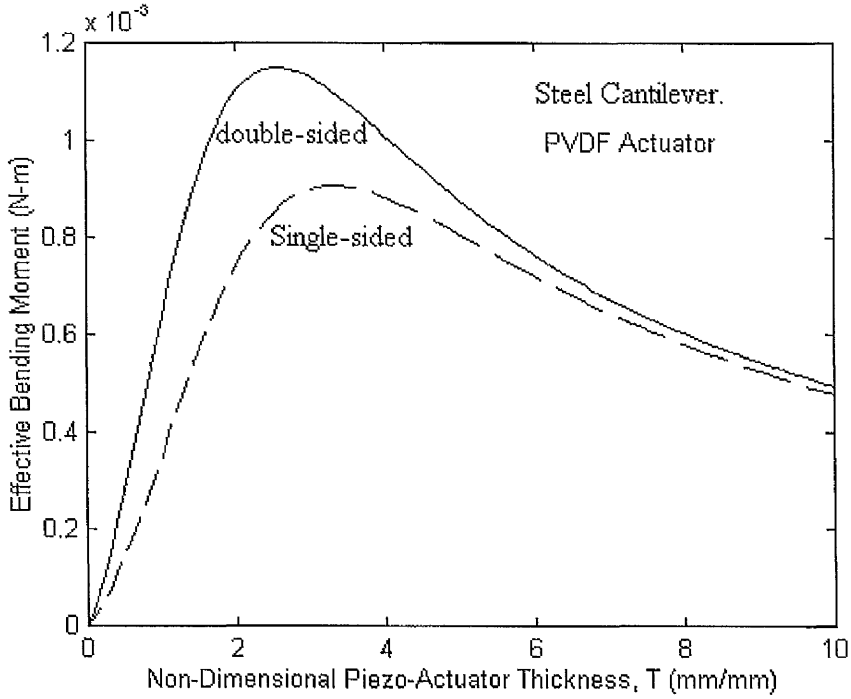

Figure (4-4). A comparison of the effective bending moment induced by double and single PVDF-Actuators.

Figure (4.5) describes the same comparison given in figure (4.3), using an aluminium cantilever. The optimal thickness of the double-sided piezo-actuator is about 40 % and about 50 % for the single-sided PZT actuator.

Figure (4.6) shows the effective bending moment as a function of the piezo-actuator thickness using the maximum allowable electric field strengths for both single layer PZT and PVDF actuators. As can be seen, the optimal thickness of the PVDF actuators necessary to maximise the applied bending moment is approximately four times that of the PZT actuators

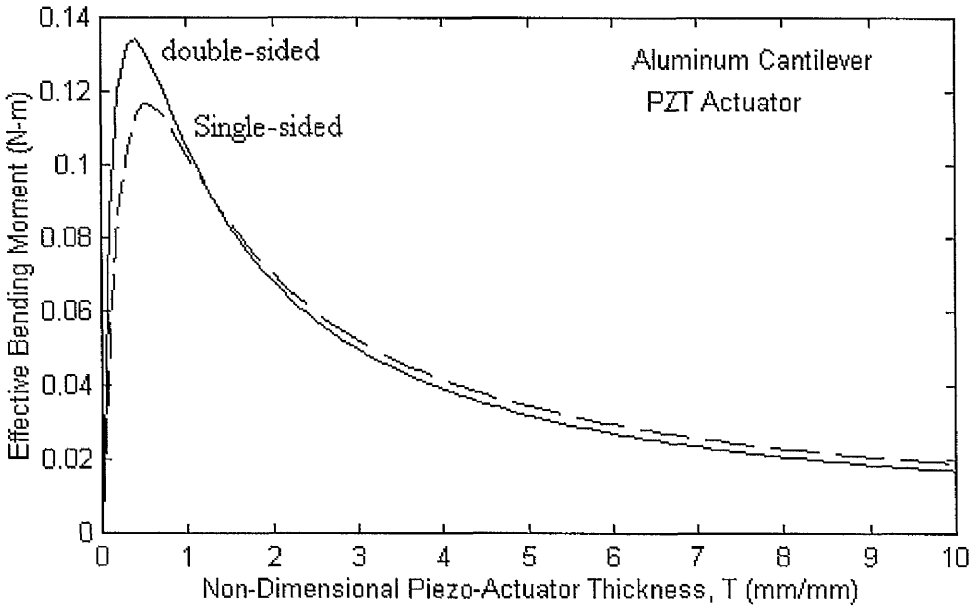

Figure (4-5). A comparison of the bending moment induced by double and single PZT actuators.

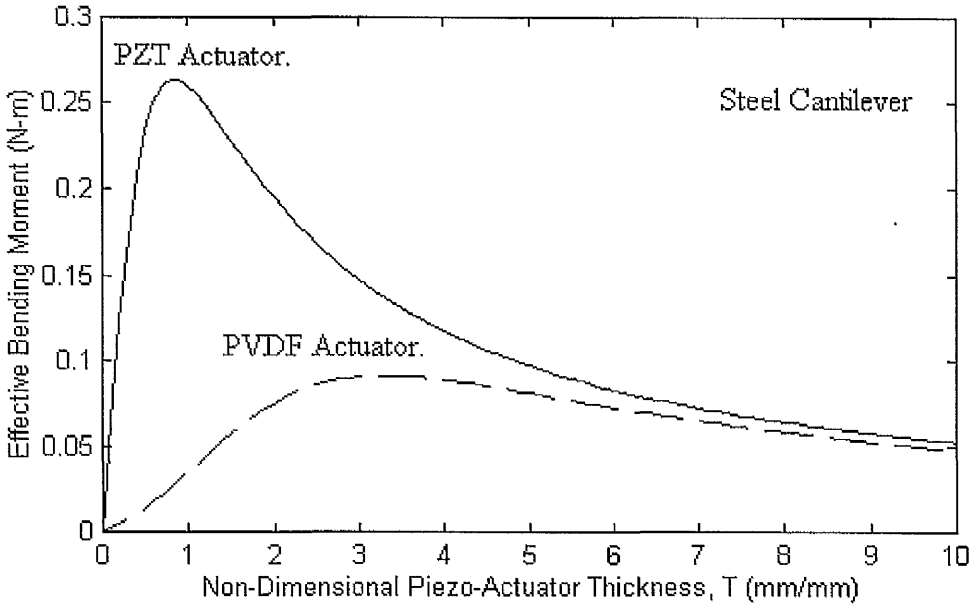

Figure (4-6). Comparison of PZT Actuator with PVDF Actuator.

In general, for a given thickness of cantilever and actuator the effective bending moment is dependent only on the Young's modulus of the cantilever, assuming the same actuator material is used. Table (4.1) gives Young's modulus for a number of commonly used materials. These have been used to determine the effective bending moment as a function of the actuator to cantilever thickness ratio. Figure (4.7) shows the results obtained and it can be seen that for each material there is an optimum thickness for maximum actuation. This result is intuitively correct since a thicker actuator produces larger actuation until the stiffening effect of the actuator dominates. The validity of these theoretical predictions has not been experimentally demonstrated before. In this thesis, an experimental system has been developed to investigate this behaviour. This is described in the following section .

Stainless Steel	Silicon	Silicon Nitride	Glass	Aluminium
2.1×10^{11}	1.79×10^{11}	1.5×10^{11}	8.1×10^{10}	7.1×10^{10}

Table (4-1) Elastic properties of suitable materials used (Young's modulus (N/m^2)).

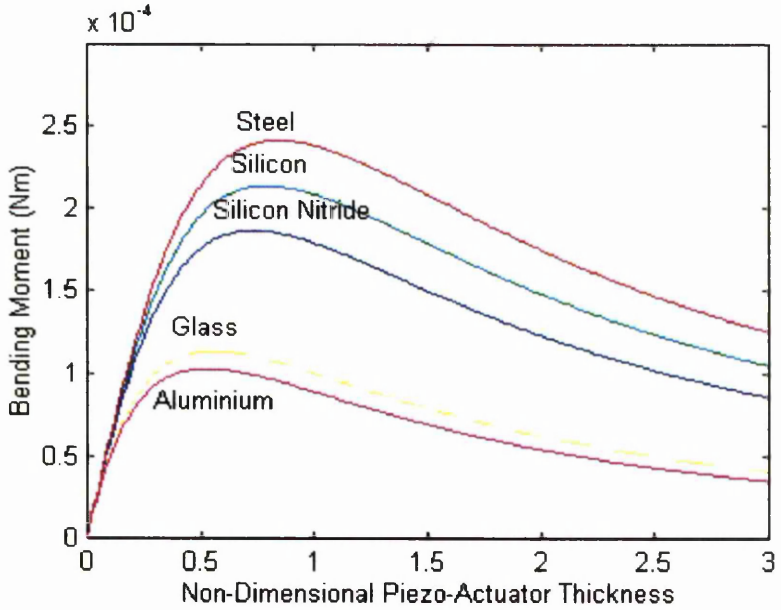

Figure (4-7). Effective bending moment curves illustrating the influence of the material's Young's modulus on the optimal piezoactuator thickness.

4.3 Experimental investigation.

The objective of this work is to determine experimentally, for a given cantilever material, the relationship between the thickness of the piezoelectric actuator and the thickness of the cantilever. The experimental work can be considered in two separate parts: the change in the cantilever thickness and the measurement of the magnitude of cantilever deflection.

4.3.1 Mechanical set-up.

For this work stainless steel and aluminium were used as cantilevers, since as figure (4.7) shows the optimum thickness ratio is very different. The piezoelectric actuator used was made from PZT (Advanced Ceramics ACL4050). The experiment was designed so that the piezoelectric element thickness is held constant while the cantilever thickness was reduced. A mechanical system was designed to enable the cantilever to be well supported and permanently attached to a holder while the cantilever was manually polished using carborundum to successively reduce the cantilever thickness. The assembly was made in three pieces with location pins to enable the cantilever holder to be precisely and reproducibly located onto the polishing head and also subsequently onto the experimental system as shown in figure [4.8] . The cantilever was bonded to the holder using electrically conducting epoxy resin to make fixed cantilever length for all measurements. The dimensions of the piezoelectric element were 1mm × 1mm × 0.2mm. The cantilever was 4 mm long and 1mm wide and its thickness varied from 0.7 mm to 0.1mm for stainless steel and from 1.5 mm to 0.1 mm for aluminium. The piezoelectric element was bonded to the cantilever (about 0.5 mm from the clamp) using electrically conducting epoxy resin. At the end of the cantilever a small mirror (1mm x 1mm) was attached for the optical sensing system, which is described in the next section. A dial gauge was used to monitor the cantilever thickness as it was polished. The cantilever thickness was reduced in small incremental steps and its thickness confirmed using a micrometer.

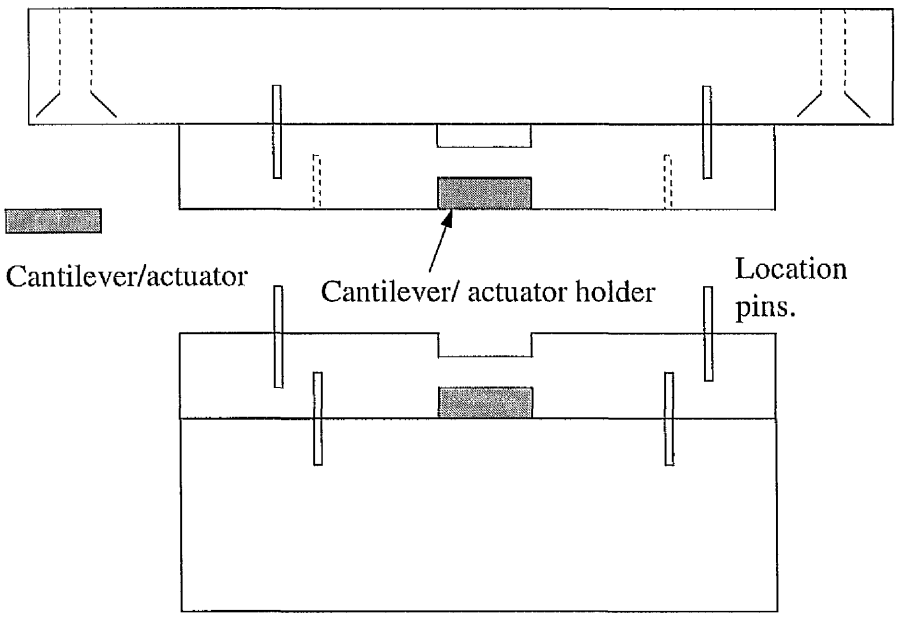

Figure (4-8) Cantilever holder set-up.

4.3.2 Actuation Measurement

The measurement of the amount of cantilever deflection was made using an experimental arrangement which is very similar to that described by Cunningham *et al* [2]. The arrangement is shown schematically in figure (4.9) . The piezoelectric element was driven by an ac voltage of constant amplitude (Jupiter 2000), so that constant electric field can be applied at the cantilever resonance frequency. The end deflection of the cantilever was measured using optical beam deflection (OBD), which can be considered to have a linear response for small displacements encountered. In OBD light from a diode laser (Vector Technology Beta TX at 670nm) is focused onto the mirror at the end of the cantilever and the reflected light collected by a position sensitive detector in the form of a quadrant photodetector

(Hamamatsu S5981). The OBD system was calibrated using a series wired piezoelectric bimorph, the behaviour of which is well characterised [7]. The signals from the quadrant position sensitive detector were differentially amplified and filtered using a second order high pass filter (Bessel type), with a -3 dB point of 250 Hz. After further pre-amplification the lock-in amplifier (EG&G 5210) was used to recover signal from the noise. The function generator provided the reference signal for the lock-in amplifier. The signal measured at the lock-in amplifier was recorded as a function of the piezo-actuator thickness to cantilever thickness ratio. Figures (4.10) shows the results obtained using this method for stainless steel and aluminium. At each cantilever thickness the cantilever was removed from the assembly and reinserted five times in order to test the assembly reproducibility and average values were calculated. The error bars shown in figures (4.11) and (4.12) indicate a 95 % confidence level.

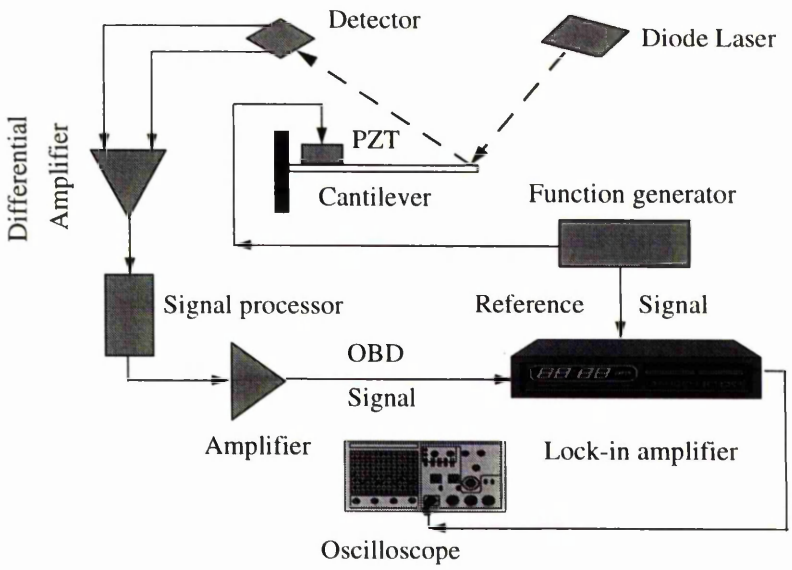

Figure (4-9) Experimental arrangement.

4.3.3 Discussion:

Figure (4.10) shows that the model prediction of an optimum actuator to cantilever thickness ratio for maximum deflection of the cantilever has been validated experimentally. In this figure the experimental and theoretical results are compared for stainless steel and aluminium cantilevers and it can be seen that the agreement is good. This indicates that the simple model accurately predicts the optimum thickness ratio and so equation (4.15) can be used to give the optimum actuator thickness for a given cantilever for a wide range of practically significant cantilever materials for actuation and micro-actuation such as stainless steel, aluminium, silicon, silicon nitride and glass. It can be seen that the actuation of the cantilever for actuation thickness below optimum gives much lower deflections than predicted by the model. It is therefore important that, if possible, the actuator thickness be no less than the optimum value, as the reduction in deflection for thicker than optimum actuators is fairly small whereas a very drastic reduction in deflection occurs for thinner rather than for optimum actuators.

The model used in section (4.2) was based on the stated assumptions in order to facilitate solution. It is clear that the model is not a good representation of the experimental situation where the cantilever is thick at the beginning of the polishing procedure. Robbins and Reddy for piezoelectrically actuated beams [10] and Hess for the similar problem of differential expansion of composite strips [11] have shown that the model becomes invalid when the actuator length is comparable with the composite thickness. This situation pertains just while the cantilever remains thick.

However, the model is valid in the practically important region of optimum thickness ratio and above. This work shows the importance of good actuation in using an actuator thickness at least similar to that predicted by the model given. This analysis is valid for a wide range of cantilever dimensions from the conventional to the 100 μm long micro-cantilevers used in scanning probe microscopes.

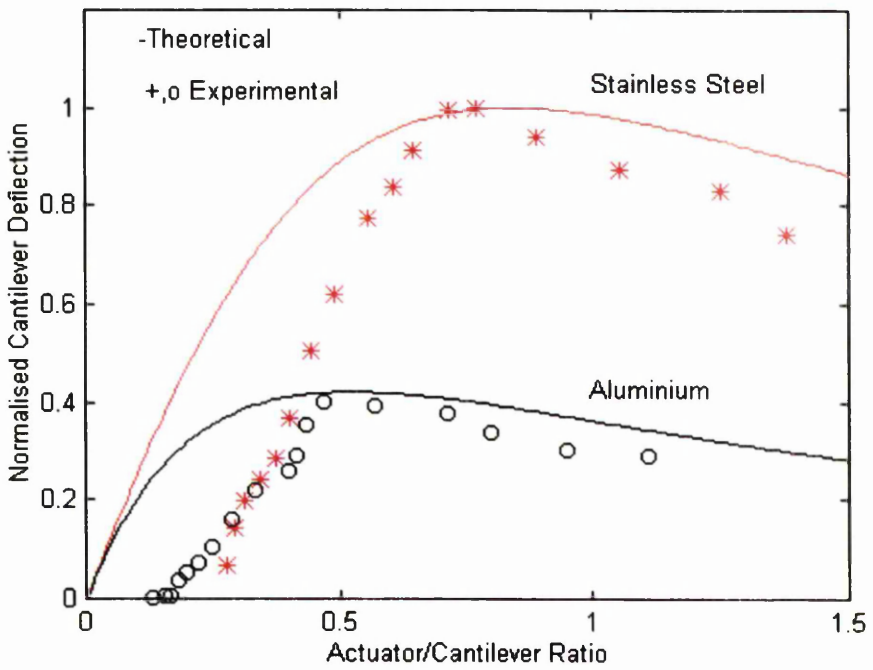

Figure (4-10). Comparison of the end deflection as a function of piezoactuator to cantilever thickness ratio for stainless steel and aluminium cantilevers.

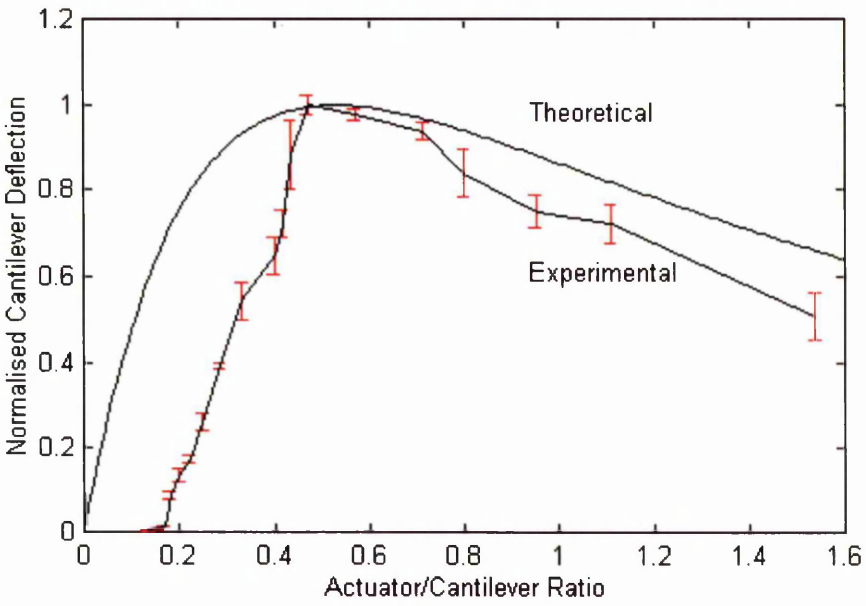

Figure (4-11) Normalised cantilever end deflection as a function of piezoelectric element to cantilever thickness ratio for an aluminium cantilever.

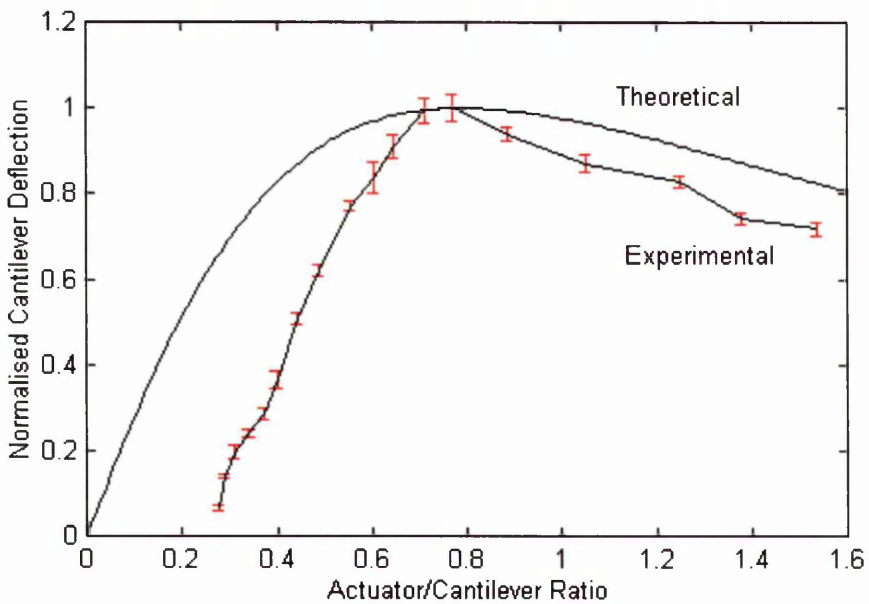

Figure (4-12) Normalised cantilever end deflection as a function of piezoelectric element to cantilever thickness ratio for a stainless steel cantilever.

4.3.4 Summary.

Based on ideas which were first published by Kim *et al* for plate substructure, an analytical model that describes the optimal thickness of piezoelectric elements attached to the simple cantilever is presented. The model shows that for each cantilever material there is an optimum thickness for maximum actuation. The validity of this model has been demonstrated experimentally.

4.4 References.

1. Cunningham, M.J, Cheng, S.T and Clegg, W.W. "A differential interferometer for scanning force microscopy". *Measurement Science and Technology*. 5, 1994, pp. 1350-1354
2. Cunningham, M.J, Jenkins, D.F.L, Clegg, W.W and Bakush, M.M. "Active Vibration Control of a Small Cantilever Actuator". *Sensors and Actuators A (Physical) - Micromechanics*, Vol. A50, 1995, pp 147-150.
3. Kim, S.J and Jones, J.D " Optimal design of piezoactuators for active noise and vibration control" *Am. Inst. Aeronaut. Astronaut J.* ,Vol. **29,** No **12,** (1991) pp 2047-2053.
4. Crawley, E. F, and de Luis, J., " Use of Piezoelectric Actuators as Elements of Intelligent Structures", *Am. Inst. Aeronaut. Astronaut J.* Vol. **25** No **10** (1987) pp 1373-1384
5. Plantier, G, Guigou, C, Nicolas, J, Piaud, J.B and Charette, F. "Variational analysis of a thin finite beam excitation with a single asymmetric piezoelectric actuator including bonding layer and dynamical effects". *Acta Acustica* 3 (1995) 135-151.
6. Cunningham, M.J, Jenkins, D.F.L and Bakush, M.M " Experimental investigation of the optimum thickness of a piezoelectric element for cantilever actuation " submitted to IEE proceeding *Measurement Science and Technology, 1996,* accepted for publication.

7. Jenkins, D.F.L, Bakush, M.M and Cunningham, M.J " An investigation into the optimum design of a piezo-actuator" Conference presentation: Sensors and Actuators, Manchester Business School, July 1996.
8. Baz, A and Poh ,S. "Performance of an active control system with piezoelectric actuators". *Journal of Sound and Vibration* 126(2) (1988) 327-343.
9. Morgan-Matroc Ltd., Thornhill, Southampton, SO9 5QF, UK. Piezoelectric Ceramics - Technical Literature.
10. Robbins, D.H and Reddy J. N. "Analysis of piezoelectrically actuated beams using a layer-wise displacement theory". *Computers and Structures* Vol. 41 No. 2 (1991) 265-279.
11. Hess, M.S "The end problem for a laminated elastic strip - II. differential expansion stresses". *Journal of Composite Materials*, Vol.3 (1969) 630-641.

Chapter 5

5. Electrostatic actuator.

5.1 Introduction.

In the last few years, there has been a growing interest in actuation that is capable of operating at the micrometre level such as electrostatic [1,2], piezoelectric [3], electromagnetic [4], thermal and shape memory alloy [5]. Recently Wood *et al* [6] have reviewed a variety of actuation mechanisms used in microengineering and have shown that electrostatic actuators have a strong position in microengineering applications due to their compatibility with CMOS processes and low temperature dependence. Lang *et al* [7] in their consideration of the monolithic microfabricated actuators have presented basic arguments which favour electrostatic drive: the electrostatic actuator is more efficient and consumes less power in micro scales, and they are capable of producing more power and force than electromagnetic actuators with the same dimensions. In 1987, Trimmer and Gabriel [8] have also discussed the advantages of the electrostatic drive for a microfabricated actuator and described the advantages of the miniaturisation of manipulators for handing small parts. In the scanning probe microscope area, Erlandsson *et al* [9] have used of an electrostatic force by the application of a small voltage between the sample and the cantilever tip to obtain topographic images of graphite surface.

Although electrostatic actuators have been recently used advantageously in many micromechanical structures, such as electrostatic motors [10], valves [11,12], pumps [13] and in vibration control and microposition applications [14], there are however disadvantages, namely

- The electrostatic force is non linear at low excitation frequency.
- It is restricted mainly by the dielectric strength of the insulating barrier and is sensitive to the permittivity of the gap separation.
- If air is used as the separating dielectric, variations due to temperature and humidity will affect its operation.

Our literature survey indicates that the non-linear behaviour has not been fully investigated, therefore, the aim of this study is to evaluate theoretically and experimentally the behaviour of small cantilever excited electrostatically in order to appreciate the low frequency non-linear behaviour.

5.2 Theoretical considerations.

The electrostatic actuator is a non-contact device. This actuator uses the principle that any two electrodes (Cantilever and fixed electrode in our case) separated by an insulating barrier will attract towards one another if there is an electric potential difference between them. In 1994, Brugger *et al* [15] have reported that the mathematical complication comes from the deflection of the cantilever and the non-uniform electrostatic forces present along its length. Their analysis shows that for small deflection the effective electrostatic force can be assumed at the free end of the cantilever. Therefore, for mathematical simplicity the cantilever free end

and the electrode are assumed as parallel-plates (only small length is effective) in this thesis as shown in figures (5.1) and (5.2).

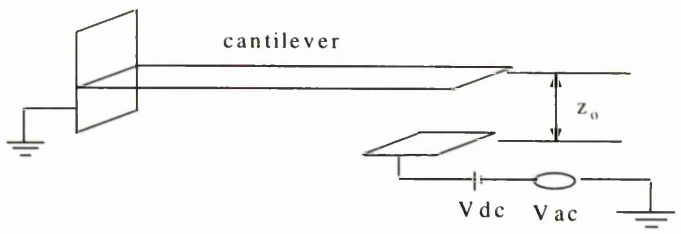

Figure (5-1) Cantilever and electrode configuration.

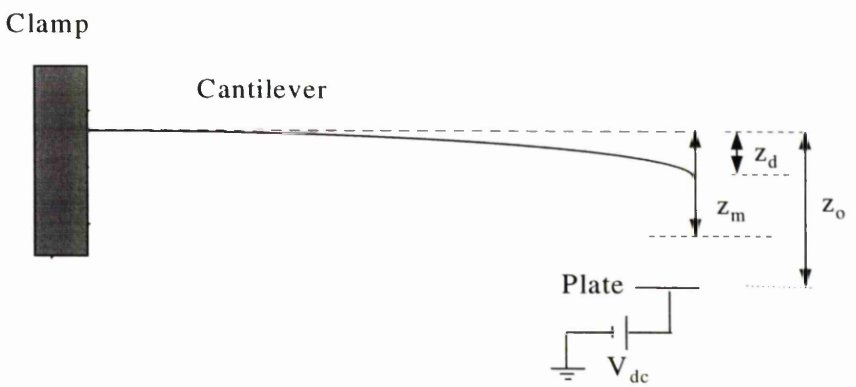

Figure (5-2) Deflection caused by dc voltage.

As can be found in the literature [15,16], the electrostatic force between any parallel -plates is a function of the applied voltage and the capacitance changes with respect to the gap between plates. This force can be expressed as

$$F_{es} = -\frac{1}{2}.V^2 \frac{\partial C}{\partial z} \tag{5.1}$$

In the case of parallel - plates of an area A and gap = z_o as shown in the above figures, the capacitance between two plates can be expressed as [17]

$$C = \frac{\varepsilon_o A}{z_o - z_d} \tag{5.2}$$

Therefore, the electrostatic force is

$$F_{es} = \frac{\varepsilon_o . A}{2.(z_o - z_d)^2} V^2 \tag{5.3}$$

Assuming the excitation voltage as

$$V = V_{dc} + V_m \sin \omega t$$

Thus,

$$F_{es} = \frac{1}{2}\left[V^2{}_{dc} + 2V_{dc}V_m \sin \omega t + \frac{V^2{}_m}{2}(1 - \cos 2\omega t) \right] \frac{\varepsilon_0 A}{(z_o - z_d)^2}$$

$$F_{es} = \frac{1}{2}\frac{\varepsilon_0 A}{(z_o - z_d)^2}\left(V^2{}_{dc} + \frac{V^2{}_m}{2} \right) + \frac{\varepsilon_0 A}{(z_o - z_d)^2} V_{dc} V_m \sin \omega t$$

$$- \frac{\varepsilon_0 A}{2(z_o - z_d)^2} V^2{}_m \cos 2\omega t . \tag{5.4}$$

so $$F_{es} = F_{dc} + F_{ac}(\omega) + F_{ac}(2\omega)$$

Therefore, the total deflection is composed of static deflection due to d.c voltage and dynamic deflection (vibration) due to a.c voltage.

$$D = z_d(\text{static}) + z_v(\omega) + z_v(2\omega). \quad (5.5)$$

Where $$z_v(\omega) = A(\omega)\cos(\omega t + \phi_1). \quad (5.6a)$$

$$z_v(2\omega) = A(2\omega)\cos(2\omega t + \phi_2). \quad (5.6b)$$

5.2.1 Static deflection:

In the static deflection case, the electrostatic force (F_{dc}) and restoring spring constant force (F_{spring}) can be calculated by [16]

$$F_{dc} = \frac{1}{2}\varepsilon_o \frac{A}{(z_o - z_d)^2} V_{dc}^{\ 2} \quad (5.7)$$

$$F_{spring} = k_o.Z_d \quad (5.8)$$

Therefore, the net force ***F*** can expressed as

$$F = F_{dc} - F_{spring} \quad (5.9)$$

where z_d is the deflection distance (see figure 5.2) and k_o is dynamic cantilever spring constant.

In the practical case, there is a maximum value of V_{dc} beyond which no stable equilibrium position exists and the cantilever can no longer withstand the attractive electrostatic force and will ' snap ' into the electrode. This voltage is called the pull-in voltage (V_p). In 1967 Nathanson *et al* [16] described this phenomenon and showed that the equilibrium position of the cantilever occurs when the electrostatic force is counterbalanced by the restoring force of the cantilever spring.

$$F_{dc} - Fspring = 0$$

$$\frac{\varepsilon_o A V_{dc}^2}{0.5(z_o - z_m)^2}\Big|_{V_{dc}=Vp} - k_o(z_m) = 0 \qquad (5.10)$$

The equilibrium position $\mathbf{z_m}$ can be calculated by setting the derivative of equation (5.9) equal to zero

$$\frac{\partial F}{\partial z_m} = -\frac{\varepsilon_o A}{(z_o - z_m)^3} V_d^2(max) + k_o = 0 \qquad (5.11)$$

By solving equations (5.10) and (5.11) together yields

$$z_m = \frac{z_o}{3} \qquad Vp = \sqrt{\frac{8.k_o.z^3{}_o}{27.\varepsilon_o.A}} \qquad (5.12)$$

The effective cantilever spring constant k_1 can be calculated by differentiating equation (5.9)

$$k_1 = \frac{dF_{dc}}{dz} = k_o - \frac{27.\varepsilon_o A}{8.z_o^3} V^2{}_{dc} \qquad (5.13)$$

The above equation shows that the effective spring "constant" is not constant, but varies with applied d.c voltage. The variation in k_1 causes a shift in the resonant frequency from the mechanical resonant frequency $\omega_o = \sqrt{\frac{k_o}{m}} = 2\pi f_o$ to $\omega_{or} = \sqrt{\frac{k_1}{m}}$. The ratio between these frequencies can be expressed as

$$\frac{\omega_{or}}{\omega_o} = \sqrt{\frac{k_1}{k_o}} \approx \sqrt{1 - \left(\frac{V_{dc}}{Vp}\right)^2}$$

The elastic curve of the cantilever due to an electro-static force can be expressed by [17]

$$y(x) = \frac{z_d}{3L^4}\left(x^4 - 4x^3L + 6x^2L^2\right) \qquad (5.14)$$

5.2.2 Dynamic deflection.

The forced vibration of a cantilever due to the driving a.c electrostatic force is

$$F_{ac} = F_{ac}(\omega) + F_{ac}(2\omega)$$

Where $$F_{ac}(\omega) = \frac{\varepsilon_o A}{(z_o - z_d)^2} V_{dc} V_{ac} \sin \omega t.$$

$$\left|F_{ac}(\omega)\right| = \frac{\varepsilon_o A}{(z_o - z_d)^2} V_{dc} V_{ac}. \qquad (5.15)$$

and $$F_{ac}(2\omega) = -\frac{\varepsilon_o A}{4(z_o - z_d)^2} V^2_{ac} \cos 2\omega t.$$

$$|F_{ac}(2\omega)| = \frac{\varepsilon_o A}{4(z_o - z_d)^2} V^2_{ac}. \qquad (5.16)$$

The equation of motion for this system is given by Sarid [17] as ,

$$m\frac{\partial^2 z}{\partial t^2} + \frac{\omega_o m}{QF}\frac{\partial z}{\partial t} + kz = F_{es}$$

where m is the effective mass of the cantilever. QF is the quality factor of the system. For one ω, the equation of motion can be written as

$$\left[k_1 - m\omega^2 + j\frac{m\omega\omega_o}{QF}\right]A(\omega) = F_{ac}(\omega)$$

and (5.17)

$$A(\omega) = \frac{|F_{ac}(\omega)|}{k_1\sqrt{\left(1 - \frac{\omega^2}{\omega^2_{or}}\right)^2 + \frac{\omega^2\omega^2_o}{QF^2\omega^4_{or}}}}$$

Similarly the A(2ω) can be expressed as

$$A(2\omega) = \frac{|F_{ac}(2\omega)|}{k_1\sqrt{\left(1 - \frac{4\omega^2}{\omega^2_{or}}\right)^2 + \frac{4\omega^2\omega^2_o}{QF^2\omega^4_{or}}}} \qquad (5.18)$$

Substituting equations (5.15), (5.16), (5.17) and (5.18) into equations (5.6 a) and (5.6 b), the dynamic deflections (z_v (ω) and z_v (2ω)) can be calculated. The phase angles in equations (5.6 a and b) are given as

$$\phi_1 = \tan^{-1}\left(\frac{\frac{\omega\omega_o}{QF.\omega^2_{or}}}{1-\frac{\omega^2}{\omega^2_{or}}}\right)$$

$$\phi_2 = \tan^{-1}\left(\frac{\frac{2\omega\omega_o}{QF.\omega^2_{or}}}{1-\frac{2\omega^2}{\omega^2_{or}}}\right)$$

5.2.3 Results and discussion.

In performing the calculation, the following dimensions and values were used.

Length	20 mm
Width	2 mm
Thickness t	0.1 mm
Spring constant k_o	4.28 N/m
Gap z_o	60 μm
Quality factor QF	100
Resonance frequency ω_o	1256 Rad
ε permittivity	8.84E-12

Table (5-1). Typical cantilever dimensions.

Figure (5.3) (a and b) shows the calculated static deflection of a cantilever as a function of the cantilever length and different applied d.c. voltages. Figure (5.3a) shows that the static deflection is under the equilibrium position value as d.c voltage is less than the maximum allowable voltage (V_{max} = 71.4 volt in this case). When the applied dc bias exceeds this value the cantilever snaps to the other plate as shown in figure 5.3 b .

Figure 5.4 shows the static deflection as a function of the applied d.c bias . As can be seen from this figure the relation between the dc electrostatic displacement and the applied dc bias is a non-linear behaviour.

Figure 5.5 shows the predicted cantilever vibration as a function of time . The cantilever was excited at resonance frequency. It is clear from this figure that the cantilever response is linear in this case.

Figure (5.6) illustrates the shift in the actual cantilever resonant frequency as function of applied dc voltage. This shift is due to the variation in the cantilever spring constant k_l caused by its dependency on the attractive forces resulting from the electrostatic field . Although this case is correct for small cantilevers where the actual spring constant is very small (i.e. SFM cantilevers , k_o = 0.03-0.5 [18]), it is not easy to notice this shift as the cantilever's dimensions become bigger where k_o = 5 as has been demonstrated by Brugger *et al* [15].

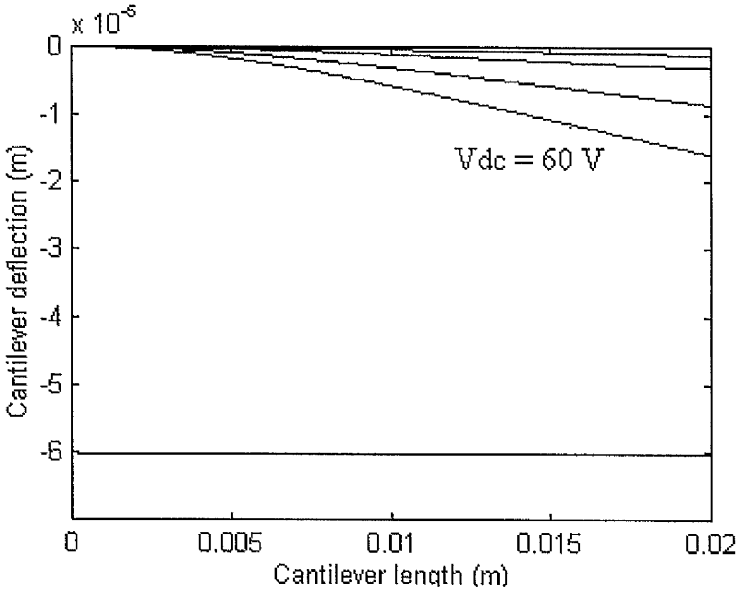

(a)

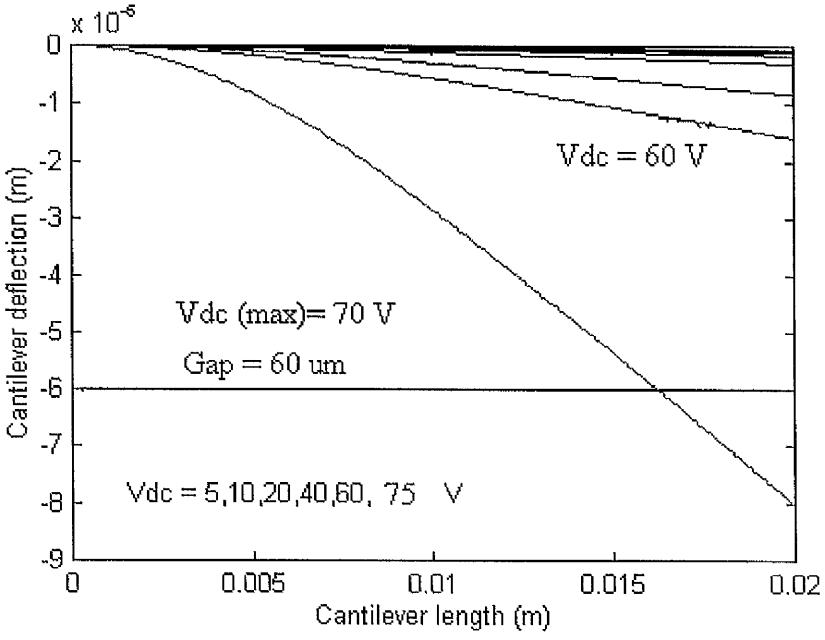

(b)

Figure 5-3 (a,b). Cantilever static deflection as function of the cantilever length.

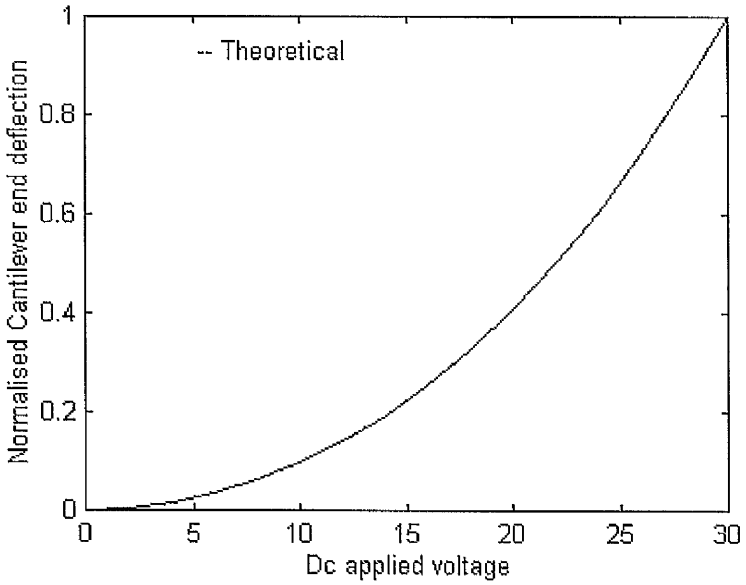

Figure (5-4). Static deflection as a function of applied d.c bias voltage.

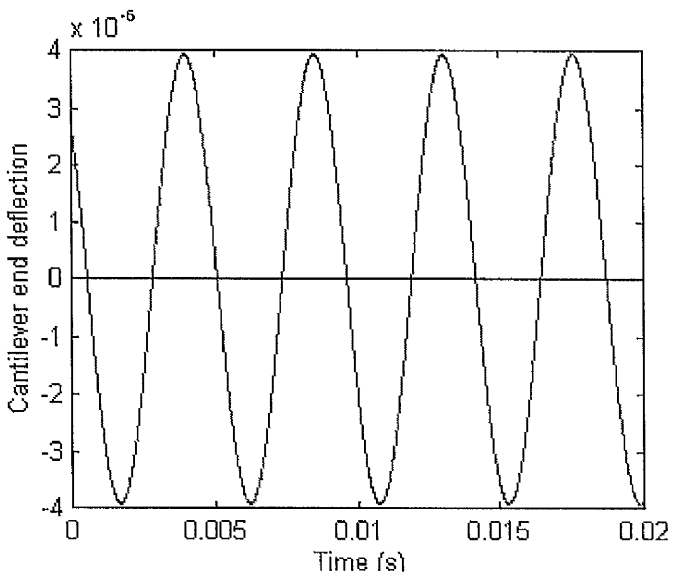

Figure (5-5). The cantilever vibration as a function of time due to excitation voltage (a.c = 6 V and d.c = 4 V).

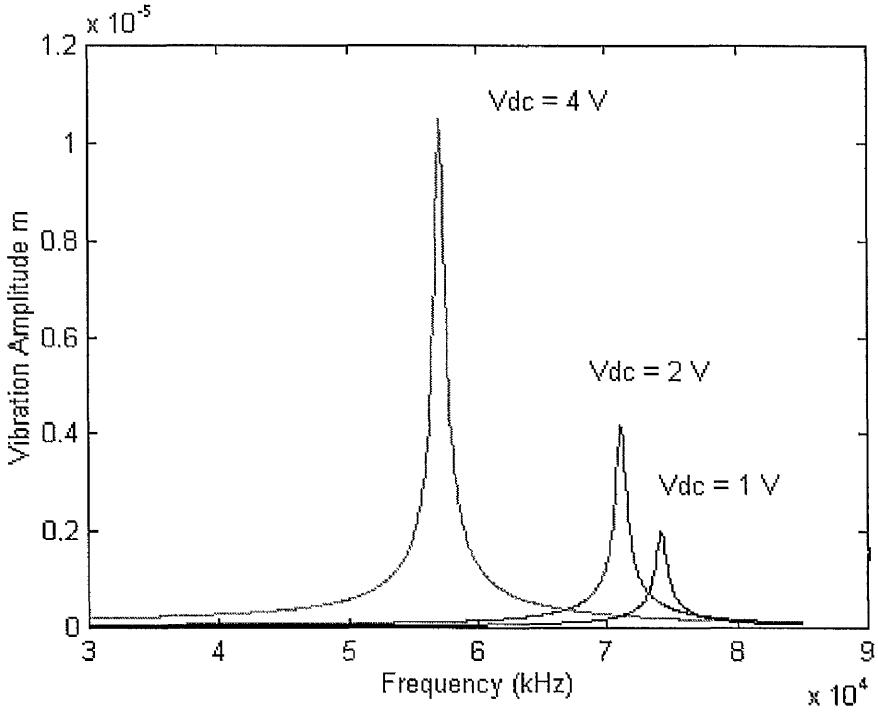

Figure (5-6). Cantilever vibration amplitude as function of the excitation frequency and dc voltage for constant ac drive voltage.

Figure (5.7) describes the effects of varying the changing field for a given dc bias field. It is clear that the actuation system is linear at low ac field, and the system starts to deviate from the linearity as varying ac field is increased. This is probably due to the enhancement of the second cantilever frequency as can be seen from figure (5.8). The linear response can be realised if the square root of the total drive field is applied as can clearly be shown by figure (5.9).

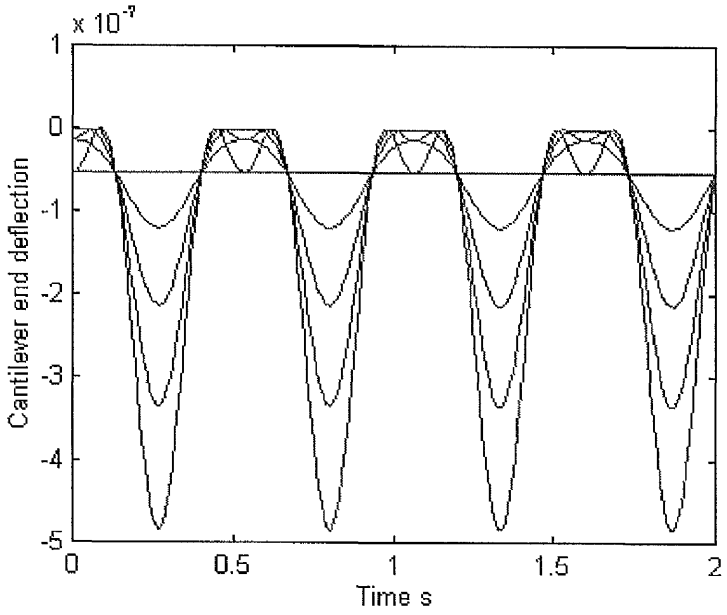

Figure (5-7) The predicted cantilever vibration as function of the a.c voltage (0,1,4,5,7 V) with V_{dc} = 4 V and f = 2 Hz.

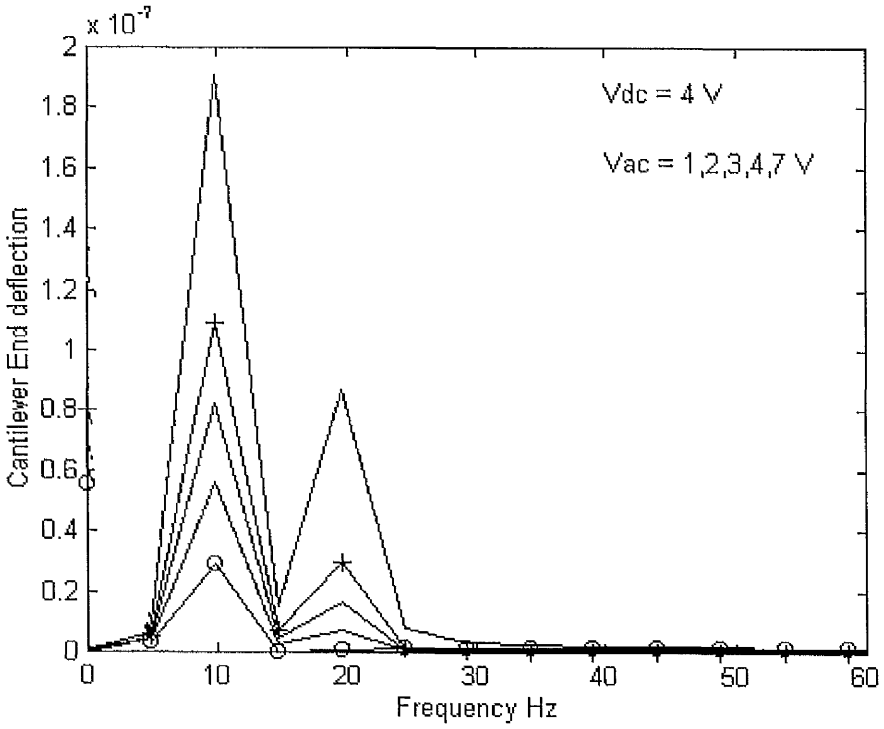

Figure (5-8) Spectrum of cantilever deflection signal showing the first and second frequencies.

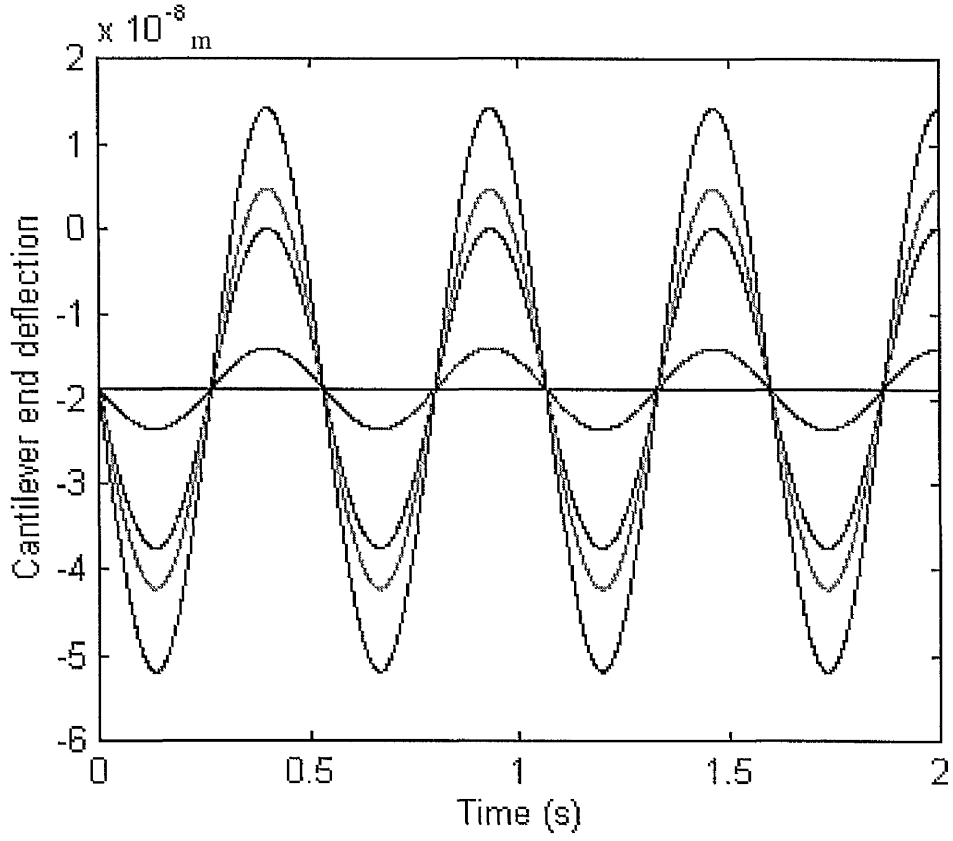

Figure (5-9) The predicted cantilever vibration as function of the a.c voltage (0,1,4,5,7 V) with $V_{dc} = 4$ V and f = 2 Hz. Using square rooter.

5.3 Experimental investigation.

In order to investigate experimentally the behaviour of the cantilever when excited by an electrostatic force the following situations were taken into consideration.

- Study the static deflection when only a d.c. bias voltage is applied.
- Study the dynamic deflection (vibration) when a d.c. and an a.c. voltage are applied.

- Investigation of the non-linear behaviour.

5.3.1 Experimental set up.

In the electrostatic drive, two parallel plates are separated by an air gap. One plate is usually fixed (electrode) and the other (Cantilever) is free to move as shown schematically in figure (5.10). To study the behaviour of the electrostatic actuation, a small cantilever was used. The cantilever was fabricated from a glass with 20 mm x 2 mm x 0.11 mm dimensions. The cantilever is coated with a 75 nm permalloy film to provide a good optical reflector (permalloy is nearly 80% nickel and 20% iron). Permalloy was chosen because it has good properties of reflection and easy to stick with the glass cantilever.

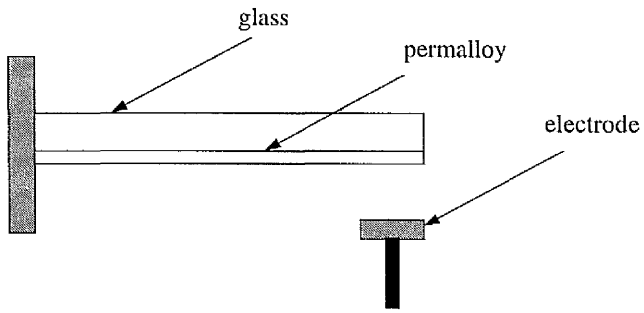

Figure (5-10) Experimental cantilever and electrode configuration.

Due to the attractive nature of the electrostatic device and the interacting behaviour between the two electrodes, it is very difficult to estimate the initial gap between them. Therefore, a series of experiments were carried out to estimate the initial gap and to make a comparison with the theoretical work presented in the previous section. Initially the gap was estimated by the vertical movement of the

electrode. The electrode movement was calibrated mechanically by attaching a small scaled wheel at the bottom of the electrode. This wheel is divided into equal sectors with 15 μm each. The experimental arrangement used in this work is depicted schematically in figure (5.11).

5.3.2 Static deflection.

In this experiment the gap is assumed to be that given by the wheel scale (15, 30, 45 μm). While the gap is assumed, the applied d.c. voltage is varied from 0 to 30 V. The cantilever deflection was monitored optically using the optical beam deflection method measured by the FLUKE 8000 A multimeter. The measured values show the expected V^2 behaviour. Figure(5.12) shows the measured data together with predicted values for a given gap. The results obtained show that the agreement between predicted and measured data is good.

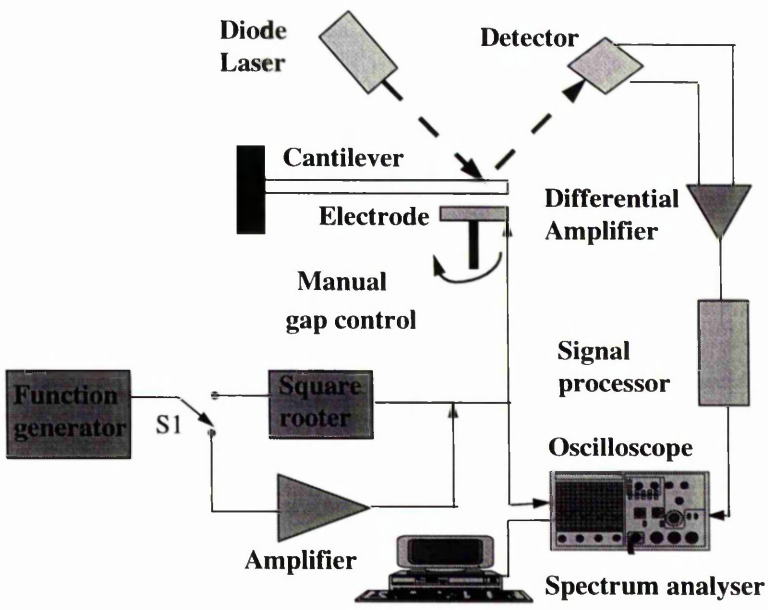

Figure (5-11) Experimental arrangement.

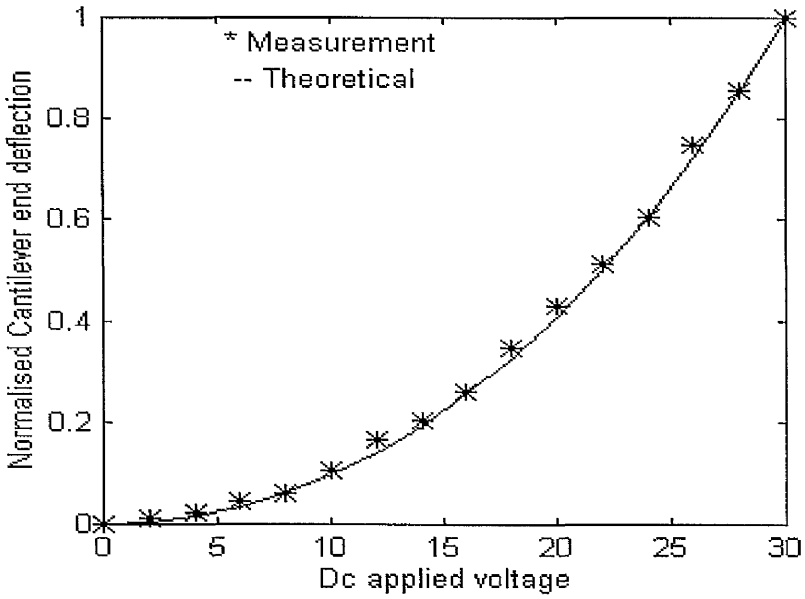

Figure (5-12). Static deflection curve of the cantilever as a function of the applied d.c. voltage with an estimated gap = 60 μm.

5.3.3 Dynamic deflection

In this section the dynamic behaviour of the cantilever is described. To analyse the dynamic cantilever behaviour the set-up given in figure (5.10) was used. The cantilever is deflected electrostatically by driving the fixed electrode by constant dc voltage and varying ac voltages using a function generator (Jupiter 2000). For this work sinewave and triangular excitation signals with frequency equal to 2 Hz were used. The low frequency value was used to represent the real movement of the cantilever when the micropositioning is undertaken. The signal from the photodetector was amplified and filtered using a simple RC filter with a cut off frequency greater than ten times the fundamental frequency of the output signal in

order to cancel the 50 and 100 Hz noises. The signal was monitored using a HAMEG 20 MHz Storage Scope HM 205-3 and sampled by a PC 30 PG A/D converter and its FFT was obtained The following figures illustrate the cantilever behaviour when it is statically deflected by applying 4 V dc voltage and dynamically vibrated by varying ac voltages from 0 to 8 V. As can be seen from these figures the cantilever has non-linear behaviour as expected by the theoretical model described in previous section.

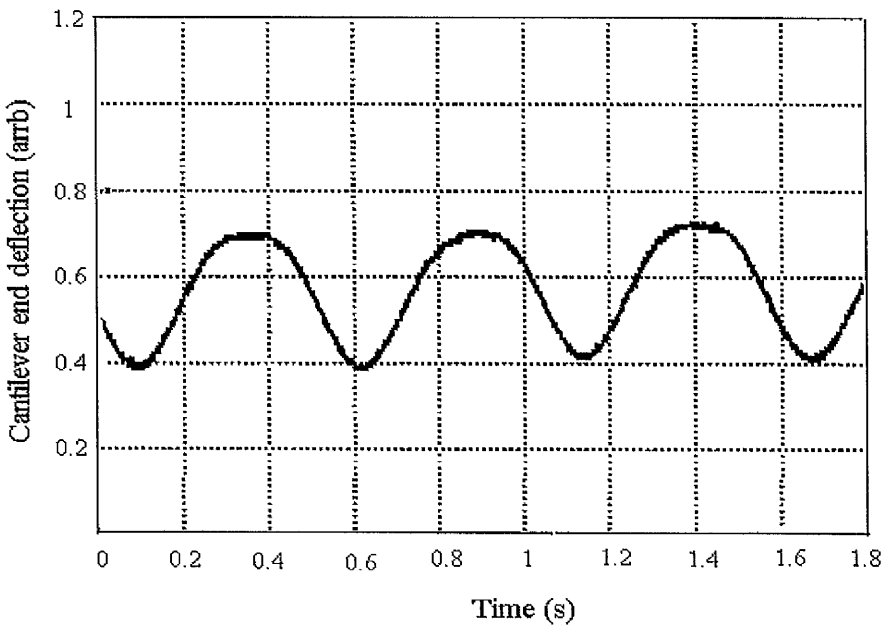

Figure (5-13) Cantilever dynamic deflection (V_{dc} = 4 V and V_{ac}= 2 V) sinewave signal

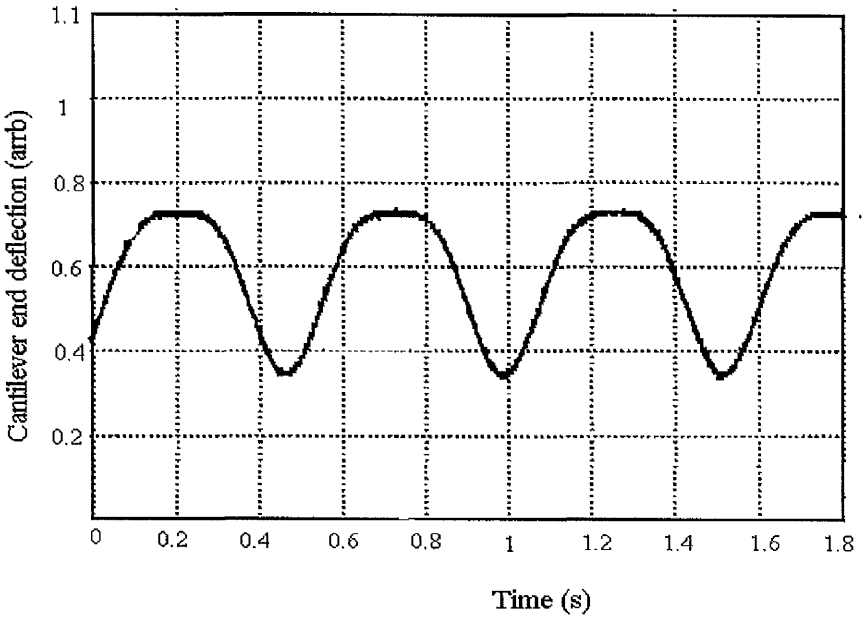

Figure (5-14) Cantilever dynamic deflection (dc = 4 V and ac = 4 V).

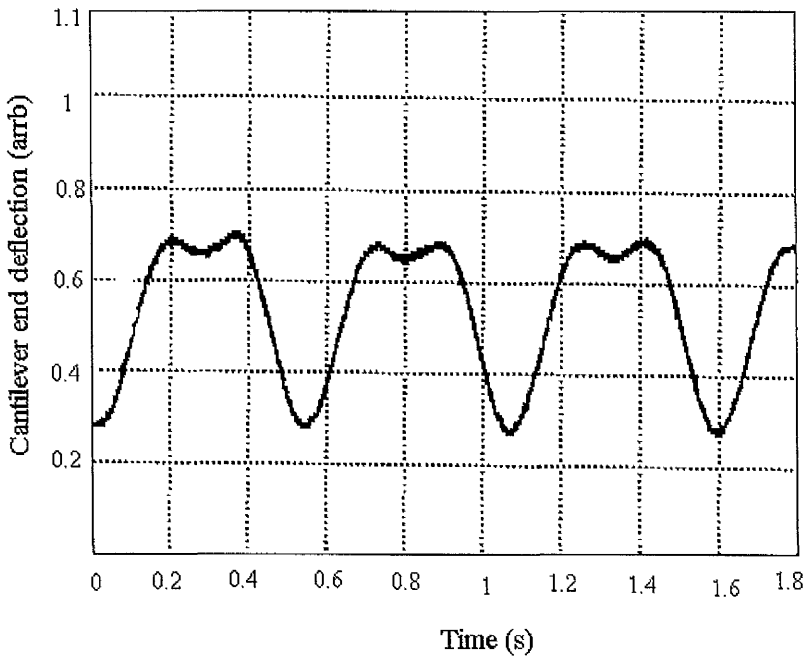

Figure (5-15) Cantilever dynamic deflection (dc = 4 V and ac = 6 V).

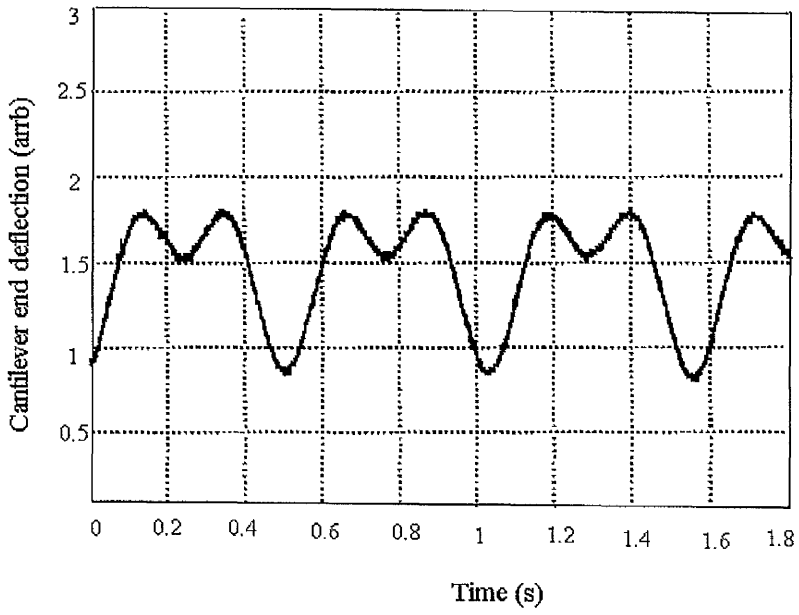

Figure (5-16) Cantilever dynamic deflection (dc = 4 V and ac = 8 V).

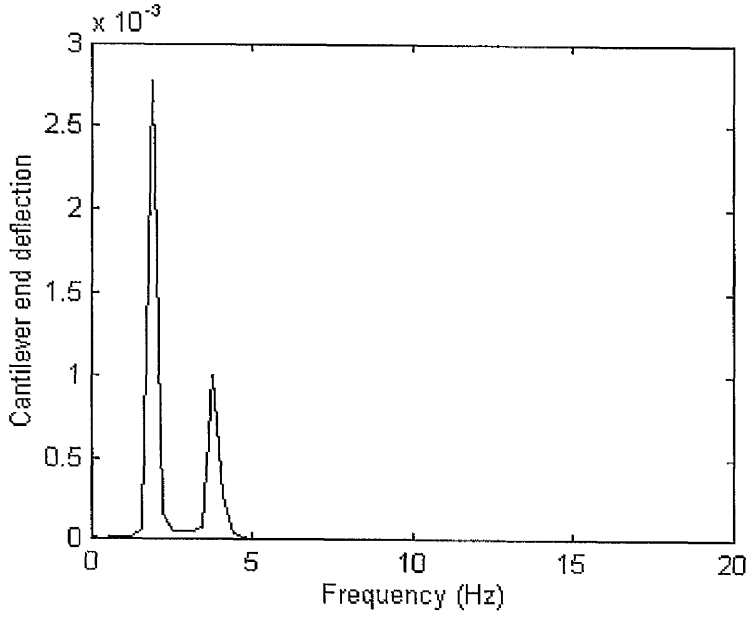

Figure (5-17) Power Spectrum of deflection cantilever signal (dc = 4 V and ac = 8 V)

5.4 The use of square rooter.

The square rooter circuit (MPY 634 kp) shown in figure (5.18) was used to investigate the problem of linearisation of the cantilever behaviour whilst actuated by a d.c. and an a.c. signals. Since the electrostatic interaction between the cantilever and the electrode introduces a V^2 law, a linear behaviour is to be expected by square rooting the input signal before applying to the cantilever. The experimental results given in the following figures (5.19-5.23) show (for two input waveforms) that if the square root of the total drive field is applied then the cantilever response is linearised as predicted from theoretical considerations .

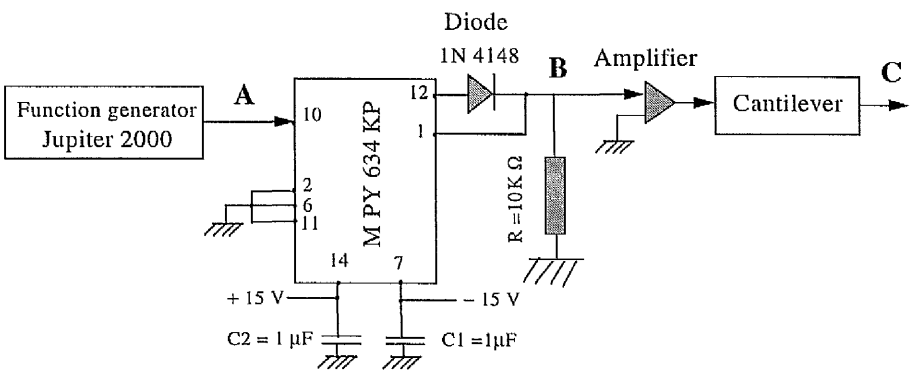

Figure (5-18) The square rooter circuit diagram.

Figure (5.19) shows the cantilever behaviour (Sinewave input signal) as a function of time when the square rooter circuit was used. It is clearly seen that the cantilever behaviour is linear as expected from the theoretical model. The effect of the square

root operation can be clearly seen from the spectrum in Figure (5.20). This figure shows that only the excitation frequency is produced.

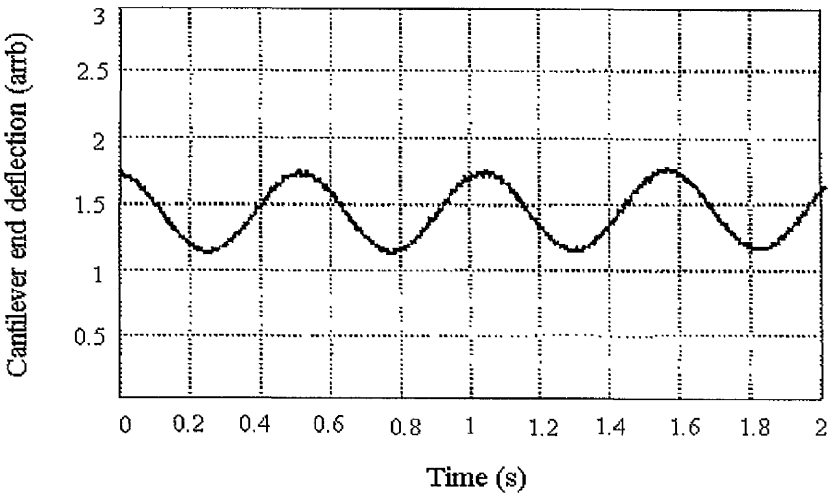

Figure (5-19) Cantilever behaviour after square rooter is used (sinewave signal). At point C in figure (5.18). (dc = 4 V and ac = 8 V)

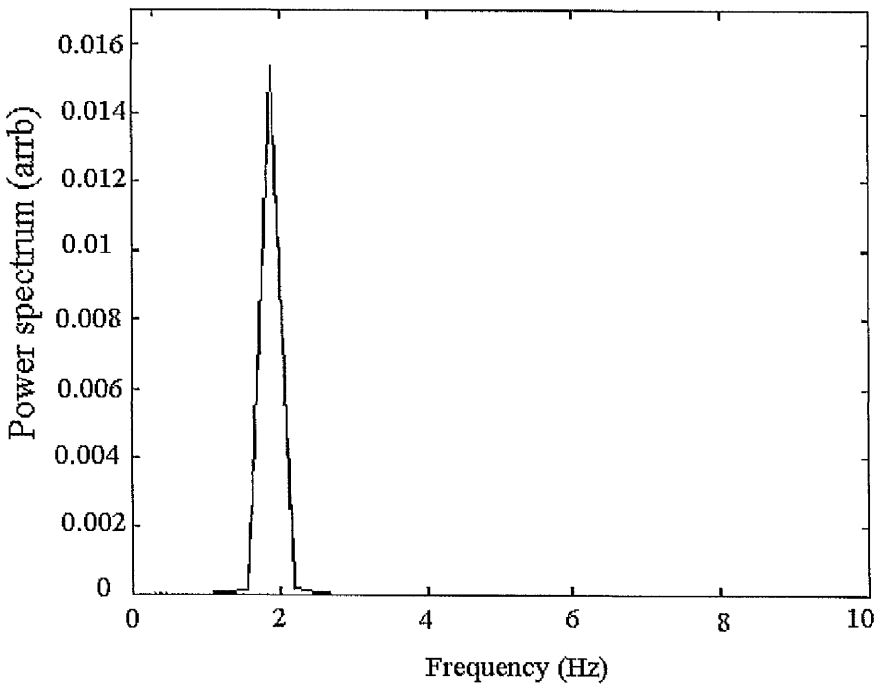

Figure (5-20) The power spectrum of the above signal.

Figures (5.21), (5.22) and (5.23) describe the same results for the triangular input signal. The triangular signal is used to represent the true behaviour of the cantilever when it is used in micropositioning applications. Figures (5.21) and (5.22) illustrate the drive signal (Triangular) (point A) output of the square rooter (point B) and the cantilever response (point C) . Again similar results were obtained as can be clearly seen from figure (5.23).

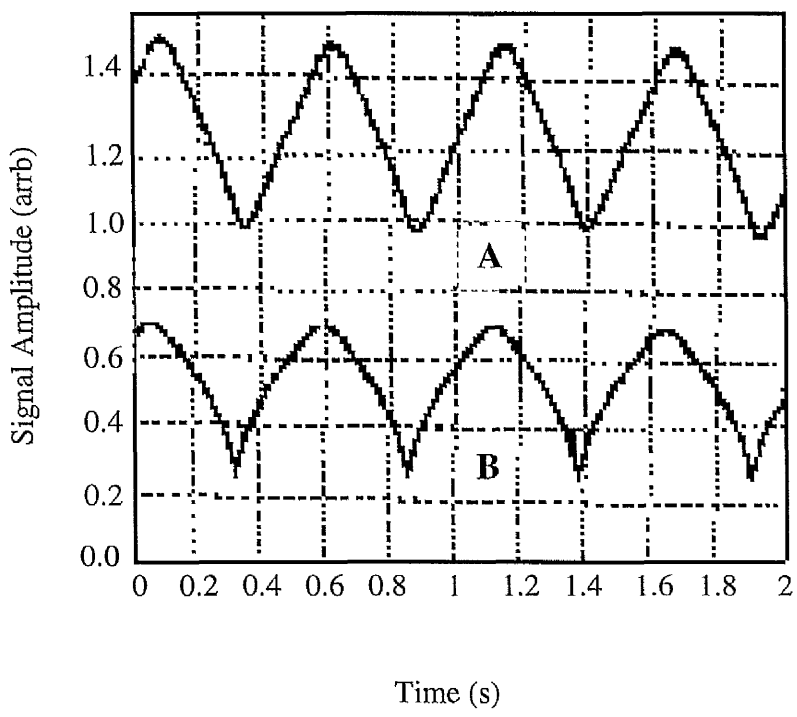

Figure (5-21). Input (point A) and output (point B) of the square rooter circuit.

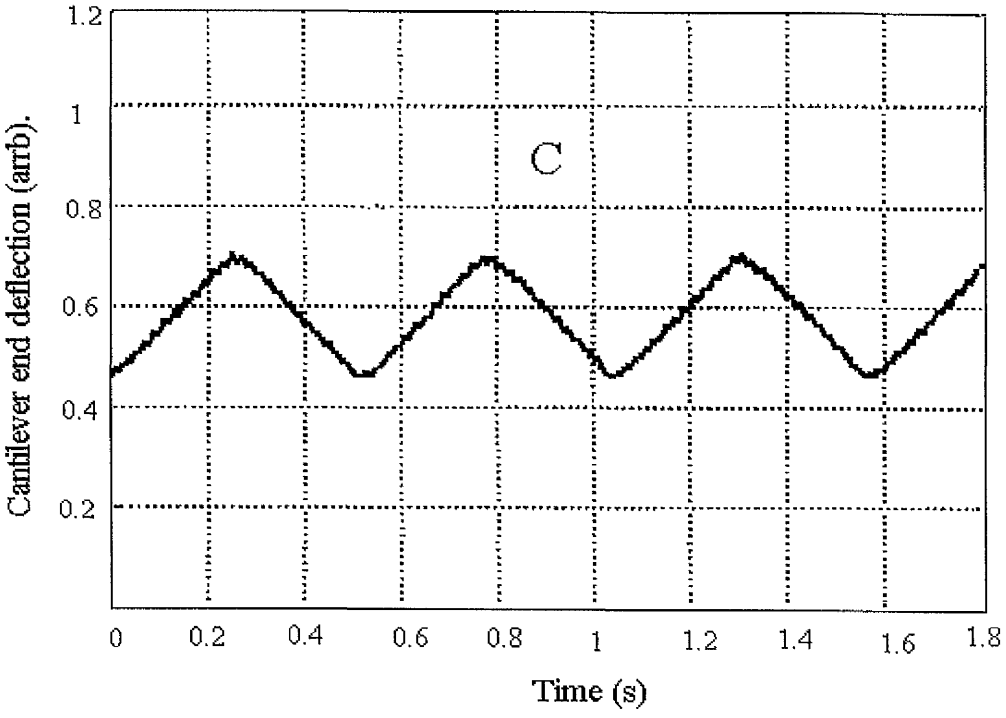

Figure (5-22) Cantilever behaviour after square rooter is used (triangular input signal).Point C in figure (5.18).

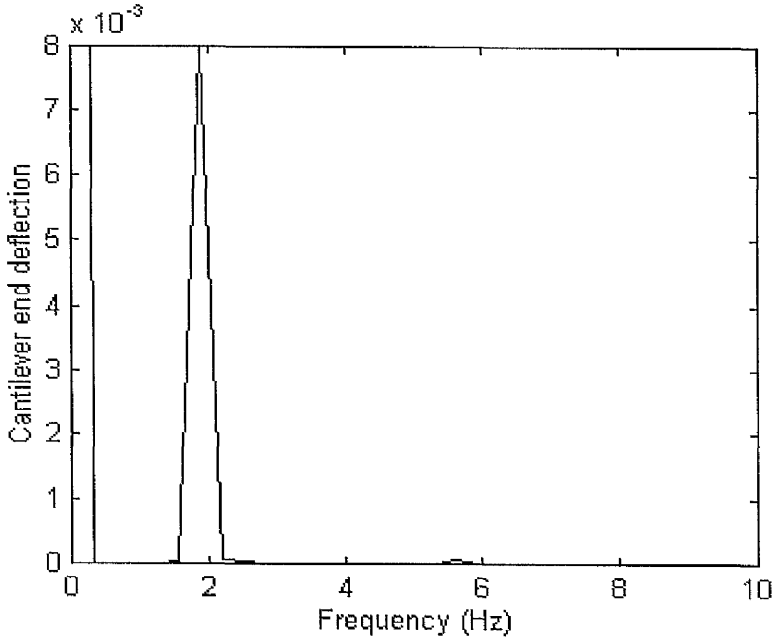

Figure (5-23) The power spectrum of cantilever behaviour.

5.5 Summary.

The performance of the electrostatic actuator with applied dc and ac voltages is theoretically and experimentally demonstrated. This study is carried out to investigate the ability of this type of actuation and its use in micropositioning applications . The results produced show that the agreement between the theoretical and experimental data is very good. The non-linear characteristic was also investigated and linear behaviour is produced by means of a square root circuit.

5.6 References.

[1] Price, R.H, Wood, J.E and Jacobsen, S.C " Modelling of electrostatic forces in small electrostatic actuators" Conference Title: Technical Digest- IEEE Solid State and Sensor and Actuator workshop, USA, 1988, p 131-135.

[2] Ward, M.C.L and King, D.O " Comparison electrostatic and magnetic actuation for micromechanical systems" Conference Title: IEE Science, Education and Technology Division Colloquium on Active Drives for Microengineering Application, UK, 1995, pp 4-10.

[3] Cunningham, M.J, Jenkins, D.F.L, Clegg, W.W and Bakush, M.M, " Active vibration control and actuation of a small cantilever for applications in scanning prope instruments", *Sensors and Actuators*, A 50 (1995), pp 147-150

[4] Busch, V. I. J " The case for magnetically driven microactuators" *Sensor and Actuators* **A(33),** 1992, pp 207-220.

[5] Gardner, J.W and Hingle, H.T " *Developments in Nanotechnology*" Volume **1**, " From Instrumentation to Nanotechnology " pp 301-317.

[6] Wood, D, Burdess, J.S and Harris, A, J " Actuators and their mechanisms in microengineering" *IEE digest no: 96/110*, 1996.

[7] Lang, J.H, Schlecht, M.F and Howe, R.T " Electric micromotors: electromechanical characteristics" Proc. *IEEE Micro Robots and Teleoperators Workshop*. Hyannis. MA USA, 1987, pp 9-11.

[8] Trimmer, W.S.N and Gabriel, K.J " Design considerations for a practical electrostatic micro-motor ", *Sensor and Actuator*, Volume **11**, 1987, pp 189-206.

[9] Erlandsson, R , McClelland, G.M , Mate, C.M and Chiang, S " Atomic force microscopy using optical interferometery ", *Journal of Vacuum Science and technology*, A **6** (2) , Mar/Apr (1988), pp 266- 270 .

[10] Fan, Tai, and Muller, " IC-processed Electrostatic micro-motors" Proc, 1988 IEEE Int, *Electro Devices Meet.,* IEEE Electron Devices Soc., San Fracisco CA., 1988, pp 666-669.

[11] Branedbjerg and Gravesen, " A New Electrostatic Actuator providing improved length and force" , proc *IEEE workshop on microelectromech.* Sys., 1992, pp 6-11.

[12] Huff ,Mettner, Lober and Schmidt, " A pressure- balanced elecrostatically-actuated microvolve", *Technical Digest of the IEEE Solid-State Sensor and Actuator workshop*, Hilton Head, SC, 1990, pp 123-127.

[13] Zengerle, Richter and sandemaier, " A Micro Membrane Pump with electrostatic actuation", *proc, IEEE workshop on microelectromech. Sys.*, 1992, pp 19-24.

[14] Cunningham, M.J, Jenkins, D.F.L and Khalid, M.A.Hj, " Cantilever vibration control by electrostatic actuation for probe microscopes " *Submitted to Sensors and Actuators* 1996.

[15] Brugger, J, Blanc, N, Renaud , Ph and de Rooij, N.F " Microlevel with combined integrated sensor/actuator functions for scanning force microscopy " *Sensors and Actuator A*, Volume **43** , 1990, pp 339-345

[16] Nathhanson, H.C, Newell, W.E, Wickstrom, R.A and Davis, J.R ," The Resonant Gate Transistor " *IEEE Transactions on Electron Devices* , Volume, ED - 14 , No 3, March 1967, pp 117-133

[17] Sarid, D, " Scanning force microscopy with applications to electric, magnetic and atomic forces." Oxford University Press, New York, 1994.

[18] Park Scientific Instruments Inc, 1171 Borregas Ave, Sunnyvale, CA 94089, USA.

Chapter 6

6. Further experimental work on sensors and actuators for active vibration control :

6.1 Introduction:

After the analysis of the possible methods of exciting, sensing and measuring the cantilever vibration given in chapter 2, different active techniques to control unwanted cantilever vibration have been investigated experimentally in this chapter. For control and actuation purposes a single piezoelectric element has been deposited onto the cantilever close to the root (clamped end). The employment of suitable actuation permits a substantial reduction in the instrument size and cost whilst maintaining the ability to control the cantilever deflection. The piezoelectric materials are chosen as actuators for their suitability as discussed in chapter 2, and their ability to cover a wide range of the structure's resonant frequencies. The overall control performance is not determined by the actuator alone, but also by the sensor measuring the response of the system. Generally, the position of the sensor within the control loop has to be chosen carefully to ensure the immediate and accurate sensing of the wanted parameter and to detect all influences on the system. In addition to the optical beam deflection method used in Chapters 4 and 5, the following methods have been selected for investigation.

(a) the capacitance detection method.

(b) the piezo-element detection method.

6.2 The capacitance detection method.

6.2.1 Design of the detection system:

The main components of the capacitance -detection device can be designed as described below.

6.2.1.1 Mechanical design.

Based on a three nearly equally spaced parallel plates a differential capacitance transducer was constructed as shown schematically in figures (6.1 and 6.2). The position of each of the two outer electrodes is fixed with respect to the other, and a third common, electrode moves relatively towards them. A displacement of the middle plate causes one of the two capacitances so formed, say C_1 to increase and the other, C_2 to decrease. When this transducer forms the variable arms of a bridge circuit, it forms a differential sensor which has major advantages. So, both these arms are close together and have nearly the same response to environmental changes, greatly increase transducer stability and double the output. Other advantages are improved linearity and reduced excitation forces. Aspects of the design and performance of a capacitance displacement sensor in bridge circuits have been discussed by many authors, for example Hugill [1], Garratt [2] and Jones and Richards [3]. A theoretical consideration of this type of transducer is reviewed in chapter 2 .

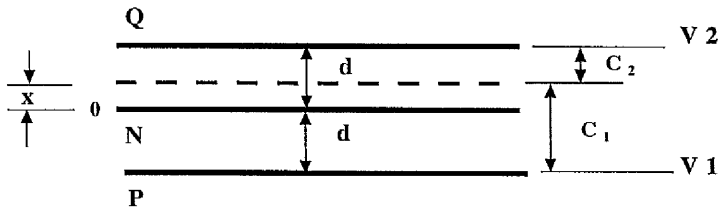

Figure (6-1). Capacitance displacement transducer.

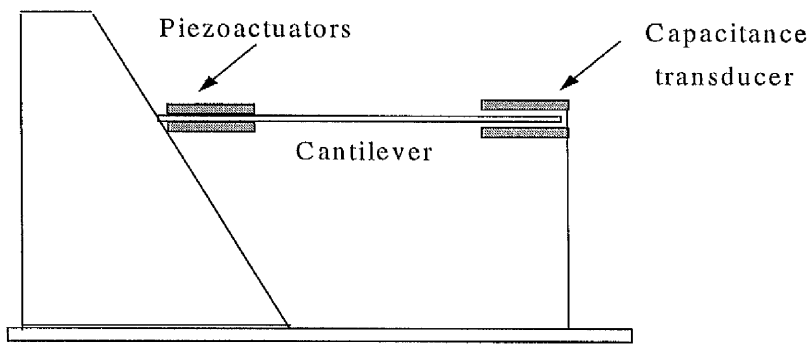

Figure (6-2). Mechanical mounting of the transducer.

6.2.1.2 Electronic design:

(a) Design considerations:

When using capacitance techniques the measuring circuits should have [4]:-

a) low drift

b) high and stable sensitivity.

c) immunity to temperature variations.

d) immunity to stray capacitances.

e) high measurement frequency, for example 20 kHz.

b) System block diagram:

The block diagram of the system built in this project is given in figure 6.3. The transducer was housed in a metal screened box. The three plates were left floating whilst the transducer supports and the screen were all earthed to the common point with the electronic circuit. Capacitive systems generally require well designed processing electronics to detect the small capacitive changes and unless properly shielded pick up stray signals.

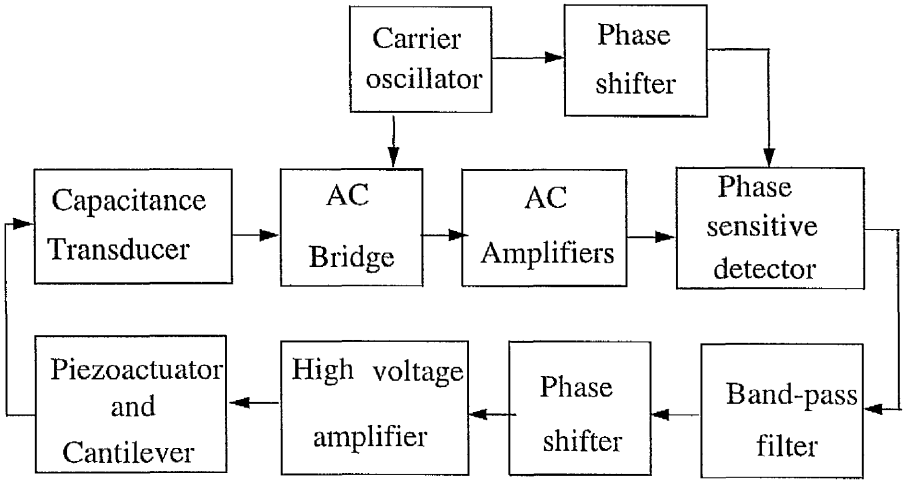

Figure (6-3). System block diagram.

To measure the variations in the capacitance transducer due to cantilever vibration, an AC bridge, given in figure (6.4), was used [5]. The transducer constituted the two arms of bridge C_1 and C_2 and was driven by the carrier oscillator. To satisfy the bridge balance conditions, two variable resistors were used. C_3 was used to achieve a final balance point. The transducer signal modulated by the carrier frequency appears at the bridge output. This waveform was then amplified, demodulated and fedback to the piezoactuator through phase shifter and a high voltage amplifier as shown in figure 6.3.

Although the balance conditions for an ideal bridge are independent of the impedance to earth, the sensitivity to inbalance will depend on any impedance to earth across the bridge output unless a detector amplifier with a very low input impedance is used (current detector).

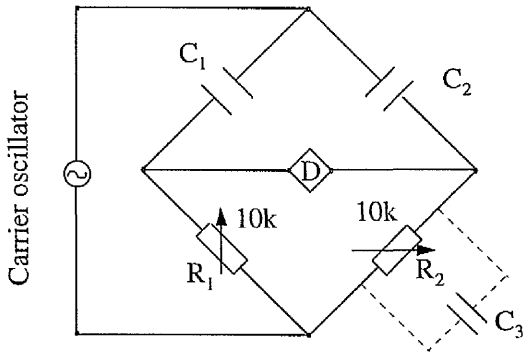

Figure (6-4). A.C bridge arrangement.

6.2.2 Experimental investigation.

For this thesis a flexible aluminium cantilever beam was used to demonstrate the feasibility of using a capacitance transducer and piezoelectric actuator in an active control loop to suppress the beam vibrations. The control law was based on constant gain feedback. The cantilever was excited using a loudspeaker. For the constant-gain controller, the gain was set so that the maximum voltage would not exceed the breakdown voltage of the piezoelectric actuator. The transducer has been designed so that it can detect very small displacements. The sensitivity of this sensor was 0.012 V/μm [6]. The experimental cantilever beam used is shown in figure (6.5).

Two piezoelectric elements were bonded to the upper and lower faces of the cantilever near the root using a quickset epoxy resin hardener adhesive. The

polarisation axes of these plates were arranged to give effect in the same direction. The natural frequency of free vibration of the cantilever was 25 Hz.

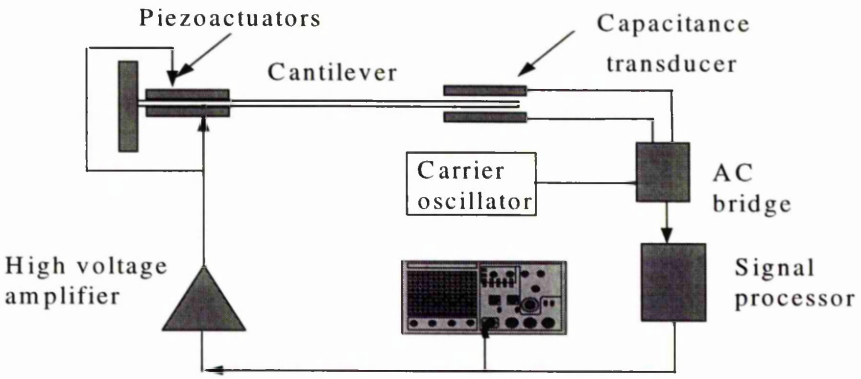

Figure (6-5). Schematic experimental arrangement.

6.2.3 Experimental results.

In this experiment, the cantilever and piezo-actuators dimensions used are given in the following table

Dimensions	Cantilever	Piezoactuator
Length mm	250	40
Width mm	17	17
Thickness	1.5 mm	25 μm

Table (6-1). The cantilever and piezoactuator dimensions used in the experimental investigation.

The typical decay envelope after switching off the loudspeaker of an uncontrolled cantilever is shown in figure (6.6). The damping ratio was equal 0.0185.

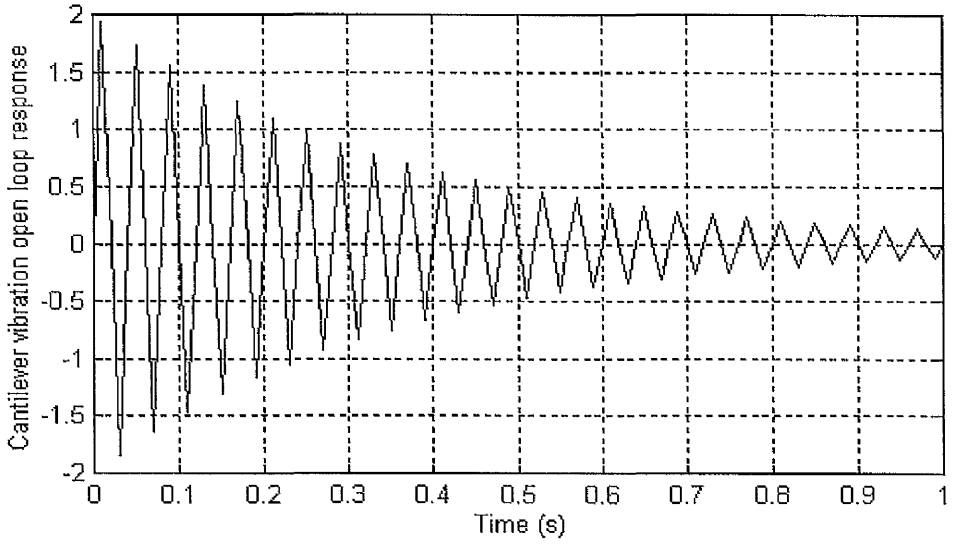

Figure (6-6). The open loop response.

Figure (6.7) shows the effect of the feedback control signal. It is clear that the vibration was damped faster than at open loop. The damping ratio in this case was equal 0.0318.

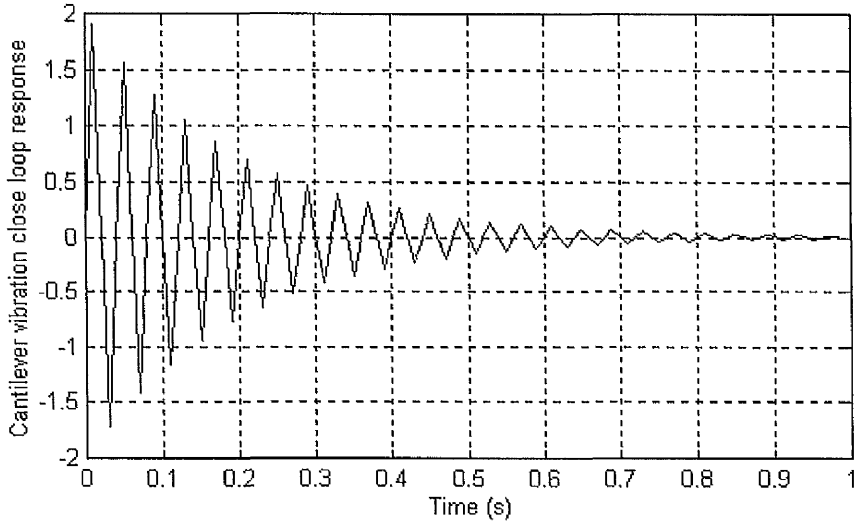

Figure (6-7) Closed loop response.

Figure (6.8) represents the effect of increasing the feedback signal gain. It can be seen from this figure that the cantilever vibration is damped quicker than in the first case due to an increase in the damping ratio. In this case the damping ratio was 0.089.

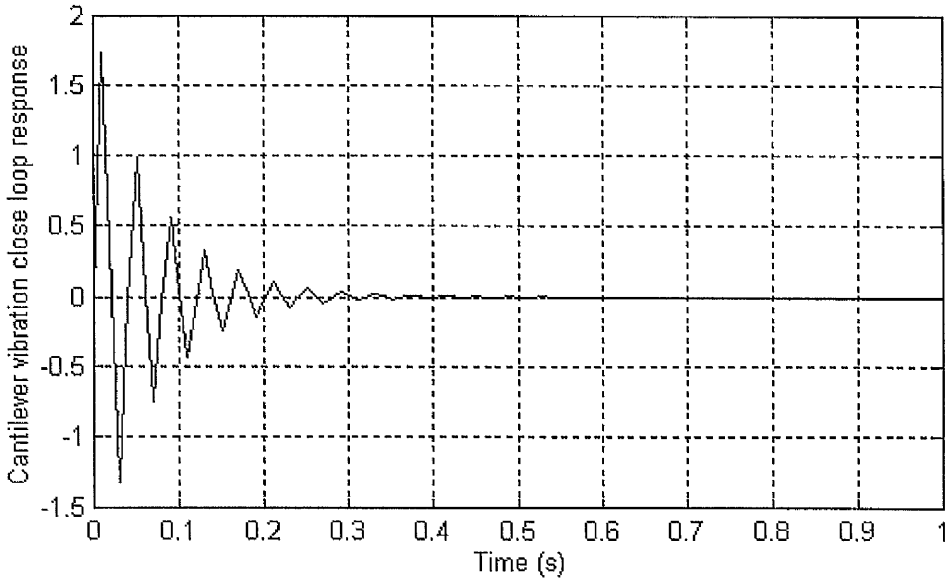

Figure (6-8) Closed loop response at higher feedback signal .

The damping ratio can be calculated by two methods (from graphs)

a) The time constant method.

The damping ratio is defined as

$$\zeta \omega_n = 1/T$$

The envelope has the exponential decay as shown in figures 6.6-6.8

The time constant is defined as the time which makes the exponent of e equal to -1 .

In an open loop case, the time constant T was

$$T = 0.33 \text{ s} \quad \zeta \omega_n = 3.03 \quad \zeta = 0.0185$$

For a closed loop (figure 6.7): $T = 0.23$ s $\zeta\ \omega_n = 5$ $\zeta = 0.0318$

For a closed loop (figure 6.8) : $\zeta\ \omega_n = 7$ $\zeta = 0.089$

6.3 Piezoelectric detection method.

Several experiments were carried out using the piezoelements as sensor and actuator. The configuration of the test structure is shown in figure (6.9). The cantilever vibrations were excited by small a loudspeaker. In this experiment the PVDF film was used as a sensor because of its high piezoelectric voltage constant (g_{31}), and a piece of PZT (Ceramic) was used as an actuator due to its higher piezoelectric charge constant (d_{31}). The sensor and actuator are located at the clamped end where the curvature of the deformed cantilever and the electromechanical coupling are at a maximum.

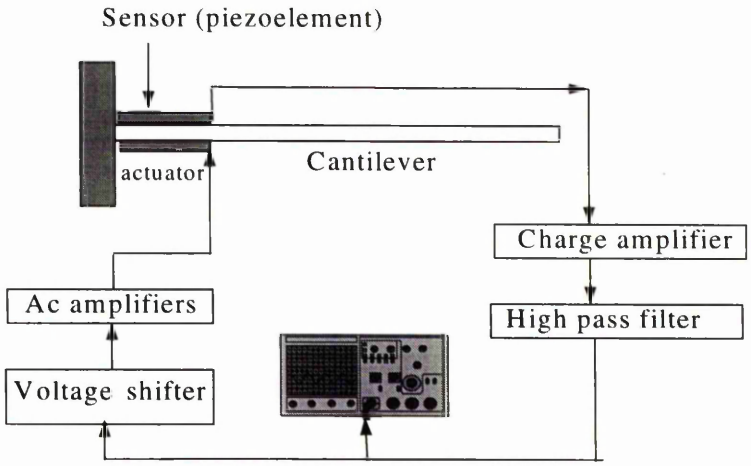

Figure (6-9). Active analogue control cantilever arrangement.

6.3.1 System calibration.

To implement the effective vibration control in removing the cantilever vibrations, the sensitivity of the measured system must be calibrated. The system was calibrated in these experiments using a PZT bimorph element. The end deflection, Δx, of a such a series of bimorph elements may be determined from its physical properties and the exciting voltage. This is given by [7]

$$\Delta x = \frac{3d_{31}L^2}{2t_p^2} V,$$

Figure (6.10) shows the relation between the bimorph end deflection and the sensor output. As can be seen from this figure the system sensitivity is in the range of less than 1nm .

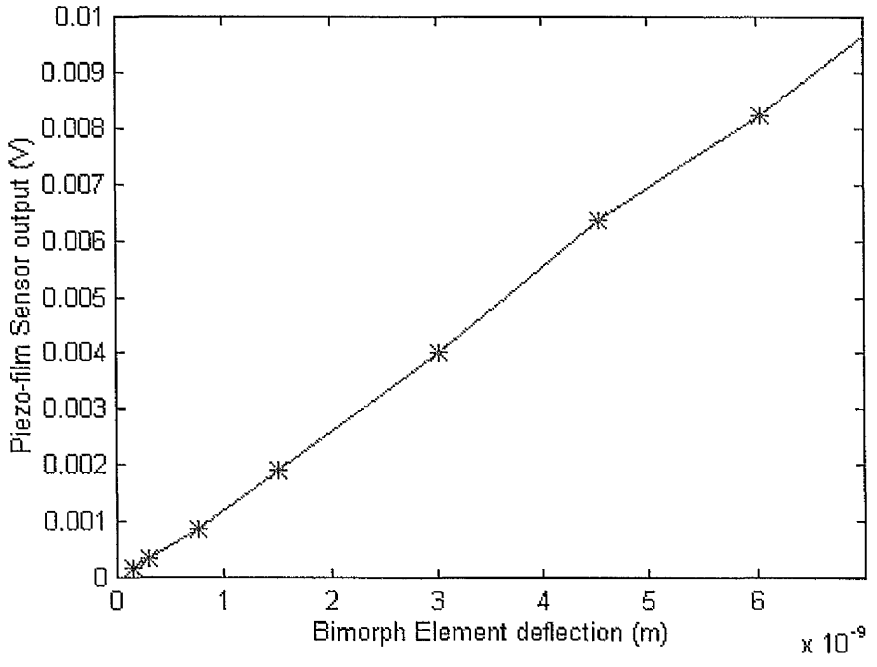

Figure (6-10). System calibration.

6.3.2 Control strategy.

A number of feedback strategies have been proposed for active vibration control [8 -11]. In this study a constant gain feedback control algorithm is implemented by an analogue loop. The output of the sensor (conditioned by a charge amplifier) is fed to the actuator through the ac-amplifier and thus suppresses the vibration as seen in figure (6.11). The charge amplifier is a current operated circuit with zero input impedance which results in no voltage being generated across the piezoelement. The charge amplifier quickly soaks up charges developed on the piezo-sensor.

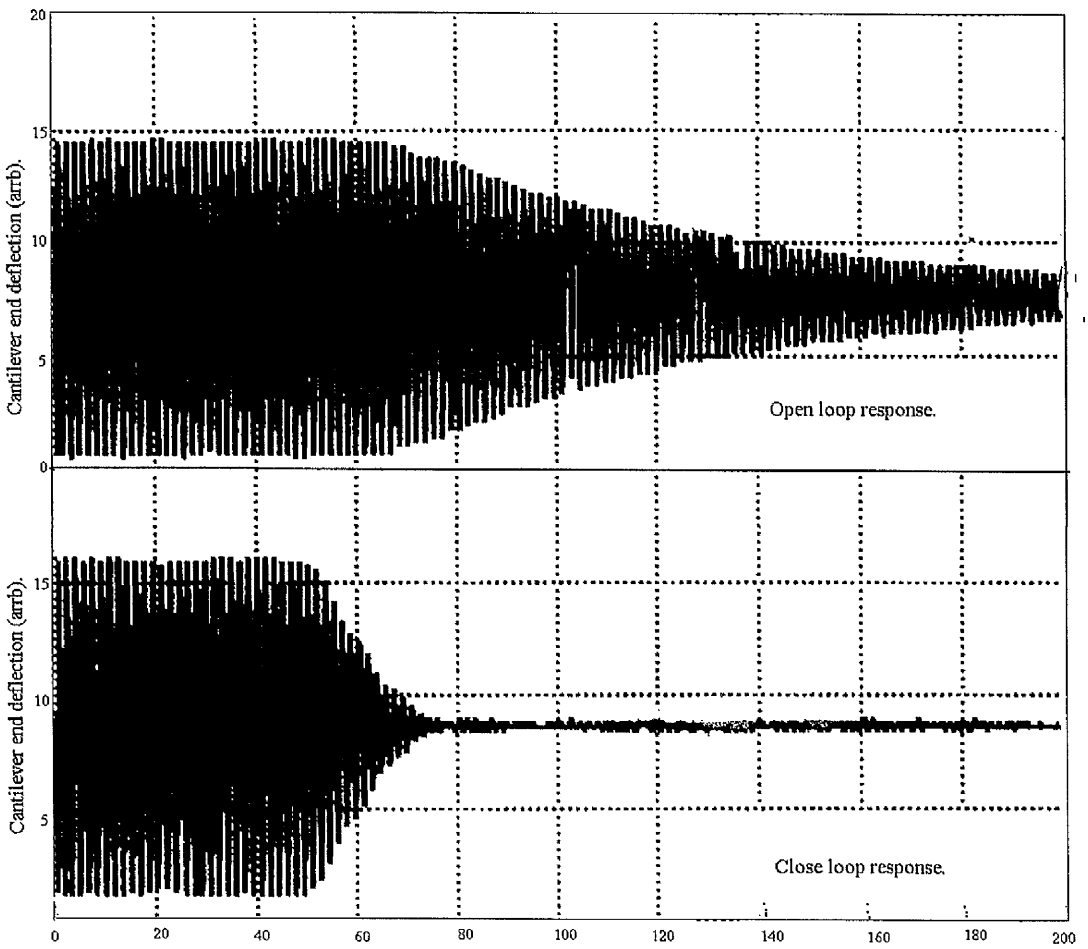

Figure (6-11) Open and close loop response. Using piezoelectric sensor.

6.4 References.

[1] Hugill, A.L "Displacement transducers based on reactive sensors in transformer ratio bridge circuits" *Journal Physics E .Scientific Instrumentation* ,Volume **15**, pp 597-605, 1982.

[2] Garratt, J.D " Survey of displacement transducers below 50 mm", *Journal Physics E .Scientific Instrumentation*, 1979, Volume **12**, pp 563-573.

[3] Jones, R.V and Richards, J.C.S " The design and some applications of sensitive capacitance micrometres", *Journal Physics E .Scientific Instrumentation*, 1973, Volume **6**, pp 589-600.

[4] Huang, S,M, Stott, A.L, Green, R.G and Beck, M,S, " Electronic transducers for industrial measurement of low value capacitances " *Journal Physics E .Scientific Instrumentation* ,Volume **21,** 1988, pp 242-250.

[5] Jones, B.E, " Instrumentation measurement and feedback" McGraw-Hill U.K.

[6] Margrete,k " M.Sc. theses submitted to the University of Manchester" 1993.

[7] Cunningham, M.J, Jenkins, D,F,L , Clegg, W,W and Bakush, M,M " Active Vibration control of a small cantilever actuator" *Sensor and Actuator A (Physical) - Micromechanics*, Volume **A 50**, 1995, p 147-150.

[8] Tzou, H.S " Distributed model identification and vibration control of continua: Theory and applications " *Journal of dynamic systems, measurement, and control*, Volume **113** ,September 113, pp 494 - 499.

[9] Varadan, V.K , Hong, S,Y and Varadan, V.V, " Piezoelectric sensors and actuators for active vibration damping using digital control." *Ultrasonic symposium* ,1990, pp 1211-1215.

[10] Rao,V, Damle, R, Tebbe, C and Kern, F , " The adaptive control of smart structures using neural networks " *Smart Materials and Structures*, Volume **3**, No. 3, 1994, pp 354-366.

[11] Zeinoun, I and Khorrami, F " An adaptive control scheme based on fuzzy logic and its application to smart structures" *Smart Materials Structures*, Volume **3** 1994 pp 266-276.

Chapter 7

7. Conclusions.

To understand the properties (Modal shape, deflection and resonance frequencies) of small cantilevers such as used in scanning probe instruments, different models that characterise these properties as a function of material and geometrical parameters are analytically presented in this thesis.

The SFM cantilevers are typically 100 μm long and have QF values of the order of tens in air and up to thousands in vacuum. Such instruments are extremely sensitive to building and air-borne vibrations. Although, great care is taken to isolate the instruments from such sources, for example, by the use of massive air-bearing table, mechanical vibration of the cantilever limits the resolution of the instruments. In this thesis, the behaviour of active vibration control, to minimise the cantilever vibration, has been theoretically and expirementaly investigated using suitable actuation and sensor methods.

Also, to maximise the actuator function, a generalised approach for the optimisation of piezoactuator / cantilever coupling is studied analytically and confirmed experimentally.

In summary, this thesis is divided into three parts:

7.1 The cantilever model.

Chapter 3 demonstrates analytical models which characterise the general behaviour of scanning probe microscope cantilevers. These models are helpful to appreciate the main design problems.

7.1.1 Behaviour of inhomogeneous cantilevers.

A new model to estimate the behaviour of inhomogeneous cantilevers (i.e. resonance frequencies and deformation) as a function of the structure material and its dimensions is derived using energy criteria. The results of this model have been compared with our experimental work and with the previous published measured data found in the literature. The theoretical prediction and experimental data were found to correlate very well. The effect of PZT element material and dimensions in a structure behaviour are also demonstrated. The behaviour of such cantilevers under feedback control system is also studied.

The advantages of this model are,

1. Simplicity in use.
2. It enables the affects of different parameters such as PZT element dimensions and its position on the cantilever to be seen.

The drawback of this model is that it neglects the effect of the bonding layer (i.e. it assumes perfect bonding). However, the discrepancy between the predicted and measured data is very small and can be neglected.

7.1.2 Modal shape.

A new expression to describe the modal shapes of inhomogeneous rectangular cantilevers is derived. In this model, the actuation by a discrete PZT element located near the cantilever root and the effective clamped point due to the non-ideal behaviour of the clamp are considered. The modal shapes predicted were compared with the measured data. This model overcomes the discrepancy between measured data and the previous analytical models, and provided a very good fit to measured data.

7.1.3 V-shaped cantilever.

Since the cantilever is in the heart of the scanning force microscope, it is important to characterise its behaviour. Most of scanning force microscope cantilevers are V-shaped because they provide low mechanical resistance to vertical deflection and high resistance to lateral torsion. In the past, V-shaped cantilevers have been treated as two rectangular beams in parallel, and their fundamental and harmonic resonate can be calculated by using the rectangular beam model. The experimental results indicate that the rectangular beam model can not provide a true representation of the V-shaped behaviour. In chapter 3 of this thesis, the behaviour of the V-shaped cantilevers is investigated using the Finite Element Technique (FEM). In this study, the effect of various parameters such as cantilever arm width and angle between arms have been taken into consideration. The results of FEM have been compared with the measured data. The agreement is good.

7.2 Investigation of the piezoelement and electrostatic actuation.

7.2.1 Optimum thickness of piezoelement actuators.

A generalised approach that describes the optimal thickness of piezoelectric elements attached to the simple cantilever is presented in chapter 4. The model shows that for each cantilever material there is an optimum thickness for maximum actuation. The predictions of this model are experimentally verified. Experimental results indicate that the simple model can accurately predict the optimum thickness ratio under a constant electric field. It is also demonstrated that the optimal thickness of single-sided piezo-actuators is slightly thicker than that of double-sided piezo-actuators. Although these results clearly show that the model is not a good representation of the experimental situation for the case where the cantilever is thick, however, it is valid in the practically important region of optimum thickness ratio and above and can also provide a foundation for general design guidelines of piezo-actuators.

7.2.2 Linearisation of the electrostatic actuators.

The performance of the electrostatic actuators under applied dc and ac voltage is theoretically and experimentally demonstrated. The results obtained have shown that the agreement between the theoretical and experimental data is very good. These results show that the behaviour of a cantilever excited by an electrostatic actuator is non-linear. This non-linearity is mainly due to square law phenomena. The

cantilever's response is linearised by a circuit which forms the square root of the total drive field. This study indicates that electrostatic actuator can be used in different applications such as microposition and active vibration control once linearity is achieved

7.3 Experimental investigation on active vibration control.

This experimental part of the work demonstrates the properties of capacitance and piezoelectric material as transducers in active vibration loop.

7.3.1 Capacitance transducer.

A capacitance transducer has been successfully designed as a sensor to monitor vibration of the small cantilever. The results obtained indicate that the capacitance transducer can be used effectively as sensor in the vibration control. However, environmental effects such as humidity and temperature, stray and fringe capacitance and mechanical design must be carefully considered if a high accuracy is to be achieved in practice. In general a capacitive system needs well designed processing electronics to detect the small capacitance changes and achieve a very high resolution.

7.3.2 Piezoelement transducer.

The experimental results show that the piezoelectric materials can be used very effectively as sensors and actuators in the active vibration control if enough control signal is supplied. This is due to their fairly simple processing electronics, large electro-mechanical coupling constant, inexpensive, availability in different thickness and size, and they also offer a wide range of operating voltages. Most of these piezo-materials can be attached to the structure without greatly changing the mechanical properties of the structure due to their light weight.

Disadvantage of this method are:

a) The control provided by this method is determined by the position of both actuator and sensor on the cantilever.
b) Temperature and humidity dependent.
c) Problems could arise from the capacitance coupling between the sensor and the actuator elements.

7.3.3 Comparison between Optical beam deflection, piezoelement and capacitance transducers.

As demonstrated in Chapter 6, the piezoelement and capacitance transducers can be used effectively as sensors in active vibration control systems owing to their inexpensive cost, high resolution and other advantages listed in Chapter 2. They have

disadvantages such as the non-linear law, stray capacitance problem, temperature, humidity and position dependency.

As sensor, optical beam deflection is superior to the piezoelement and capacitance because it offers the following advantages:

1. It is suited to the measurement of cantilever displacement at a series of discrete points.
2. It is extremely sensitive with a displacement resolution better than 0.1 nm.
3. It is experimentally simple.
4. It is a non-intrusive system;

In conclusion, this work has added to the understanding of sensors and actuators for use with small cantilevers such as those found in scanning probe instruments which can be used to simultaneously position the cantilevers and to remove unwanted vibrations.

This work provides the basis for applications of sensing and actuation in small structures. Typical applications would include the direct manipulation of optical fibres for medical and other uses and the control of cantilevers for ink jet printers

Appendices.

Appendix A .

The Matlab routine used to evaluate the cantilever and piezoelectric plate composite structural behaviours is given as:

```
% Script file to define the cantilever and piezoelemnts constants.

constant;

q = input ('ENTER NO OF SHAPE FUNCTIONS ');
Q = input ('NUMBER OF POINTS EACH SIDE OF RESONANCE ');
n = input ('NUMBER OF RESONANCES ');
type = input ('ANALYSIS TYPE 1=displacement, 2=velocity , 3=acc ');

% This function to calculate the mass matrix (M) and stiffens matrix (K)
[M,K,C,P1p,Pd,phit] = matflex(q,stif,loss,t,L,V,b,A,m,I,Ib,mu);
% To calculate the eigvalus and eigen function
[omega] = eigfreq(M, K,1e-10);
% To calculate the frequencies points around the resonate frequency.
[w] = freqpoint (omega,Q,n);
% To calculate the resonate frequency.
[fr] = loopfr1(M,K,C,w,V,P1p,Pd,phit,type);
%[fr] = loopfr1(M,K,C,w,V,P2p,Pd,phit,type);

plot (w,abs(fr),'r')
xlabel('Frequency-Hz')
ylabel (' Amplitude')
end

% Script file to find the mode shape.
w = input('ENTER FREQUENCY OF INTEREST ');

[x,y] = shape1(M,K,C,V,P,L,Pd,phit,wsp,q);
plot(x,(y))
xlabel('Beam length (m) ')
ylabel('Beam deflection (m) ')
end
```

```
% Script file that selects required constants
dat = input ('DATA FILE (in quotes)   ');
[m,stif,loss,wi,V,I,Ib,A,t,b,L,mu] =eval(dat);
end

function [m,stif,loss,wi,V,I,Ib,A,t,b,L,mu] = beamcons
% file containing data for building beam matrices

stif (E)   = [ Eb  Ep];
loss  (L) = [ Lb  Lp];
rho = [ρb       ρp];
t = [tb  tp]*1e-3;
wi= [wb    wp]*1e-3;
wb =
wp =
D = (stif(2).*(t(2))^2 + 2*stif(2).*t(2)*t(1) + stif(1)*t(1)^2);
D1= 2*(stif(2)*t(2) +stif(1)*t(1));
DD = D/D1;
XX = DD - t(1)/2;
V =  ;
Lb = ;
bb= [x1/ Lb     x2/ Lb ];
% piezoelectric charge constant (C/N)
d31 =
p = bb* Lb
A = wi.*t;
m = rho.*A;

% for sandwich beams(two piezoelectric layers)
I = wi.*(t.^3)./12;
% for one piezoelectric.
I1= wb.*(t(1).^3)./12;
Ib = I1 + wb*t(1).*XX^2;
 mu = d31/t(2);
end

%function [M,K,C,P2p,Pd,phit] = matflex(q,stif,loss,t,L,V,p,A,m,I,Ib,mu).
function [M,K,C,P1p,Pd,phit] = matflex(q,stif,loss,t,L,V,p,A,m,I,Ib,mu).
% calculates mass, stiffness (constant & variable), damping and forcing
% matrices for the flexural motion of a beam with q assumed shapes.
% phit is the shape at the tip  of the beam
```

```
[IDphi,dummy1, IsdDphi] = mbuild1(L,0,L,q);
 [IDPhiB,dummy2,IsdDphiB] = mbuild1(L,p1,p2,q);
[dummy3,dummy4,IsdphiB] = Int2(L,p1,p2,q);
Sp = A(2)*(t(1)^2/4 + t(1)*t(2)/2 + t(2)^2/3);
 Sf = A(2)*(t(1) + t(2));

M = m(1)*IDphi + 2*m(2)*IsdDphiB;
K11 = stif(1)*Ib*IsdDphi ;
K12 = stif(1)*I(1)*IsdDphi ;

% k22 two piezoelectric bounded to beam.
K22 = 2*stif(2)*Sp*IsdDphiB;
% k21 one piezoelectric bounded to beam.
K21 = stif(2)*Sp*IsdDphiB;
%K = K12+K22;
K = K11+K21;
%C = K12*loss(1) + K22*loss(2);
C = K11*loss(1) + K21*loss(2);
%P = mu*PHIDDB;
% p2p two piezoelectric bounded to beam.
%P2p = 2*stif(2) * Sp * mu *V*IsdphiB;
% p1p one piezoelectric bounded to beam.
P1p = stif(2) * Sp * mu *V*IsdphiB;
%Pd = P2p * loss(2);
Pd = P1p * loss(2);
 [phit] = Int3(L,L,q,q);

end

function [P,PD,PDD] = mbuild1(L,a,b,qh)
% [P,PD,PDD] = mbuild1(L,a,b,qh)
% builds maitrices of order qh for phi*phi and its derivatives

P = zeros(qh);
PD = P;
PDD = P;
for vi = 1:qh;
 [li,cfi] = lamph(vi);
 cfi1 = [-cfi(2) cfi(1) cfi(4) cfi(3)];
 cfi2 = [-cfi(1) -cfi(2) cfi(3) cfi(4)];

 for vj = 1:qh
  [lj,cfj] = lamph(vj);
  cfj1 = [-cfj(2) cfj(1) cfj(4) cfj(3)];
  cfj2 = [-cfj(1) -cfj(2) cfj(3) cfj(4)];
```

```
  [P(vi,vj),I] = c2phi(li,lj,b1,b2,L,cfi,cfj);
   PD(vi,vj) = sum(sum((cfi1'*cfj1).*I))*li*lj/L^2;
   PDD(vi,vj) = sum(sum((cfi2'*cfj2).*I))*li^2*lj^2/L^4;
 end

end
  end

function [PHI,PHID,PHIDD,MP] = Int2(L,a1,a2,qh)
% [PHI,PHID,PHIDD,MP] = Int2(L,a1,a2,qs)
% calculates the integral from a1 to a2 of phi and  its derivatives.

for v = 1:qh;
  [li,c] = lamph(v);
  s1 = li*a1/L;
  s2 = li*a2/L;
  pp1 = c(1)*(sin(s2)-sin(s1)) + c(2)*(cos(s2)-cos(s1));
  pp2 = c(3)*(sinh(s2)-sinh(s1)) + c(4)*(cosh(s2)-cosh(s1));
  PHID(v,1) = pp1 + pp2;
  p1 = c(2)*(sin(s2)-sin(s1)) - c(1)*(cos(s2)-cos(s1));
  p2 = c(4)*(sinh(s2)-sinh(s1)) + c(3)*(cosh(s2)-cosh(s1));

  PHI(v,1) = (p1 + p2)*(L/li);
  PHIDD(v,1) = (li/L)*(p2-p1);
 Pa = ((li/L)^2)*(-c(1)*sin(s2) - c(2)*cos(s2) + c(3)*sinh(s2) + c(4)*cosh(s2));
 Pb = ((li/L)^2)*(-c(1)*sin(s1) - c(2)*cos(s1) + c(3)*sinh(s1) + c(4)*cosh(s1));
 Ma = (li/L)*(c(1)*cos(s2) -c(2)*sin(s2) +c(3)*cosh(s2) + c(4)*sinh(s2));
 Mb = (li/L)*(c(1)*cos(s1) -c(2)*sin(s1) +c(3)*cosh(s1) + c(4)*sinh(s1));
 MP(v,v) = (Pa.*(Ma) - Pb.*(Mb));
end;
end

function [PHIX,PSIX] = Int3(L,x,qh,qs)
% [PHIX,PSIX] = Int3(L,x,qh,qs)
% builds vector for phi  at any position x
for v = 1:qh;
  [lh,c] = lamph(v);
  s = lh*x/L;
phi1 = c(1)*sin(s) + c(2)*cos(s);
phi2 = c(3)*sinh(s) + c(4)*cosh(s);

  PHIX(v,1) = phi1 + phi2;
end
  end
```

```
function I = iss(lam1,lam2,b1,b2,L)
% I = iss(lam1,lam2,a,b,L);
% calculates the integral from b1 to b2 for sin(lam1*x/L)*sin(lam2*x/L)
if  lam1 == lam2,

I = ((b2-b1) - (sin(2*lam1*b2/L)-sin(2*lam1*b1/L))*L/(2*lam1))/2;
else,


g = (lam1+lam2)/L;
 h = (lam1-lam2)/L;
I1 = (sin(g*b2)-sin(g*b1))/g;
 I2 = (sin(h*b2)-sin(h*b1))/h;
 I = -(I1-I2)/2;
end
  end

function I = isc(lam1,lam2,b1,b2,L)

% I = isc(lam1,lam2,a,b,L);
% calculates the integral from b1 to b2 for  sin(lam1*x/L)*cos(lam2*x/L).
if  lam1 == lam2,
 I =  -(cos(2*lam1*b2/L)-cos(2*lam1*b1/L))*L/(4*lam1);
else,
 g = (lam1+lam2)/L;
 h = (lam1-lam2)/L;
 I1 = (cos(g*b2)-cos(g*b1))/g;
 I2 = (cos(h*b2)-cos(h*b1))/h;
 I = -(I1+I2)/2;
end
   end

function I = issh(lam1,lam2,b1,b2,L)
   % I = issh(lam1,lam2,a,b,L);
% calculates the integral from b1 to b2 for sin(lam1*x/L)*sinh(lam2*x/L)

I1 = sin(lam1*b2/L)*cosh(lam2*b2/L) - sin(lam1*b1/L)*cosh(lam2*b1/L);
I2 = cos(lam1*b2/L)*sinh(lam2*b2/L) - cos(lam1*b1/L)*sinh(lam2*b1/L);
I = (lam2*I1 - lam1*I2)*L/(lam1^2+lam2^2);
end

function I = isch(lam1,lam2,b1,b2,L)
% I = isch(lam1,lam2,a,b,L);
% calculates the integral from b1 to b2 for sin(lam1*x/L)*cosh(lam2*x/L).
I1 = sin(lam1*b2/L)*sinh(lam2*b2/L) - sin(lam1*b1/L)*sinh(lam2*b1/L);
```

```
I2 = cos(lam1*b2/L)*cosh(lam2*b2/L) - cos(lam1*b1/L)*cosh(lam2*b1/L);
I = (lam2*I1 - lam1*I2)*L/(lam1^2+lam2^2);

end

function I = icc(lam1,lam2,b1,b2,L)
% I = icc(lam1,lam2,a,b,L);
% calculates the integral from b1 to b2 for cos(lam1*x/L)*cos(lam2*x/L).
if  lam1 == lam2,
 I = ((b2-b1) + (sin(2*lam1*b2/L)-sin(2*lam1*b1/L))*L/(2*lam1))/2;


else,
 g = (lam1+lam2)/L;
 h = (lam1-lam2)/L;

 I1 = (sin(g*b2)-sin(g*b1))/g;
 I2 = (sin(h*b2)-sin(h*b1))/h;
 I = (I1+I2)/2;
end
   end

function I = icsh(lam1,lam2,b1,b2,L)
% I = icsh(lam1,lam2,a,b,L);
% calculates the integral from b1 to b2 for cos(lam1*x/L)*sinh(lam2*x/L).

I1 = cos(lam1*b2/L)*cosh(lam2*b2/L) - cos(lam1*b1/L)*cosh(lam2*b1/L);
I2 = sin(lam1*b2/L)*sinh(lam2*b2/L) - sin(lam1*b1/L)*sinh(lam2*b1/L);
I = (lam2*I1 + lam1*I2)*L/(lam1^2+lam2^2);

end

function I = icch(lam1,lam2,b1,b2,L)
% I = icch(lam1,lam2,a,b,L);
% calculates the integral from b1 to b2 for cos(lam1*x/L)*cosh(lam2*x/L).
I1 = cos(lam1*b2/L)*sinh(lam2*b2/L) - cos(lam1*b1/L)*sinh(lam2*b1/L);
I2 = sin(lam1*b2/L)*cosh(lam2*b2/L) - sin(lam1*b1/L)*cosh(lam2*b1/L);
I = (lam2*I1 + lam1*I2)*L/(lam1^2+lam2^2);
end

function I = ishsh(lam1,lam2,b1,b2,L)
% I = ishsh(lam1,lam2,a,b,L);
% calculates the integral from b1 to b2 for  sinh(lam1*x/L)*sinh(lam2*x/L).
```

```
if  lam1 == lam2,
 I1 = sinh(2*lam1*b2/L) - sinh(2*lam1*b1/L);
 I = (I1*L/(2*lam1) - (b2-b1))/2;
else,
 g = (lam1+lam2)/L;
 h = (lam1-lam2)/L;
 I1 = (sinh(g*b2)-sinh(g*b1))/g;

I2 = (sinh(h*b2)-sinh(h*b1))/h;
 I = (I1-I2)/2;
end
end

function I = ishch(lam1,lam2,b1,b2,L)
% I = ishch(lam1,lam2,a,b,L);
% calculates the integral from b1to b2 for sinh(lam1*x/L)*cosh(lam2*x/L).

if  lam1 == lam2,
 I1 = cosh(2*lam1*b2/L) - cosh(2*lam1*b1/L);
 I = I1*L/(4*lam1);
else,
 g = (lam1+lam2)/L;
 h = (lam1-lam2)/L;

I1 = (cosh(g*b2)-cosh(g*b1))/g;
 I2 = (cosh(h*b2)-cosh(h*b1))/h;
 I = (I1+I2)/2;
end
end

function I = ichch(lam1,lam2,b1,b2,L)
% I = ichch(lam1,lam2,a,b,L);
% calculates the integral from b1 to b2 for  cosh(lam1*x/L)*cosh(lam2*x/L).

if lam1 == lam2,
 I1 = sinh(2*lam1*b2/L) - sinh(2*lam1*b1/L);
 I = (I1*L/(2*lam1) + (b2-b1))/2;
else,
 g = (lam1+lam2)/L;
 h = (lam1-lam2)/L;
I1 = (sinh(g*b2)-sinh(g*b1))/g;
 I2 = (sinh(h*b2)-sinh(h*b1))/h;
 I = (I1+I2)/2;
end
end
```

```
function [B,I] = c2phi(lam1,lam2,b1,b2,L,cf1,cf2)

% B = c2phi(lam1,lam2,a,b,L,cf1,cf2)
% calculates the integral from b1 to b2 of phi*phi.

% cf1 & cf2 are vectors of trig function coefficients
% i.e. A1*sin(px) + A2*cos(px) + A3*sinh(px) + A4*cosh(px)

I(1,1) = iss(lam1,lam2,b1,b2,L);
I(1,2) = isc(lam1,lam2,b1,b2,L);
I(1,3) = issh(lam1,lam2,b1,b2,L);
I(1,4) = isch(lam1,lam2,b1,b2,L);
I(2,1) = isc(lam2,lam1,b1,b2,L);
I(2,2) = icc(lam1,lam2,b1,b2,L);
I(2,3) = icsh(lam1,lam2,b1,b2,L);
I(2,4) = icch(lam1,lam2,b1,b2,L);
I(3,1) = issh(lam2,lam1,b1,b2,L);
I(3,2) = icsh(lam2,lam1,b1,b2,L);
I(3,3) = ishsh(lam1,lam2,b1,b2,L);
I(3,4) = ishch(lam1,lam2,b1,b2,L);
I(4,1) = isch(lam2,lam1,b1,b2,L);
I(4,2) = icch(lam2,lam1,b1,b2,L);
I(4,3) = ishch(lam2,lam1,b1,b2,L);

I(4,4) = ichch(lam1,lam2,b1,b2,L);

B1 = cf1'*cf2;
B2 = B1.*I;
B = sum(sum(B2));

end

function [W,EV] = eigfreq(a,b,acc)
% [W,EV] = eigfreq(a,b,acc)
% This function finds the natural frequencies (Hz) and eigenvectors
% if the mass maitrix (a) and stiffness maitrix (b) are entered

s = iterat(a,b,acc);
[vect,wsq] = eig(s);

p = length(s);
om = diag(wsq)/1e9;
E(1,:) = om';

 for n = 1:p;
  E(n+1,:) = vect(n,:);
```

```
 end
omeg = sort(om');
 for n = 1:p
 for m = 1:p;

if  E(1,m) == omeg(n),
   EV(:,n) = E(2:p+1,m);
 end

 end
end

W = sqrt(omeg*1e9)/(2*pi);
end

function[w]=freqpoint(omega,Q,n);
 % [w] = freqpoints(omega,Q,n)
 % Builds frequency vector 'w' concentrating points around 'n' resonances
 % Uses 'Q' points either side of each resonance
 % Spacings increase geomertically
 adder = 1;
 omeg = abs(sort(omega));
 for m= 1:n;
  if m ==1;

p1=0.5;
  p2 = (omeg(m) + omeg(m+1))/(omeg(m)*2);
  elseif m ==length(omeg);
  p1= (omeg(m) + omeg(m-1))/(omeg(m)*2);
  p2 = 1.08;
  else
  p2 = (omeg(m+1) + omeg(m))/(omeg(m)*2);
  p1= (omeg(m) + omeg(m-1))/(omeg(m)*2);
  end;
  B1 = (1-p1)/Q^2;
  B2 = (p2-1)/Q^2;
  count = adder +Q;
  for nn = -1:2:1

   if nn == -1,
     z= -B1;
     else,
      z = B2;
    end
    for r = 0:Q;
    w(count) = omeg(m)*(1 +z*r*r);
```

```
adder = count+(nn/abs(nn));
    count = adder;
    end;
    count = adder + Q+ 1;

end
    end;
    end;

function [fr] = loopfr1(M,K,C,w,V,P1p,Pd,phit,type);
%function [fr] = loopfr1(M,K,C,w,V,P2p,Pd,phit,type);
%function[fr,w] = openlopfr1(M,K,C,P,V,H,Sx,Pd,phit,type,para)
% plots the frequency response function.

adder = 1;
for count = 1:length(w)
wr = w(count)*2*pi;
if type == 1,
  ana= 1;
 elseif type == 2,
  ana= i*wr;
else,
  ana = -wr*wr;

 end
s1 = K - wr^2*M + i*C ;
s2 = (P1p- i*Pd)*V;
%s2 = (P2p- i*Pd)*V;
%  s=iterat(s1,s2,1e-9);
   s =s1\s2;
count = adder;
fr(count,1) = ana*phit'*s;
adder = count + 1;

 end
end
```

Appendix B .

Cantilever modal shape modelling.

For a uniform cantilever beam , the free vibrations are governed by the well known Euler differential equation given by.

$$EI \frac{\partial^4 y}{\partial x^4} + \rho A \frac{\partial^2 y}{\partial t^2} = 0 \qquad \text{(B-1)}$$

In the case of applied external force, the above equation becomes

$$EI \frac{\partial^4 y}{\partial x^4} + \rho A \frac{\partial^2 y}{\partial t^2} = F(x, t) \qquad \text{(B-2)}$$

The solution of the above equation can be expressed as

$$y(x, t) = \Phi_n(x). e^{jw_n t} \qquad \text{(B-3)}$$

where Φ_n (x) is the normal mode function. w_n are the cantilever harmonic frequencies.

Substituting equation (B-3) into equation (B-2) yields

$$\frac{\partial^4 \Phi_n(x)}{\partial x^4} - \lambda^4{}_n \Phi_n(x) = 0 \qquad \text{(B-4)}$$

where $$\lambda^4{}_n = \frac{\rho A}{EI} \omega^2{}_n$$

The general solution of equation (B-4) can be given as

$$\Phi_n(x) = C_1 \cosh(\lambda_n x) + C_2 \sinh(\lambda_n x) + C_3 \cos(\lambda_n x) + C_4 \sin(\lambda_n x). \quad \text{(B-5)}$$

The boundary conditions for the case of one end fixed, and other end free are

$$\Phi_n(x = -\Delta L) = 0 \qquad \Phi_n'(x = -\Delta L) = 0 \quad \text{(B-6)}$$

$$\Phi_n''(x = L) = 0 \qquad \Phi_n'''(x = L) = 0 \quad \text{(B-7)}$$

where ΔL (inside the clamp) is included to compensating the effect of non-ideal clamp at the fixed end.

Substituting the above boundary conditions into equation (B-5) yields

$$0 = C_1 \cosh(\lambda_n \Delta L) - C_2 \sinh(\lambda_n \Delta L) + C_3 \cos(\lambda_n \Delta L) - C_4 \sin(\lambda_n \Delta L). \quad \text{(B-8)}$$

$$0 = -C_1 \sinh(\lambda_n \Delta L) + C_2 \cosh(\lambda_n \Delta L) + C_3 \sin(\lambda_n \Delta L) + C_4 \cos(\lambda_n \Delta L). \quad \text{(B-9)}$$

$$0 = C_1 \cosh(\lambda_n L) + C_2 \sinh(\lambda_n L) - C_3 \cos(\lambda_n L) - C_4 \sin(\lambda_n L). \quad \text{(B-10)}$$

$$0 = C_1 \sinh(\lambda_n L) + C_2 \cosh(\lambda_n L) + C_3 \sin(\lambda_n L) - C_4 \cos(\lambda_n L). \quad \text{(B-11)}$$

From equation (B-8) yields

$$C_2 = \frac{C_1 \cosh(\lambda_n \Delta L) + C_3 \cos(\lambda_n \Delta L) - C_4 \sin(\lambda_n \Delta L)}{\sinh(\lambda_n \Delta L)} \quad \text{(B-12)}$$

Substituting equation (B-12) into equation (B-9) yields

$$C_1 = -AC_3 - BC_4 \quad \text{(B-13)}$$

where

$$A = \cos(\lambda_n . \Delta L) \cosh(\lambda_n . \Delta L) + \sin(\lambda_n . \Delta L) \sinh(\lambda_n . \Delta L).$$

$$B = \cos(\lambda_n . \Delta L) \sinh(\lambda_n . \Delta L) - \sin(\lambda_n . \Delta L) \cosh(\lambda_n . \Delta L)$$

Similarly, from equations (B-12) , (B-13) yields

$$C_2 = -DC_3 - FC_4 \tag{B-14}$$

$$D = \cos(\lambda_n . \Delta L) \sinh(\lambda_n . \Delta L) + \sin(\lambda_n . \Delta L) \cosh(\lambda_n . \Delta L)$$

$$F = \cos(\lambda_n . \Delta L) \cosh(\lambda_n . \Delta L) - \sin(\lambda_n . \Delta L) \sinh(\lambda_n . \Delta L).$$

From equations (B-13) , (B-14) and (B-9) there follows

$$C_4 = -\gamma . C_3 \tag{B-15}$$

$$C_1 = -\alpha . C_3 \tag{B-16}$$

$$C_2 = -\beta . C_3 \tag{B-17}$$

where

$$\gamma = -\frac{D \sinh(\lambda_n L) + A \cosh(\lambda_n L) + \cos(\lambda_n L)}{B \cosh(\lambda_n L) + F \sinh(\lambda_n L) + \sin(\lambda_n L)},$$

$$\alpha = -\frac{(AF - BD) \sinh(\lambda_n L) + A \sin(\lambda_n L) - B \cos(\lambda_n L)}{B \cosh(\lambda_n L) + F \sinh(\lambda_n L) + \sin(\lambda_n L)},$$

$$\beta = -\frac{(DB - AF)\cosh(\lambda_n L) + D\sin(\lambda_n L) - F\cos(\lambda_n L)}{B\cosh(\lambda_n L) + F\sinh(\lambda_n L) + \sin(\lambda_n L)}$$

Substituting equations (B-15), (B-16) and (B-17) into equation (B-5) yields the expression for modal shape $\Phi_n(x)$:

$$\Phi_n(x) = -C_3\left(\left[\left(\alpha\cosh(\lambda_n x) - \cos(\lambda_n x)\right) + \left(\beta\sinh(\lambda_n x) + \gamma\sin(\lambda_n x)\right)\right]\right) \quad \text{(B-18)}$$

The constant C_3 can be found using additional boundary condition at the edges of piezoelement . This boundary condition accounts for the moment produced by the piezoelement .

At $x = X_2$ (see figure in chapter 3)

$$EI\frac{d^2\Phi_n(x)}{dx^2} = \pm gV. \quad \text{(B-19)}$$

Therefore the constant C_3 can be given as

$$C_3 = \frac{g.\ V}{\lambda^2_n EI\left[\alpha\cosh(\lambda_n X_2) + \cos(\lambda_n X_2) + \beta\sinh(\lambda_n X_2) - \gamma\sin(\lambda_n X_2)\right]} \quad \text{B-20)}$$

where V is the applied voltage. g dependence on the cantilever and piezoelement parameters and can be expressed as.

$$g = d_{31}\left(\frac{h_b + h_p}{2}\right)\frac{E_b h_b E_p w}{E_b h_b + E_p h_p}$$

Appendix C

SFM Cantilevers Modelling with ABAQUS.

ABAQUS is a finite element program designed for advanced structural analysis. It includes features specifically designed for the analysis of beam-like structures. With ABAQUS a structure like a cantilever can be modelled by dividing the cantilever into nodes and elements. A finite element model consists of a geometric description, which is specified by elements and their nodes. Moreover, a set of properties associated with the elements like material definitions and boundary conditions are included to the geometric description in a finite element model.

The ABAQUS input data contains model data and history data. Model data define a finite element program, i.e. the nodes, elements, element properties , material definitions and any other data that specify the model itself. History data define what happens to the model, i.e, the sequence of events for which the model's response is calculated. ABAQUS provides static and dynamic stress analysis, eigevalue extraction, resonant frequency detemination, transient heat transfer analysis etc, and can involve a linear and non-linear response.

In the following, the general description of how to model and analyse the structures using ABAQUS is discussed. As an example the resonant frequency of V-shaped SFM cantilevers will be calculated. Table C.1 shows the input file for a V-shaped cantilever used in our research group.

```
* HEADING
SFM cantilevers (V-shaped)
*NODE, NSET = ONE1
1, 0.E-6 , 0.E-6 , 0.
20, 115e-6 , 0, 0.
*NGEN, NSET=ONE
1 , 20
*NODE , NSET=TWO2
501, 0E-6 , 82.5E-6 , 0.
520, 190E-6, 0E-6 , 0.
*NGEN, NSET=TWO
501 , 520
*NFILL , NSET=FACE
ONE ,TWO , 5,100
*NCOPY, OLD SET=FACE, CHANGE
NUMBER = 600, NEW
SET=FACE1,REFLECT=LINE.
-5, 0,0 ,5 ,0 ,0
*ELEMENT, TYPE=S4R
1,1,2,102,101
*ELGEN, ELSET=ALL
1,19,1,1,5,100,19
*ELCOPY, OLD SET=ALL, NEW SET=ALL1,
ELEMENT SHIFT=95 ,SHIFT NODE = 600
*ELSET, ELSET=A
ALL,ALL1
*SHELL SECTION, ELSET=A,
MATERIAL=SILICON
0.3E-6
*MATERIAL, NAME=SILICON
*DENSITY
2330
*ELASTIC
1.79E+11, 0.3
*NSET , NSET=FIXED
1,101,201,301,401,501
*NSET, NSET=FIXED1
```

```
601,701,801,901,1001,1101
*MPC
TIE, 20,620
*MPC
TIE, 120,720
*MPC
TIE, 220,820
*MPC
TIE, 320,920
 *MPC
TIE, 420, 1020
*MPC
TIE, 520,1120
*BOUNDARY
FIXED  ,ENCASTRE
FIXED1,ENCASTRE
*DRAW, NODENUM
*DRAW,ELNUM
*STEP, PERTURBATION
FREE MODES AND FREQUENCIES
*FREQUENCY
3
*PLOT
*DISPLACED
U
*MODEL FILE
*END STEP
```

Table (C-1) Input file used in Finite element model for V-shaped cantilevers

All data definitions in ABAQUS are accomplished with option blocks, i.e. set of data describing a part of the problem definition. Each option is introduced by a * and a keyword card. The first option is the header for the analysis and will be taken as the heading for each page of the printed output job:

```
*HEADING
SFM cantilevers V-shape
```

The model data now follow. There is no particular order for defining a model, but it begin with the mesh , i.e. the nodes and elements that model our structure.

```
*NODE, NSET = ONE1
1, 0.E-6 , 0.E-6 , 0.
20, 115e-6 , 0, 0.
```

The * NODE option begins the reading of nodes and their co-ordinates. The (optional) parameter NSET has been included, with the value ONE1. This means that the two nodes read in this option will included in the node set ONE1.

ABAQUS contains several simple mesh generation capabilities. Here, we have used the *NGEN option for node generation along a line:

```
*NGEN, NSET=ONE
  1 , 20
```

The following *NFILL option to generate nodes for a region of a mesh with 500 nodes in total.

```
*NFILL , NSET=FACE
 ONE ,TWO , 5,100
```

The * NCOPY option to create nodes of the otherside by copying the old generated nodes. Likewise, we have to define the elements:

```
*ELEMENT , Type = S4R
1,1,2,102,101
```

The *ELEMENT option includes the TYPE parameter with the value S4R, a linear interpolation shell element for three dimensional problems. The first element is defined by the nodes 1,2,102,101. The mesh generation option is again used

*EIGEN, ELSET=ALL

1,19,1,5,100,19

The parameter ELSET has been included with the value ALL. This introduces an element set ALL, and adds all of the elements generated in the option to the set (see abaqus manual for details). The cantilever thickness is set by the * SHELL SECTION option,

*SHELL SECTION, ELSET=ALL, MATERIAL SILICON

0.6E-6

The material properties used are defined as

*MATERIAL, NAME=SILICON

All keywords that follow the *MATERIAL option produce the cantilever material

*DENSITY (mass density)

*ELASTIC (Young's modules)

The model definition is completed by giving some fixed boundary conditions

*NSET, NSET=FIXED

1,101,201,301,401,501

*NSET, NSET=FIXED1

601,701,801,901,1001,1101

To join the two arms of V-shaped cantilever , the *MPC option is used

*MPC

TIE , 20,620

This option to join the node (20) with node (620).

*BOUNDARY

FIXED, ENCASTRE

FIXED!, ENCASTRE

Here, the boundary conditions for nodes sets FIXED and FIXED1 have been described by the parameter ENCASTRE (fully built-in).

The model defination is now completed . The following steps describe the history data, i.e. the sequence of loading or events occurs and what response variables can be used. The history data are divided into steps. In one case, the free modes and frequencies are interested, this can be defined by using the following option,

*STEP, LINEAR

*FREQUENCY

NO of frequencies (6)

*END STEP

The *STEP option begins the step; *END STEP ends it. The LINEAR parameter specifies that only linear response should be considered.

ABAQUS

U
MAG. FACTOR = +7.4E-02
SOLID LINES - DISPLACED MESH
DASHED LINES - ORIGINAL MESH

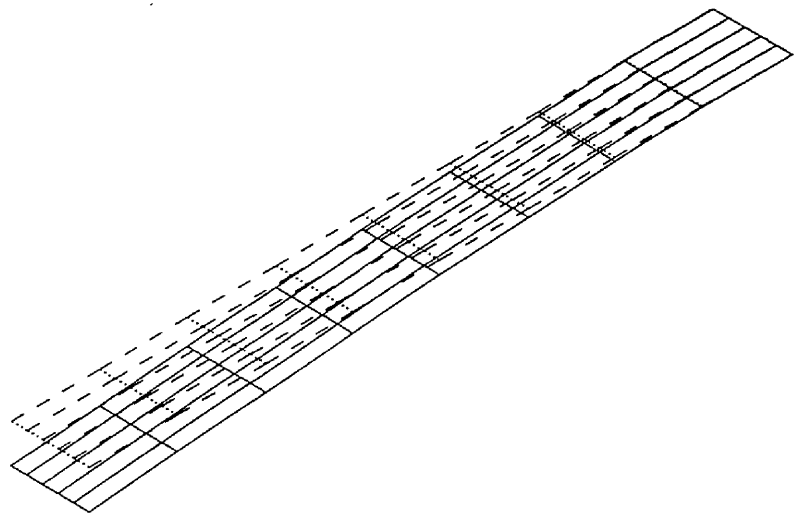

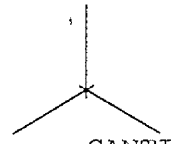

CANTILEVER RECTANGULAR-SHAPE

EIGENVALUE = +6.914E+04

ABAQUS VERSION 5.4-1 DATE: 04-JAN-95 TIME: 11:43:46

ABAQUS

U
MAG. FACTOR = +2.6E-01
SOLID LINES - DISPLACED MESH
DASHED LINES - ORIGINAL MESH

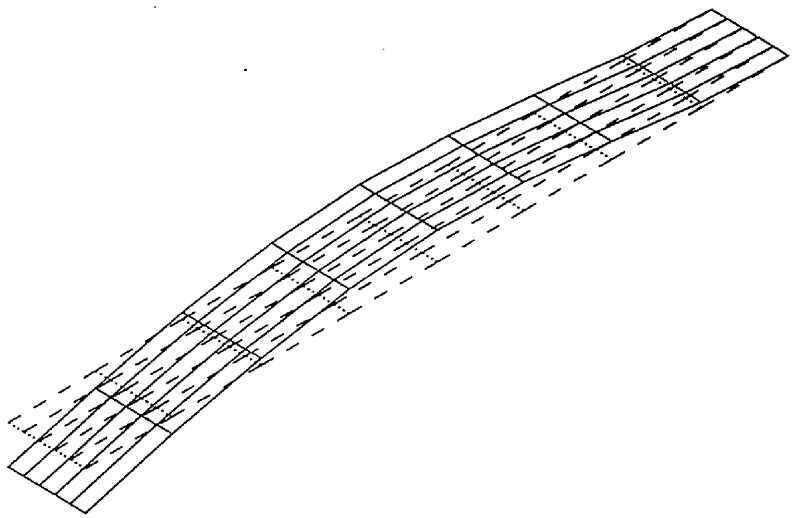

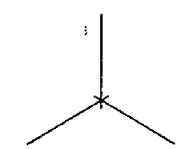

CANTILEVER RECTANGULAR-SHAPE

EIGENVALUE = +2.921E+11

ABAQUS VERSION 5.5 1 DATE: 09 JAN 95 TIME: 11:43:46

ABAQUS

U
MAG. FACTOR = +4.8E 01
SOLID LINES DISPLACED MESH
DASHED LINES ORIGINAL MESH

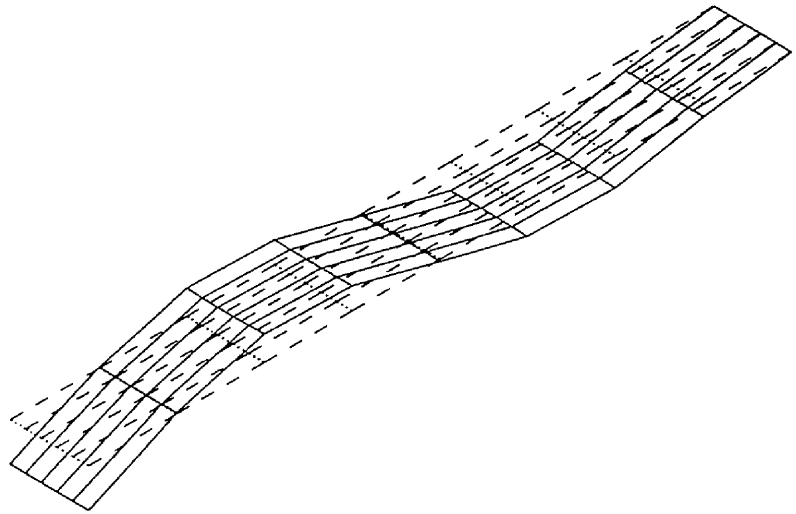

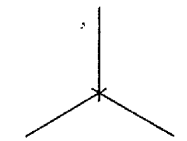

CANTILEVER RECTANGULAR-SHAPE

EIGENVALUE +2.661E+12

ABAQUS VERSION 5.3-1 DATE: 09 JAN 95 TIME: 11:43:46

ABAQUS

U
MAG. FACTOR = +6.6E-04
SOLID LINES - DISPLACED MESH
DASHED LINES - ORIGINAL MESH

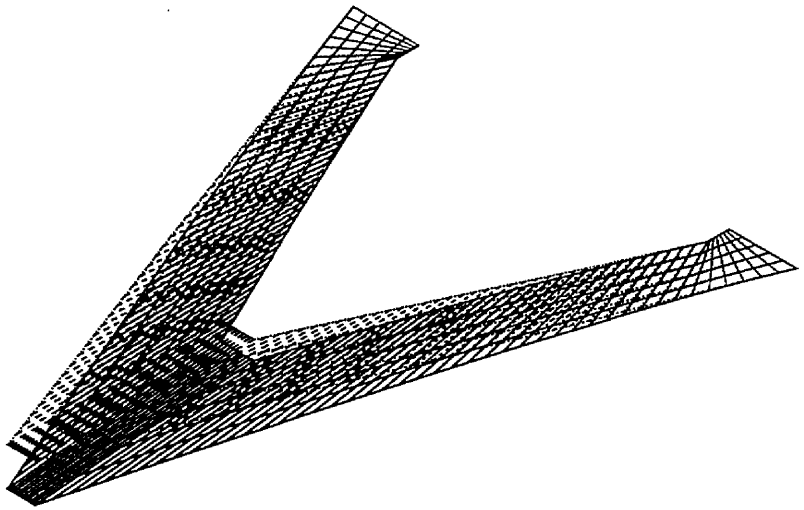

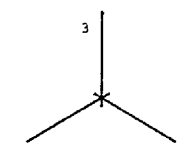

CANTILEVER V-SHAPE

TIME COMPLETED IN THIS STEP +2.220E-16 TOTAL ACCUMULATED TIME +0.000E-00 STEP 1 INCREMENT 1

ABAQUS VERSION 5.3-1 DATE: 06-FEB-95 TIME: 11:35:27

ABAQUS

U
MAG. FACTOR = +2.6E-01
SOLID LINES - DISPLACED MESH
DASHED LINES - ORIGINAL MESH

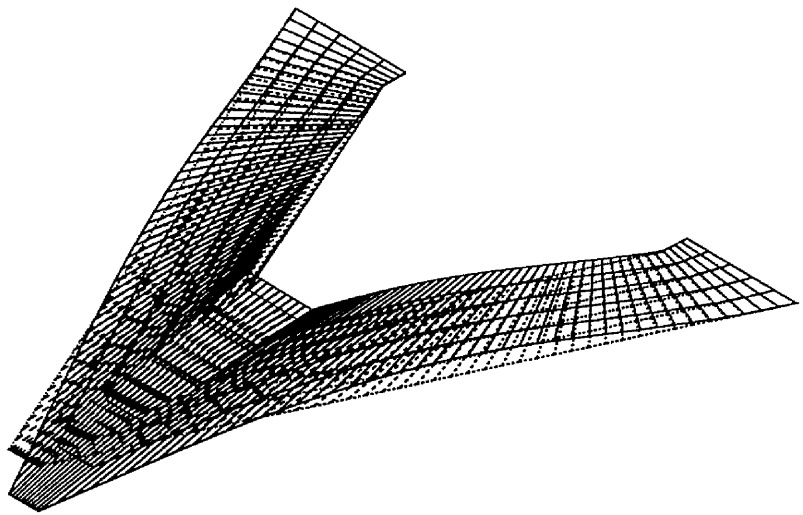

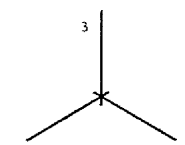

CANTILEVER V-SHAPE

EIGENVALUE = +1.321E+12

ABAQUS VERSION 5.3-1 DATE: 31-JAN-95 TIME: 12:20:33

ABAQUS

U
MAG. FACTOR = +6.8E-01
SOLID LINES - DISPLACED MESH
DASHED LINES - ORIGINAL MESH

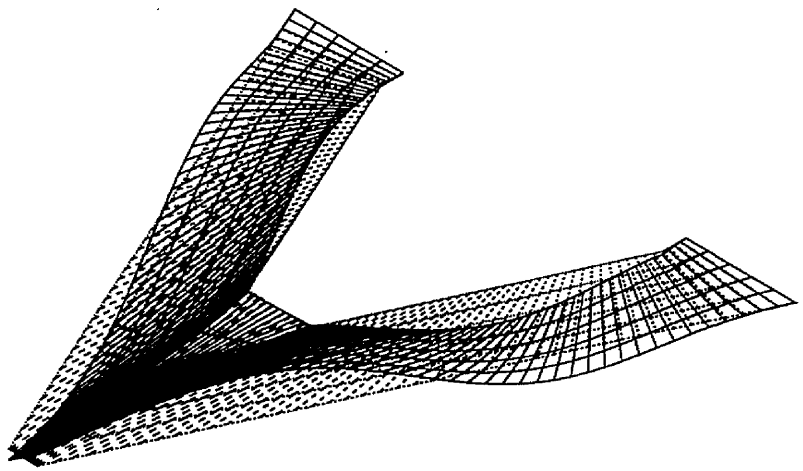

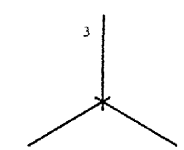

CANTILEVER V-SHAPE

EIGENVALUE = +8.913E+12

ABAQUS VERSION 5.3 1 DATE: 31 JAN-95 TIME: 12:20:33

Appendix D

Meas.Sci. Technol. 6 (1995) 160-166.

MEASUREMENT OF THE MODAL SHAPES OF INHOMOGENEOUS CANTILEVERS USING OPTICAL BEAM DEFLECTION.

D.F.L Jenkins, M J Cunningham, W W Clegg and M M Bakush.

Division of Electrical Engineering, Manchester School of Engineering, University of Manchester, Oxford Road, Manchester M13 9PL, UK.

Received 16 September 1994, in final form 10 November 1994, accepted for publication 16 November 1994.

Abstract. The study of free vibrations of systems such as simple cantilevers has been mainly concerned with the determination of the eigenvalues (frequencies) and eigenfunctions (modal shapes). A technique has been developed, using optical beam deflection, to measure the modal shape of a cantilever non-invasively at each modal frequency. A knowledge of the modal shapes of very small cantilevers incorporating suitable actuators is important in the application of active vibration control to micromechanical structures.

Sensors and Actuators A 50 (1995) physical 147-150.

ACTIVE VIBRATION CONTROL AND ACTUATION OF A SMALL CANTILEVER FOR APPLICATION IN SCANNING PROBE INSTRUMENTS.

M J Cunningham, D.F.L Jenkins, W W Clegg and M M Bakush.

Division of Electrical Engineering, Manchester School of Engineering, University of Manchester, Oxford Road, Manchester M13 9PL, UK.

Received 13 January 1995; accepted in revised form 19 June 1995.

Abstract. The deflection control of a small cantilever is described, which operates using a single active piezoelectric element and optical vibration sensing, so that unwanted vibrations in the cantilever are removed, and yet it remains possible to deflect the cantilever statically or dynamically as required. Such a control system is directly applicable to very small cantilevers found in scanning probe microscopes, such as atomic force and magnetic force microscopes, the resolution of which is limited by unwanted vibration.

AN INVESTIGATION INTO THE OPTIMUM DESIGN OF A PIEZO- ACTUATOR

D F L Jenkins, M M Bakush and M J Cunningham

Division of Electrical Engineering, Manchester School of Engineering, University of Manchester, Oxford Road, Manchester M13 9PL, England.

Sensors and actuators conference, 15-16 July, Manchester Business School.

Abstract. Piezoelectric elements as actuators have been extensively used to control structures with a wide range of sizes. The effect of piezo-actuator thickness on the magnitude of deflection of a cantilever beam has been investigated experimentally and the results compared with a theoretical model. Results indicate that there exists a piezo-actuator thickness which maximises the cantilever deflection, and this optimal thickness is a function of ratio of the Young's modulus of the actuator and the cantilever. The significance for actuator design is discussed.

IEE Proceeding Science, Meas and Technol. ***144*** *(1997) 45-48.*

EXPERIMENTAL INVESTIGATION OF THE OPTIMUM THICKNESS OF A PIEZOELECTRIC ELEMENT FOR CANTILEVER ACTUATION

M J Cunningham, D F L Jenkins and M M Bakush

Abstract. Piezoelectric elements as actuators may be used to control structures with a wide range of sizes. The magnitude of actuation which is possible is a direct function of the ratio of the thickness of the piezoelectric element to that of the cantilever. An experimental investigation has been made to determine the exact nature of this phenomenon for two materials and compared with current theoretical models. The significance for actuator design is discussed.

A LINEARISED ELECTROSTATIC ACTUATOR.

M M BAKUSH, D F L JENKINS, M J CUNNINGHAM,

C FERRARI † AND G P SCHIONA †

Division of Electrical Engineering, Manchester School of Engineering,

University of Manchester, Oxford Road, Manchester M13 9PL, England.

† Electrical Engineering Department, University of Ferrara, Italy

Sensors and actuators conference, 15-16 July, Manchester Business School.

Abstract. There is currently considerable interest in positioning miniature structures. For such structures electrostatic actuation is attractive. An electrostatic actuator is however inherently non-linear. The behaviour of such an actuator is theoretically modelled and experimentally verified. A control system has been developed which enables linear electrostatic actuation to be realised.